Study of surface flashover of insulator in gases at high pressure

By

SOMESH VINAYAK TEWARI

Enrollment no.-ENGG01201004004

Bhabha Atomic Research Centre, Mumbai – 400085 INDIA

A thesis submitted to the Board of Studies in Engineering Sciences

In partial fulfillment of requirements

For the Degree of

DOCTOR OF PHILOSOPHY

of

HOMI BHABHA NATIONAL INSTITUTE, MUMBAI

December, 2014

Homi Bhabha National Institute

Recommendations of the Viva Voce Board

As members of the Viva Voce Board, we certify that we have read the dissertation prepared by Somesh Vinayak Tewari entitled "Study of surface flashover of insulator in gases at high pressure" and recommend that it may be accepted as fulfilling the dissertation requirement for the Degree of Doctor of Philosophy.

Date: 26/8/2015

Chairman: Prof. A.P.Tiwari

Date: 26-8-15

Guide/ Convener: Prof. Archana Sharma

Date:

Co-Guide: Prof.K.C.Mittal

Date: 26.08.2015

Member 1: Prof. S.V.G.Ravindranath

Date: 26/8/2015

Member 2: Prof. A.Bhattacharjee

Date: 26.08.2015

External Examiner: Prof. R.Sarathi

Final approval and acceptance of this dissertation is contingent upon the candidate's submission of the final copies of the dissertation to HBNI. I hereby certify that I have read this dissertation prepared under my direction and recommend that it may be accepted as fulfilling the dissertation requirement.

Date: 01-09-2015

Place: Mumbai

Guide: Prof. Archana Sharma

STATEMENT BY AUTHOR

This dissertation has been submitted in partial fulfillment of requirements for an advanced degree at Homi Bhabha National Institute (HBNI) and is deposited in the Library to be made available to borrowers under rules of the HBNI.

Brief quotations from this dissertation are allowable without special permission, provided that accurate acknowledgement of source is made. Requests for permission for extended quotation from or reproduction of this manuscript in whole or in part may be granted by the Competent Authority of HBNI when in his or her judgment the proposed use of the material is in the interests of scholarship. In all other instances, however, permission must be obtained from the author.

Somesh Vinayak Tewari

Somesh Vinayak Tewari

DECLARATION

I, hereby declare that the investigation presented in the thesis has been carried out by me. The work is original and has not been submitted earlier as a whole or in part for a degree / diploma at this or any other Institution / University.

Somesh Vinayak Tewari

Somesh Vinayak Tewari

Dedicated to

My Parents

Shri. Asit Kumar Tewari

Smt. Gouri Tewari

and

My Sisters

Smt. Nitu Tewari

Smt. Neha Tewari

ACKNOWLEDGEMENTS

I express my deep gratitude to the following persons who have helped me in various ways.

- To my guides Dr. K. C. Mittal, Head, Accelerator and Pulse Power Division, BARC, (Retired on 31-05-2014), Dr. Archana Sharma, Head, Pulse Power Systems Section, Accelerator and Pulse Power Division, BARC, Mumbai and Dr.K.V.Nagesh, Head Energetics and Pulse Power Systems Section, Accelerator and Pulse Power Division, BARC (Retired on 31-07-2011) for stimulating discussions, providing facilities, cheerful help, valuable guidance through the entire period and correction of manuscript.
- To my doctoral committee, HBNI, Dr.A.P.Tiwari, Dr. S.V.G.Ravindranath and Dr. A. Bhattacharjee for their valuable guidance during writing this thesis, putting me on the right track afterwards and also for meticulous suggestions & guidance to make this work complete and correction of manuscript.
- I would specially like to thank Dr. Amitava Roy, Accelerator and Pulse Power Division, BARC, for simulating useful discussions, meticulous suggestions and corrections of the manuscript.
- To Dr.L.M.Gantayet, Director, Beam Technology Development Group, (Retired on 30-11-2014), for his support and encouragement.
- To all my seniors at Accelerator and Pulse Power Division and my colleagues at HBNI.
- Finally I express gratitude to my family for their heartful support without that I could not have done this work. In addition I express my gratitude to all persons who have not been listed here but helped to complete this work.

Somesh Vinayak Tewari

CONTENTS

ABSTRACT

Spacers are used as solid insulating support structures for HV conductors in a gas insulated system. Spacer-gas interface constitutes the electrically weakest location in the system. The high voltage pulse power system constitutes a number of composite dielectric interfaces like the solid-liquid, solid-gas and solid-vacuum interface. However surface flash over along the gas solid interface in pressurized spark gaps and in support insulators is a major problem in the operation of the high voltage pulse power systems. Further an efficient design of spacer is required in order to achieve higher spacer efficiency and also minimize the problem of surface flashover. The research focuses on development of a model to study discharge along gas-solid interface under nanosecond time regime using particle-in-cell code with a spacer efficiency of nearly 81% in an insulator bridged gap. The work involves the discharge characteristics by varying insulator geometries to optimize the insulator geometry with maximum spacer efficiency and effect of spacer surface protrusions. The maximum efficiency of 97% has been achieved for negative angled and bushbar spacers. A compact Marx generator based on pulse forming network is developed which is utilized as a pulsar for high pressure surface flashover studies. Furthermore surface potential decay experiments are carried out on Polymethyl methacrylate (PMMA) and Polyoxymethylene (POM) spacers to study the effect of potential decay on insulating material surface and the analysis is carried out based on length of the polymeric chain. Finally optical emission spectroscopic experiments are carried out on particle contaminated spacer surface to further get an insight into the breakdown process using atomic spectra lines. These results illustrate presence of H_α lines in the presence of an insulator with a reduction in plasma temperature from 0.44eV to 0.437eV and increase in electron density with increase in distance of particle contamination from cathode.

Study of surface flashover of insulator in gases at high pressure

SYNOPSIS

The growth and development in the field of pulse power technology is attributed to a number of applications in the field of medicine, industry and defense. The generation of electron, X rays and high magnetic fields using pulse power is utilized for production of high power microwaves (HPM), flash radiography (FXR) and electromagnetic welding. An important application of pulse power technology is the study on the development of discharges in gaseous, liquid and solid dielectrics exposed to strong electric fields. The increase in energy density and requirement of compact and ultra-compact systems need proper insulation which can withstand high voltage stresses. An insulator placed in between two electrodes at different potentials as a mechanical support structure or for isolating points operating at different potential can contribute to the formation of triple points. These are points of charge emission, which can lead to flashover at lower stresses. The surface flashover restricts the maximum operating field or leads to repeated disruption of normal operation. Furthermore, the presence of dielectric leads to a modification in the electric field lines and may lead to breakdown at a reduced voltage. Considerable experimental and theoretical work has been done to study the mechanism of surface flashover in gases and the information is available in dc, ac and microsecond regime [1]. An attempt has been made in this thesis to understand the surface flashover along gas solid interface under nanosecond pulse regime for improvement in the spacer efficiency leading to higher system operating voltage for different insulator configurations.

Chapter 1 of this thesis introduces the subject of insulation aspects in pulse power systems followed by the study of surface flashover in vacuum. Based on the review of available literature

on surface flashover in vacuum, it is felt that a lot of theories exist in this field explaining the mechanism of flashover in dc, ac and pulse voltage regime. The differences between surface flashover in vacuum and in high pressure environment is analyzed which initiates the need for further research in the area of surface flashover of insulator in compressed gas environment. Consequently, the following areas were identified for investigation in this thesis.

a) surface discharge study along a gas solid interface under nanosecond pulse regime
b) effect of spacer surface and geometry on discharge voltage and spacer efficiency.
c) development of a nanosecond pulse generator and its use as a pulsar for nanosecond surface flashover study in a pressurized gas environment
d) surface potential decay study in polymethymethacrylate (PMMA) and polyoxymethylene (POM) in air.
e) effect of particle contamination on flashover along insulator surface in gas environment using optical emission spectrometry (OES).

Chapter 2 of this thesis presents a review of the literature available on the breakdown mechanism in gases under pulse voltages, breakdown mechanism in solids under pulse voltages, the discharge mechanism along gas -solid interface and its applications along with the existing models of surface discharge along the gas-solid interface. Pulse power systems employ different insulation media like vacuum, gas, liquid and solid at different stages of pulse power systems. However a combination of two or more dielectric media, one of them being solid is of considerable interest in study of pulse power system.Fig.1 shows the schematic of the high voltage pulsed power system KALI 30 GW operating at APPD, BARC. It consists of a Marx generator, blumlein connected to a relativistic electron beam diode (REB) and operates with a maximum voltage and current ratings of 1MV and 30 kA respectively..

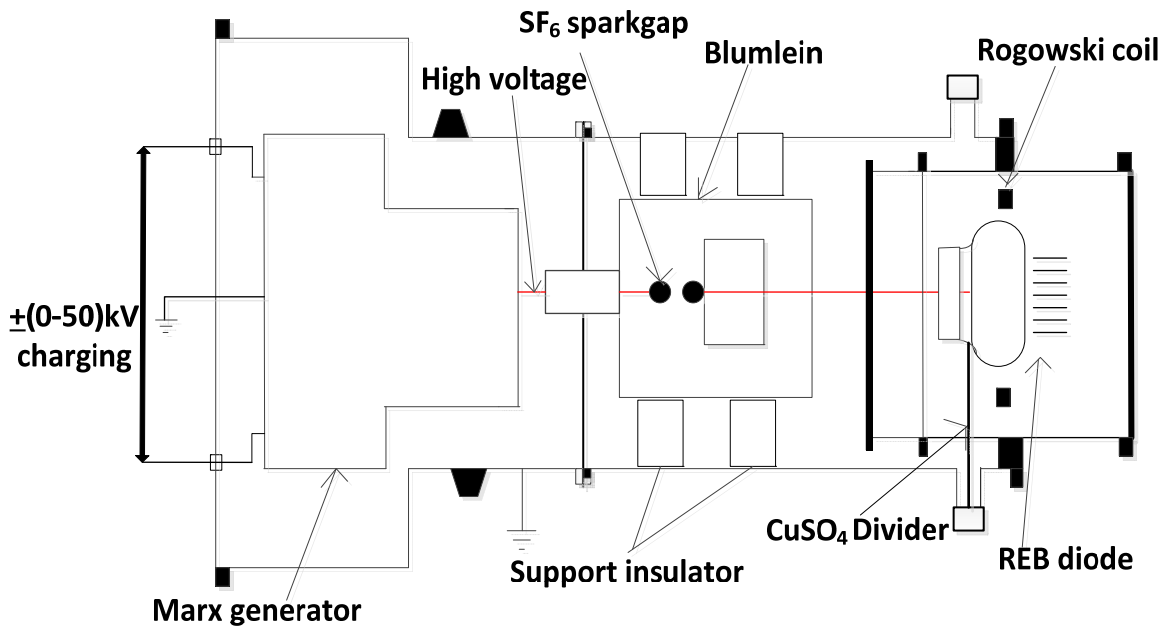

Figure 1. Schematic of KALI 30 GW Pulse Power System at APPD BARC

The 1 MV, 30kA electron beam system employs nitrogen pressurized spark gaps enclosed by Delrin chamber as spark gap assembly setup in the Marx generator. This constitutes a potential point for surface discharge as a result of the triple point (metal-dielectric-gas) interface which becomes a weak point leading to emission of electrons and breakdown at a reduced voltage. The entire Marx generator tank is filled with transformer oil to operate at higher voltages. The blumlein uses solid insulator supports between the inner and the intermediate conductor and between the intermediate and the outer conductor surrounded by transformer oil which forms a solid-liquid insulation interface. The SF_6 spark gap used for switching the blumlein output voltage to the REB diode is enclosed within a Perspex chamber which again forms a triple point [2].The REB diode chamber for flash x-ray and microwave generation uses a vacuum -solid interface [3]. These triple points become weak links or points of charge emission leading to breakdown at a reduced voltage.

A number of factors influence the breakdown voltage of spacer which includes the material of

the spacer, its geometrical configuration, its surface properties and its surrounding gas environment [4]. The breakdown strength in gases is mainly influenced by amplitude, duration of the applied voltage pulse and the gas density [5] and the breakdown phenomenon is clearly understood based on the Townsend's and Streamer mechanism[6,7]. Breakdown in a gas gap under nanosecond pulse duration is explained on the basis of runaway electron model. Runaway electrons are electrons which gain sufficient energy from the field and encounter lesser collisions as it accelerates. An electron emitted from the cathode undergoes multiple ionizations leading to formation of an electron avalanche in the gap. The ions emitted in the gap as a result of collision ionization are standstill as the drift velocity of ions is less than that of electrons. This forms a space charge field which distorts the main field. The avalanche can be considered as a localized group of electrons resulting in high velocity electrons ionizing the gas volume in its path and extending the main avalanche along a filamentary channel towards the anode. Once the avalanche touches the anode a conducting path is formed between cathode tip of avalanche and anode forming a highly conductive plasma channel which bridges the gap [8]. There are a number of breakdown mechanisms in solid like the intrinsic breakdown, streamer breakdown and electromechanical breakdown etc. with intrinsic breakdown as the mechanism which occurs in the nanosecond regime. Intrinsic breakdown is one in which electrons in the insulator gain sufficient energy to cross the band gap from valence band to conduction band and the duration is of the order of 10^{-8} sec. It follows from the establishment of conducting plasma through the gas or the liquid part of the composite insulation system along with the solid [9, 10].

Flashover of insulator in gases is mainly determined by the dielectric constant of the insulator surface relative to the gas. The nature and dielectric constant of the insulator plays a major role in determining the flashover path [11]. The insulation is effective up to the breakdown threshold.

Basically the breakdown process involves three stages: 1) primary electron generation to initiate the process, 2) exponential growth of the number of charge carriers, and 3) secondary electron generation to sustain the breakdown process. Interaction of material surface with the development of streamer is of prime importance as avalanches and streamers propagate along the surface of insulator leading to partial discharges and hence causing surface flashover of the insulator. Streamer propagation along an insulating surface takes places with an intrinsic propagation field and characteristic velocity depending on the type of the insulator material [12, 13]. The discharge along a dielectric surface under nanosecond pulse regime finds tremendous applications in the field of sterilization, medicine [14] and biomedical treatment [15]. The existing models which describe the discharge along gas-solid interface consider particle contamination as the dominant effect which leads to breakdown at a reduced voltage in compressed gas insulated system with the growth of the avalanche to 10^8 charges was considered as the criterion for discharge inception. Another model considers electron flux which is product of electron density and electron velocity to reach a critical value as the criterion of breakdown.

Chapter 3 describes the electromagnetic particle-in -cell code i.e. a finite-difference, time-domain (FD-TD) code used for simulating processes that involve interaction between space charge and electromagnetic fields and the simulation of discharge along a gas-solid interface. The code comprises of the Maxwell's equations, Lorentz equation and the continuity equation. The Maxwell time dependent equations are solved by FD-TD algorithm to obtain electromagnetic fields. The Lorentz force equation is used to obtain the relativistic particle trajectories and the continuity equation is used to obtain the current and charge densities for Maxwell's equation. The FDTD technique is utilized to develop a numerical model based on

particle-in-cell (PIC) code to study the discharge along gas-solid interface employing the explosive electron emission, neutral gas ionization and secondary emission models.

The simulation consists of spark gap electrodes (cathode and anode) with an insulator placed in between them. The outer diameter of cathode as well as the anode is 90mm and the thickness is 26mm. The insulator placed in between the cathode and anode has a radius of 18mm and a thickness of 10mm. A dielectric hollow chamber sealed from either ends is used to create a pressurized chamber. The inner diameter of the cylinder which encloses the spark gap electrode arrangement is 232mm with a thickness of 10mm. The length of the entire simulation domain is 282mm .The background gas used for simulation is nitrogen at 1atm pressure. The electrons emitted from the surface of cathode ionize the gas molecules in travelling towards the anode leading to the production of the positive ions and secondary electrons. The electrons emitted in the presence of dielectric on striking the surface leads to emission of secondary electrons from voids present on the surface of the dielectric. The positive ions move towards the cathode under the applied electric field on striking the cathode lead to the production of secondary electrons. The avalanche co-efficient (α) which describes the ionization growth is taken from the Longmire-Longley model. The interaction of electrons with the neutral gas molecules is taken as a function of electron energy [16].

The emitted electrons from cathode in the presence of spacer are directed towards the surface of spacer leading to a decrease in momentum when compared to the plain gas gap conditions. The electrons basically hop and move along the surface of the insulator towards the anode. An increase in charge density along insulator surface implies secondary electron emission (SEE) along the surface as compared to plain gas gap condition with a peak charge density of nearly 6.5μC/m^3 obtained along the insulator surface. The peak value of electron number densities is

3.38 x10^{12} m^{-3} in the presence of dielectric as compared to 6.14 x10^{11} m^{-3} in a plain gas gap condition in a velocity range from 0-20 x10^{7} m/s which highlights secondary electron emission along the insulator surface as a dominant factor for insulator flashover. A suppression is observed in the ionization growth and drift velocity in an insulator bridged gap. A reduction is observed in the output voltage in an insulator bridged gap which is attributed to the modification of space charge distribution along insulator surface. The spacer efficiency which is defined as a ratio of flashover voltage in an insulator bridged gap to the voltage plain gas gap condition [17] is 81% for the present model.

Chapter 4 of this thesis presents the effect of different insulator geometries and profiles on the spacer efficiency of insulator in compressed gases. The different insulator geometries used between the cathode and anode (AK) gap are positive angled geometry, negative angled geometry, doubled sided frustum geometry and bush bar shaped geometry. Nitrogen is used as the background gas at 1 atmospheric pressure with an AK gap of 20 mm. The electrons emitted from the surface of cathode encounter obstruction in path of electron movement leading to less net charge in the gap for negative and bush bar geometry. The positive angled spacer geometry provides no hindrance in the path of the motion of electrons leading to high net charge in the gap. The double sided frustum geometry behaves like a positive angled spacer till mid gap leading to net increase in charge and as mid gap is reached the space charge so formed aids in further ionization leading to highest net charge unlike all the remaining geometries.

The avalanche growth in the gap follows the spacer profile. The bush bar spacer has hollow profile in the mid gap that leads to increased ionization in the mid gap region and a dip in ionization near the cathode and anode regions because of the reduced volume of the gas gap. For a plain gap condition there is a continuous rise in the avalanche growth and suppression in

growth in case of cylindrical insulator. The electric field in the gap follows avalanche growth profile which governs the mechanism of the discharge process for different spacer profiles. The double sided frustum spacer has highest field at cathode among all the spacer profiles. The field near the centre is maximum (174 kV/cm) with reduced values at both the electrode ends. The bush bar spacer and negative angled spacer with highest spacer efficiencies (97%) have reduced field enhancement at cathode which grows towards the anode leading to highest discharge voltage in both the spacer profiles. The negative angled and bush bar geometry gives a maximum voltage of nearly 400kV as the geometry provides a longer tracking path in turn reducing SEE along insulator surface. The positive angled spacer geometry aids in faster ionization and secondary electron emission from the insulator surface giving a reduced voltage of 323kV.The double sided frustum geometry gives a lowest discharge voltage of nearly 300kV.The analysis of the charge as a function of voltage profile shows a decrease in charge in gap after a certain voltage for bush bar and negative angled spacer geometry whereas a continuous increase in charge with voltage is observed for positive angled and double sided frustum geometry.

The introduction of protrusions (teeth) along insulator surface shows an increase in voltage to 383kV from 354kV for a 1 mm teeth height at regular intervals of 1 mm along the surface of the insulator that further increases and settles at 400kV for a teeth height of 2 and 3mm. The presence of teeth along the surface of the insulator leads to an increase in effective flashover length. The electric field profile shows a field enhancement for a teeth height of 1mm at cathode as compared to teeth of 2 and 3mm with an increased field value in the middle of the gap from 5mm to 19mm for a teeth height increase from 1mm to 2 and 3mm and field stabilization for protrusions of 2 and 3mm as a result of trapping of the charge carriers.

Chapter 5 of the thesis describes the design and development of a compact Marx generator

based on pulse forming network which is utilized as a pulsar for surface flashover studies. It consists 20 stages staked one upon the other in vertical towering shape. Each stage consists of six capacitors each of 1200 pF and 30 kV connected in parallel in a PFN configuration across the charging and grounding resistors. The maximum output voltage of the Marx generator is 300kV on a matched load with a pulse width of 150ns. The output of the last stage of the Marx generator is connected to peaking gap electrode enclosed within a peaking capacitor. The introduction of peaking capacitor at the output of the Marx generator reduces the rise time of the output pulse from 25ns to 5ns. The entire assembly is placed inside a stainless steel chamber of 0.6 m inner diameter and length of 1.5 m pressurized with nitrogen and the output of the other peaking gap electrode is connected to the load along with aqueous copper sulphate voltage divider and current shunt used for voltage and current measurements respectively. Both the experimental and simulation studies have been carried out on the system and are found consistent.

The output of the Marx generator is fed to a high pressure spark gap switch designed for surface flashover studies. The high pressure spark gap chamber (test cell) is a Perspex chamber of 125mm outer radius, 105mm inner radius and a length of 237mm.The spark gap chamber is designed so as to withstand pressures up to 5kg/cm^2. Two Rogowski profile electrodes each of 90mm diameter and 26mm thickness serves as the spark gap electrodes with a spacer of 10mm thickness placed between the electrodes. A view port of 100mm inner diameter and 150mm outer diameter is made on the surface of the switch which serves as a service port. The surface flashover studies are carried out using PMMA and POM in a compressed nitrogen environment. The operating pressure range is 1kg/cm^2 to 4kg/cm^2. An increase in the flashover voltage with pressure is observed in both PMMA and POM. A reduction in flashover voltage is observed in POM (ε_r =3.7) as compared to PMMA (ε_r =2.6) because a higher permittivity mismatch between

the spacer and surrounding gas medium leads to a higher field enhancement resulting in reduction in the breakdown voltage. A spacer efficiency of 91% is observed with PMMA at a pressure of 1kg/cm^2. The reduction in spacer efficiency with PMMA is 11%as compared to 18% for POM.

Chapter 6 of this thesis presents the surface potential decay study of PMMA and POM. The surface potential decay experiments are carried out on both the samples subjected to positive and negative dc voltages of 8 kV for time duration of 5 minutes. The Trek 341B Electrostatic Voltmeter (ESVM) is used for surface potential decay measurements. An increase in peak surface potential and time to decay in PMMA as compared to POM both for positive and negative dc voltages is attributed to the length of the polymeric chain which is responsible for chain retentivity in the material. The maximum density of electron and hole traps in the surface layer of PMMA is ~1.5 x 10^{17} $eV^{-1}m^3$ and 0.8 x 10^{17} $eV^{-1}m^3$ respectively, and the energy level of its electron and hole traps are in the range 0.60 - 0.90 eV and 0.78 - 0.9 eV respectively. The introduction of roughness on POM surface leads to an increase in energy level from 0.55-0.87 eV to 0.55-0.89 eV. The presence of roughness on POM surface leads to an increase in density of electron trap centres from 2.33 x$10^{16}eV^{-1}m^3$ to 2.77 x$10^{16}eV^{-1}m^3$ and the density of hole trap centers increases from 2.85 x$10^{16}eV^{-1}m^3$ to 3.18 x$10^{16}eV^{-1}m^3$.

Finally the optical emission spectroscopic (OES) studies are carried out to analyze the effect of location of particle contamination on flashover along the insulator surface. Three different conditions of particle contamination involve a needle protrusion of 3mm length and 1mm diameter at cathode, at centre and at anode along insulator surface. The experiments are carried out in ambient air and nitrogen medium at a pressure of 1kg/cm^2. The plasma temperature during bulk breakdown in air is 0.433eV which increases to 0.434eV with the pressurized nitrogen,

which further increases in the presence of insulator to 0.441eV and 0.44eV in nitrogen and air respectively. The electron density obtained from the N emission line at 746.8 nm has an estimated peak value of 2.85×10^{12} cm^{-3} in the presence of insulator.

Chapter 7 presents summary and conclusions. The following is the summary of the work reported in the thesis.

1. The PIC simulation of discharge along gas-solid interface under nanosecond pulse is modeled and analyzed. A reduction in the breakdown voltage and an increase in net charge in the gap are observed in the presence of an insulator.
2. The effect of different insulator geometries on the spacer efficiency of insulator in gas is analyzed with maximum spacer efficiency of 97% for negative angled and bush bar geometry.
3. A compact Marx generator based on pulse forming network is developed with a peaking capacitor at its output which helps in rise time reduction from 25ns to 5ns.The generator is utilized as a pulsar for surface flashover studies.
4. An increase in the flashover voltage with pressure is observed in both PMMA and POM with a reduction in spacer efficiency with pressure. A spacer efficiency of 91% is observed with PMMA at a pressure of $1kg/cm^2$. The reduction in spacer efficiency with PMMA is 11%as compared to 18% for POM.
5. The surface potential decay studies on PMMA and POM shows an increase in peak potential and time to decay for PMMA as compared to POM is attributed to the length of the polymeric chain which is responsible for chain retentivity in the material.
6. The OES studies on the effect of particle contamination on flashover along insulator surface showed a decrease in plasma temperature and an increase in electron density with

increase in distance of particle contamination from cathode.

Finally some suggested future work is outlined

a) The application of different pulse durations to study the effect on the flashover phenomena
b) The use of different gases like argon and helium and different insulator materials to further study the variations in the discharge phenomena.
c) The use of streak camera to study the spatial and temporal variation of streamer growth along different insulator materials.

Present work has contributed to a better understanding of insulation aspects of high voltage pulse power systems. The study carried out in this thesis is useful in the development of reliable and efficient insulation structure in pulse power systems.

REFERENCES

[1.] T. S. Sudarshan and R. A. Dougal, "Mechanisms of surface flashover along solid dielectrics in compressed gases: a review", IEEE Transactions on Electrical Insulation, **EI-21/5,**727-746, 1986

[2.] Amitava Roy, Rakhee Menon, Sabyasachi Mitra, D. Durga Praveen Kumar, Senthil Kumar, Archana Sharma, K. C. Mittal, K. V. Nagesh, and D. P. Chakravarthy, "Intense relativistic electron beam generation and prepulse effect in high power cylindrical diode", J. Appl. Phys., 103/1, 014905, 2007.

[3.] Amitava Roy, Sabyasachi Mitra, Rakhee Menon, D. Durga Praveen Kumar, Senthil Kumar, Archana Sharma, K. C. Mittal, K. V. Nagesh, and D. P. Chakravarthy, "Prepulse Suppression on a High-Power Electron Beam Accelerator Using a Dielectric Cathode Holder", IEEE Trans. Plasma Sci., **PS 37/1**, 67–75,2011

[4] J. R. Laghari and A. H. Qureshi, "Surface flashover of spacers in compressed gas insulated systems" IEEE Transactions on Electrical Insulation, **EI-16/5**, 373-387, 1981

[5] Chathan M.Cooke and Alan .H.Cooke, "The nature and practice of gases as electrical insulators" IEEE Transactions on Electrical Insulation, **EI-13/4,** 239-248, 1978

[6] G.R.Nagabhushana,"Breakdown mechanism and insulation design with vacuum,gas,liquid and solid", Proc.”Technology and electrical insulation and high voltage pulse techniques”, BARC,Mumbai, 43-65, March 1-5,1982

[7] .M.S.Naidu "High Voltage Engineering" Tata McGraw Hill Education, 2004.

[8] E. E. Kunhardt and W. W. Byszewski, "Development of overvoltage breakdown at high gas pressure", Physical Review **A 21/ 6**, 2069-2077,1980.

[9] J.H.Mason, “Breakdown of solid dielectrics in divergent fields" Proc. IEE part-1, **98/109**, 44-59, 1951.

[10] J.H.Mason, "The deterioration and breakdown of dielectrics resulting from internal discharges ", Proc. IEE, part-C Vol. 102/2, 254-263, 1955

[11] George.L.Jackson, “Pulsed flashover of solid dielectrics in vacuum and gases” Ph.D thesis, Texas Tech University, 1983

[12] N.L.Allen and P.N.Mikropoulos, “Streamer propagation along insulating surface”, IEEE Transactions on Electrical Insulation**, 6/3**, 357-362,1999

[13] C. Heitz, M. Piemontesi and G. Salge, "Surface discharge along solid dielectrics in atmospheric air", IEEE International Symposium on Electrical Insulation, pp.341-344, 2000

[14] Halim Ayan, Gregory Fridman, Alexander F. Gutsol, Victor N. Vasilets, Alexander Fridman, and Gary Friedman, "Nanosecond-pulsed uniform dielectric-barrier discharge" IEEE Trans. Plasma Sci., **PS 36/2**, 504-508, 2008

[15] H. Ayan, D. Staack, G. Fridman, A. Gutsol, Y. Mukhin, A. Starikovskii, A. Fridman and G. Friedman, "Application of nanosecond-pulsed dielectric barrier discharge for biomedical treatment of topographically non-uniform surfaces", J. Phys. D: Appl. Phys.,**42**, 125202 , 2009.

[16] Yukikazu Itikawa, "Cross Sections for Electron Collisions with Nitrogen Molecules", J. Phys. Chem. Ref. Data, **35/1,** 2006

[17] J.R.Laghari, "Spacer flashover in compressed gases", IEEE Trans. Dielect. Elect Insul., **EI-20/1**, p.83-92, 1985.

LIST OF PUBLICATIONS

Journals

1. "Particle-in -cell simulations of discharge along gas-solid interface "Somesh Vinayak Tewari**,** Amitava Roy, Archana Sharma, K.C.Mittal, D.P. Chakravarthy, Ayush Saxena, Navdeep.M.Singh, *IEEE Transactions on Plasma Science* ,**2013** ,*Vol. 41,No.3,* 578-584.
2. "Development and Analysis of PFN based Compact Marx generator by using FIT technique for an Antenna Load" Somesh Vinayak Tewari, R.Agarwal, P.C.Saroj, Archana Sharma, K.C.Mittal, S. Umbarkar, H.A.Mangalvedkar, *IEEE Transactions on Plasma Science*,**2013**,*Vol. 41,No.10,* 2684-2690.
3. "Optical emission spectroscopy study on flashover along insulator surface due to particle contamination" Somesh Vinayak Tewari, R.J.Kshirsagar, Amitava Roy, R. Sarathi, Archana Sharma , K.C.Mittal " *Laser and Particle Beams*,**2014,** *Vol. 32,No.4,* 681-689.
4. "Effect of spacer surface and geometry on surface discharge in gas using PIC simulation", Somesh Vinayak Tewari, Amitava Roy, Archana Sharma, K.C.Mittal*, IEEE Transactions on Plasma Science,***2015,***Vol.43,No.2,587-593* **.**
5. "Surface potential decay of PMMA and POM in air" Somesh Vinayak Tewari, Romesh Chandra ,S.K.Sharma, R.Sarathi, Archana Sharma, K.C.Mittal, *IOP Material Research Express* ,**2015**,*Vol.2,No.4,045301.*

Other Publications

1. "First results of KALI-30 GW with 1 MV flash X-rays generation and characterization by Imaging plate" A. Sharma, A.M. Shaikh, K. Senthil, S. Mitra, R. Chandra, S. Vishnu, S. Sandeep, A. Roy, M. Rakhee, V. Sharma, M.B. Danish, T.S. Kolge, K. Ranjeet, R. Agrawal,

P.C. Saroj, Somesh Vinayak Tewari and K.C. Mittal, *Journal of Instrumentation*, **2014**,*9*, P07011.

2. "Energy Balance Aspect in KALI-30GW High Voltage Pulse Power Source", Archana Sharma, S.Mitra, Senthil.K , Vishnu Sharma, Sandeep Singh, Somesh Vinayak Tewari, K.C.Mittal, *Laser and Particle Beams* ,**2014**,*Vol.32,No.4,*531-535.
3. "Explosive Emission Properties of Cathode Materials in Relativistic Electron Beam Generation" Romesh Chandra, Amitava Roy, Senthil Kalyanasundaram, Ankur S. Patel, Vishnu Kumar Sharma, Rakhee Menon, Naresh Pasula, Ranjeet Kumar, Iger Ventizenko, Alexander Mashchenko, Tanmay Kolge, Somesh Vinayak Tewari, Ritu Agarwal, Archana Sharma, and K C Mittal, *IEEE Transactions on Plasma Science*, **2014,***Vol.42,No.11,*3491-3497.
4. "Simulation of breakdown mechanism in high power spark gaps filled with nitrogen gas at atmospheric pressure " Ayush Saxena, Somesh Vinayak Tewari, N.M.Singh, Archana Sharma, K.C.Mittal, *Radiation Effects and Defects in Solids,* **2015**,*Vol.170,No.2,111-120*
5. " Development of triggering arrangement of KALI- 30GW Marx generator" S.Mitra, T.S.Kolge, Ritu Agarwal, P.C.Saroj, Ankur Patel, K Senthil, Somesh Vinayak Tewari, Archana Sharma, K.C.Mittal, *Journal of Korean Physical Society* **2015,***Vol.66,No.4,553-557.*

Conferences

1. "Flash X-Ray Generation Using Folded Pulse Forming Line Based Marx Generator" Somesh Vinayak Tewari, R.Agarwal, Archana Sharma, K.V.Nagesh, D.P.Chakravarthy; *2nd International Symposium on Material Chemistry (ISMC)*, **2010**,*363*

2. “Development of a 300kV Compact Co-axial Marx Generator Based on PFN” Somesh Vinayak Tewari, C.S.Reddy, R.Agarwal, P.C.Saroj, Archana Sharma, K.C.Mittal, D.P. Chakravarthy ,**2012,***IEEE 4th Euro-Asian Pulsed Power Conference (EAPPC/BEAMS)*
3. “Computational Model of Discharge across a Gas/Solid Interface at High Pressure” Somesh Vinayak Tewari, Amitava Roy, Archana Sharma, K.C.Mittal, D.P.Chakravarthy, Ayush Saxena, Navdeep.M.Singh, *IEEE/Springer International Conference on Emerging Trends in Engineering and Technology* ,**2012,***532-535.*
4. “Effect on electron drift velocity and ionization coefficient along a gas-solid interface " Somesh Vinayak Tewari, C.S.Reddy, Archana Sharma, K.C.Mittal *IEEE international conference on power, energy and control,***2013***, 174-176*
5. “Particle-in-cell simulations of discharge along angled insulators in compressed gases” Somesh Vinayak Tewari, Amitava Roy, C.S.Reddy, Archana Sharma, K.C.Mittal, *International Conference on Pulsed Power and Plasma Science*, **2013***,1-3*
6. “Pulsed Flashover Of Solid Dielectric Materials in Compressed Gas Environment” Somesh Vinayak Tewari, Archana Sharma, K.C.Mittal *AIP Conference Proceeding*, **2015,** *1665, 060022-1–060022-3*.
7. "Dynamic imaging of spark gap breakdown using high intensity flash x-rays" Tanmay S. Kolge, Somesh Vinayak Tewari, H.Choudhury ,Archana Sharma, K.C. Mittal *International Conference On High Voltage Engineering and Technology (ICHVET)***2015**

Somesh Vinayak Tewari

LIST OF FIGURES

LIST OF TABLES

LIST OF SYMBOLS

c	Velocity of light	3×10^{8} ms^{-1}
e	Charge on electron	1.6×10^{-19} C
ε_0	Permittivity of free space	8.85×10^{-12} C V^{-1} m^{-1}
ε_r	Relative permeability of the medium	
μ	Permeability of free space	$4\pi \times 10^{-7}$ H m^{-1}
$1eV$	Energy in electron volts	1.6×10^{-19} Joule
E_t	Tangential component of electric field intensity	
E_n	Normal component of electric field intensity	
R	Resistance (ohms)	
L	Inductance (Henry)	
C	Capacitance (Farad)	
π	3.14285	
J	Current density	

LIST OF ABBREVIATIONS

KALI	Kilo Ampere Linear Injector
LIA	Linear Induction Accelerator
ORNL	Oak Ridge National Laboratory
REB	Relativistic electron beam
GIS	Gas insulated system
PIC	Particle -in-cell
FDTD	Finite Difference Time Domain
UWB	Ultra Wide Band
PFN	Pulse forming network
SS	Stainless steel
UV	Ultraviolet
AK	Anode-cathode
ESVM	Electrostatic voltmeter
POM	Polyoxymethylene
PMMA	Polymethyl Methacrylate
OES	Optical Emission Spectroscopy
FNS	First Negative System
FPS	First Positive System
SPS	Second Positive System

CHAPTER 1

INTRODUCTION

1.1 Introduction

The growth of research and development activities in the field of high voltage pulse power technology is attributed to a number of potential applications in field of medicine, industry and defense. The commercial aspect of this technology got importance with the generation of electron and gamma beams used for sterilization of food, curing of plastics and material processing. The intense pulse power systems developed in 1960s were made to simulate the radiation output of nuclear weapons, produce flash X-rays and for plasma physics studies. These pulsed systems along with the relativistic electron beam diode forms the pulsed electron beam accelerators. The typical parameters of interest in these pulsed electron / ion beams are high voltages (100kV-1MV), high currents (1kA-1MA), high energies (100J-5MJ) and short duration (10-100ns) pulses. The recent and significant applications of accelerators include the irradiation of food, water, medical sterilization, surface treatment, high power microwave generation for shielding of electronic components and devices. Further applications areas of pulsed power systems may include magnetic confinement fusion, impact fusion, high energy physics research, synchrotron radiation production, projectile launching, metal parts forming, large area metal welding, radio graphical diagnostics, gas clean up etc. The pulse power systems are classified as single shot systems and those meant for repetitive applications. The repetitive pulse power systems application as pumping source for gas lasers, as a driving source for plasma chemical reactors, microwave radiation curing of coatings, polymerizations and sludge disinfections etc. The nanosecond pulse power technology has played an important role in developing spark and streamer chamber which are the most used instruments in nuclear physics.

For reliable operation of high voltage, high power pulse system for a particular application, proper design and selection of insulation material is very important. The desired pulse characteristic output from short duration pulse power compact system requires inductance minimization in the available volume and is a crucial aspect due to the space required for proper and robust insulation in order to avoid undesired surface flashover in the system. Therefore, optimization of insulation and inductance is necessary for best design.

1.2 Insulation feature in pulse power systems

An important application of pulse power technology is the study on the development of discharges in gaseous, liquid and solid dielectrics exposed to strong electric fields. The increase in energy density and requirement of compact and ultra-compact systems need proper insulation which can withstand high voltage strength. The Figure 1.1 below shows block diagram of a pulsed power system. High-voltage pulsed system consists of a direct current power supply, Marx generator or pulse forming line to generate pulses of MW or GW power level and high speed switch transferring the energy to the load.

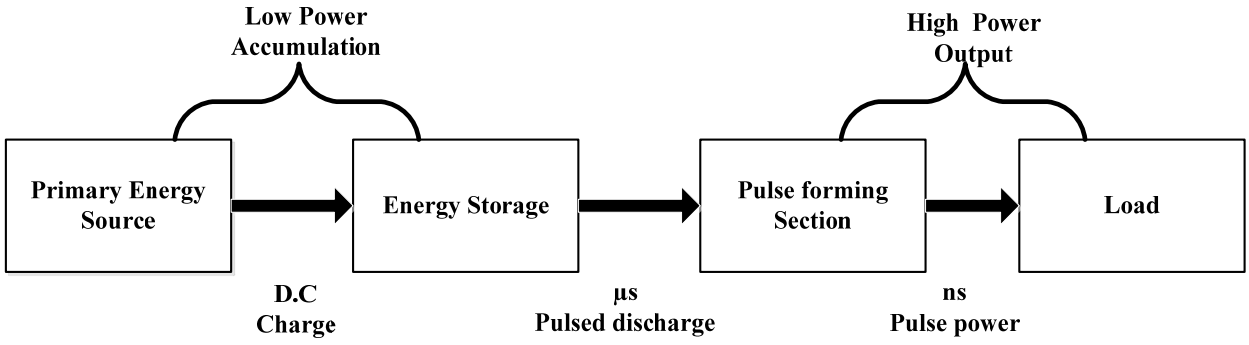

Figure 1.1 Block diagram of a typical high power pulse system [1]

Moreover different components in a pulse power system operate at different voltage levels

thereby needing proper support and separation using suitable insulators. An important property of the insulating material is its dielectric constant. A high energy density application requires a material of high dielectric constant as the energy density is directly proportional to the dielectric constant. However a medium of small dielectric constant is required if high transfer rate of energy is desired as the electromagnetic wave speed is inversely proportional to the square root of dielectric constant. The mechanical and thermal properties of the insulator also influence the breakdown strength of an insulator. Mechanical failure, deformation, ablation, crazing, current tracking and softening are some of the phenomenon which influences the breakdown strength of an insulator. These factors are very important when considering the repetitive operation of a high power switch. In most high power pulse applications liquid and gaseous insulators are mostly employed because volume breakdown takes place in a solid insulator resulting in irreparable damage to the insulating material whereas a breakdown in gas or liquid insulator can be easily cured. A combination of insulating media such as solid-vacuum, solid- gas, solid -liquid – vacuum interface are used and such an interface of two or more insulators or a metal and an insulator creates a triple point which serves as weakest link capable of charge emission which can lead to surface flashover. The phenomena of surface flashover limits maximum operating voltage and hence is matter of technological importance as mixed insulating media is widely used in a number of high energy particle accelerators. Surface flashover phenomena are known to be dependent upon a number of processes like surface property, surface roughness, system cleanliness, system configuration etc. The insulation capability reduces as the time of application of high voltage pulse increases. Many theories exist to explain the surface flashover in vacuum and are explained in brief below. The surface flashover of solid dielectric in a high pressure gaseous environment in sub-microsecond time duration is not clearly understood. The

mechanism of discharge along the insulator in compressed gases along with its effect on spacer geometry and profile are studied .The optical emission spectroscopy study of surface discharge in compressed gases along with surface charge decay of different insulating material have been studied and reported here.

1.3 Surface flashover in vacuum

The mechanism of surface flashover of insulator in vacuum is explained in detail in literature. [2-7].Each of the above theories in literature divides the process of flashover in three stages.

1. Initiation (by high field electron emission) at the cathode triple junction
2. Development (charge propagation, surface charging, secondary electron emission phenomena)
3. Electrical discharge (surface flashover)

The theories give a general agreement on the initiation of flashover that it usually begins as result of field emission of electrons from the triple junction (vacuum-electrode-dielectric interface) as shown in Figure 1.2. However there is a wide disagreement on the development of discharge in vacuum. Field emitted electron from triple junction strike the insulator surface producing secondary electrons which in turn strike the insulator surface producing tertiary electrons. Continuation of this process results in a cascade along the surface which leads to the development of secondary electron emission avalanche (SEEA). Anderson and Brainard [2] developed a flashover model based on SEEA. They considered a layer of gas adsorbed on the surface of a ceramic insulator in vacuum. The SEEA electrons strike the surface of the insulator desorbing some of the adsorbed gas molecules forming a gas cloud which is ionized by electrons in SEEA.

The positive ions so produced enhance the electric field at the triple junction resulting in increase in electron current along the insulator .This process ultimately leads to flashover. Avidenko and

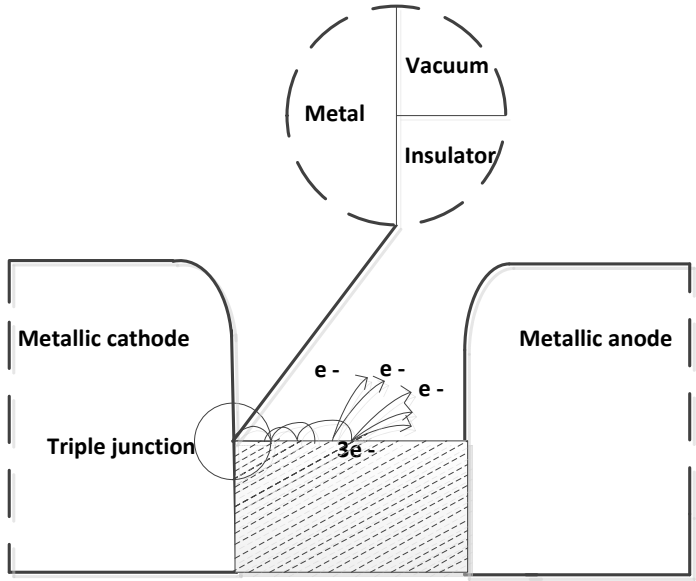

Figure 1.2 Schematic illustration of the hopping mode by which electrons travel from cathode to anode. [1]

Malev [5] said that in uniform fields the electrons emitted from the triple junction are enough to desorb gas and SEEA are not involved in surface flashover. Vigouroux [8] et.al. explained the intermediate phase of surface flashover which takes place as a result of propagation of electrons in the conduction band of the insulator as soon as their energy exceeds the band gap of the insulator .This process is termed as the electron cascade model. The insulators become positively charged due to electron removal and negative charging of the insulator is also possible if plasma is present leading to faster breakdown [9, 10]. All the authors also agree on the final stage of surface flashover that consists of discharge in gas adsorbed on the surface of the insulator. A lot has been reported on the surface flashover of insulator in vacuum under dc, ac and sub-microsecond conditions. The major differences between surface flashover in vacuum and in high pressure environment are briefly enumerated in Table 1.1 which justifies the need for further research in the area of surface flashover of insulator in compressed gas environment.

Table 1.1Comparison between surface flashover along vacuum/solid interface and gas/solid interface [11, 12]

Vacuum/solid interface	Gas/solid interface
The mean free path of the electrons is very high.	The mean free path of electrons is reduced due to a number of collisions with gas molecules.
There is no maximum limit to charge accumulation on the surface of insulator	The charge accumulated on the surface of the insulator is limited by the gas surrounding the insulator medium.
Repetitive pulses are observed in pre-discharge currents due to surface flashover in vacuum.	No repetition in current pulses observed with high pressure nitrogen environment.
There is a significant reduction in the break - down voltage in presence of insulator in vacuum	There is no reduction in the breakdown voltage at pressures below 0.5MPa and a slight reduction at pressures up to 1 MPa.
The optimum value of insulator angle for highest breakdown voltage is 45°.	The optimum value of insulator angle for highest ac breakdown voltage is 0°.

1.4 Aim of present study

The flash X-ray and high power microwave applications require high voltage pulse power systems for which a 3MV, 50kA, 100ns pulse power system is being developed at APPD, BARC. This system consists of a Marx generator rated at 3.5MV, 45kJ, 1μs which charges an intermediate storage three electrode, demineralized water Blumlein rated at 3.0MV, 6Ω, 300ns, 30kJ. The energy stored in the water blumlein is switched by a SF_6 sparkgap to another castor oil / transformer oil pulse forming line Blumlein rated at 3MV, 50kA, 100ns, 20kJ. The energy

stored is switched by another SF_6 sparkgap in to a castor oil impedance matching transmission line which will feed to relativistic electron beam (REB) diode rated at 3MV, 20 Ω, 100 ns for REB generation and flash X-ray applications. Figure 1.3 shows a basic schematic of the high voltage pulsed power system.

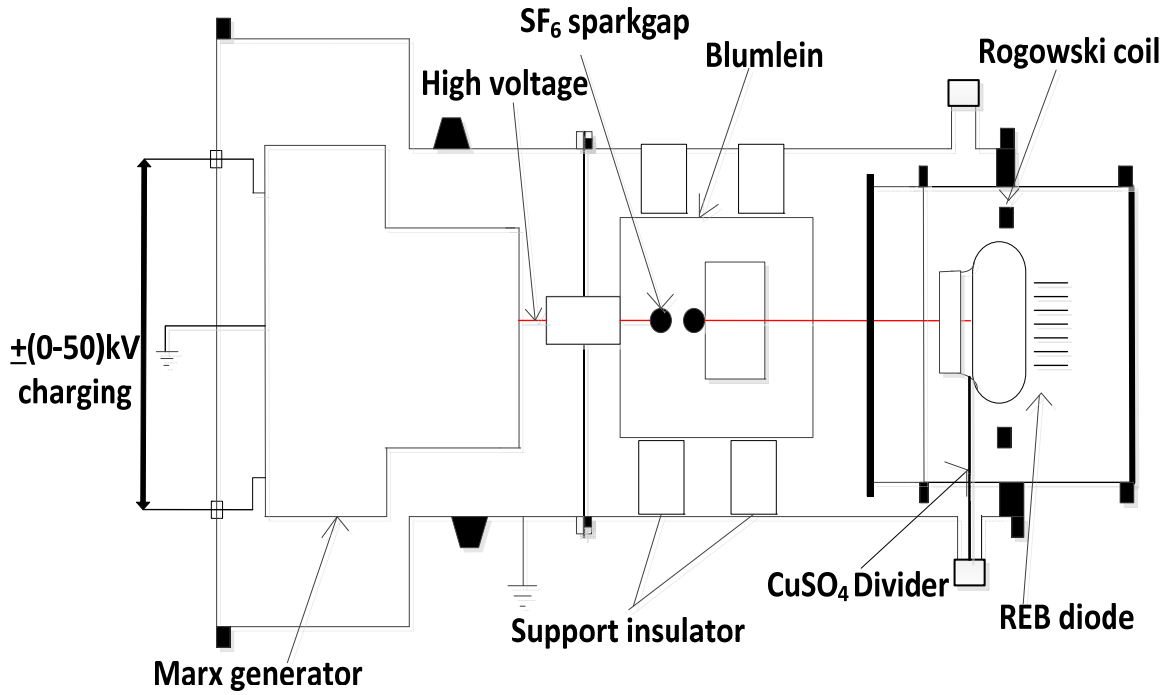

Figure 1.3 Pulse power systems with insulating support under study.

The major challenges in the development of this type of systems are (i) reliable breakdown of spark gaps in Marx generator/ Blumlein and (ii) surface flashover in Blumlein support insulator. The Marx generator uses normally pressurized nitrogen sparkgap and Blumlein uses pressurized SF_6 sparkgap. The high voltage pulsed power system has various levels of insulation from dc to sub-microsecond regime as integral parts. The reliability and consistent performance of the system depends mainly on the robustness of the insulating structure both electrically and mechanically. Present study will focus on the aspects of surface flashover in high pressure gas environment for nanosecond pulse durations.

1.5 Outline of the thesis

The thesis highlights the study on the development of discharge along the surface of an insulator in gas environment in nanosecond time regime. The study further involves the use of different insulator geometries and profiles to study the discharge characteristics in gases and its impact on spacer efficiency along with the development of a high pressure spark gap switch which is used as a test setup for surface flashover studies.

The thesis has been organized as follows:

Chapter 1 is the introduction to the insulation aspects in high voltage pulse power systems, application of pulse power system in industrial, defense and research areas, the phenomena of surface flashover in vacuum which is extensively reported in literature and the need to study the phenomena of surface flashover in compressed gas environment which forms the basis of this thesis.

Chapter 2 provides a review of the literature on surface breakdown of insulator in gases and summarizes the different factors influencing the insulator flashover .The mechanism of breakdown in gases and solid is discussed along with the different physical processes responsible for the discharge along the gas solid interface. A few of the existing models explaining physics of the breakdown process in dc, ac and microsecond regime is also discussed.

Chapter 3 gives a brief introduction to the finite difference time domain (FDTD) based particle-in-cell code and its associated algorithm. The FDTD technique is utilized to develop a numerical model based on particle-in-cell (PIC) code to study the discharge along gas-solid interface employing the explosive electron emission, neutral gas ionization and secondary emission models. The profile of the phase space movement of the electrons with and without a dielectric is studied. The ionization coefficient and drift velocity obtained from the simulation model are in

agreement with the work reported in the literature.

Chapter 4 studies the effect of different insulator geometries and profiles used in pulse power systems on the spacer efficiency of insulator in compressed gases. An analysis based on avalanche growth and temporal variation of charge in the gap is carried out to study the discharge behavior for different spacer profiles. Furthermore the effect of protrusions on the surface of insulator on discharge voltage is also studied.

Chapter 5 describes the development of a compact Marx generator based on PFN, its assembly, the design of peaking capacitor and the effect of peaking capacitor on rise time of the pulse is studied. The system has been developed and characterized. Both the experimental and simulation studies have been carried out on the system and the results have been verified. The diagnostic equipments used in the testing of the Marx generator have also been discussed. The system output is connected to a high pressure spark gap switch which is used as a test setup for surface flashover study of insulator material in compressed gas environment.

Chapter 6 deals with optical emission spectra study of discharge along an insulator surface with non–uniformity introduced on the surface of the insulator at cathode, at anode and at the centre along the surface of the insulator. The analysis has been carried out in air and in compressed nitrogen gas environment to further investigate the process of breakdown and analyze the variations in the intensity of the constituent atoms in an insulator bridged gas gap. Furthermore surface potential decay measurements are carried out on the surface of polyoxymethylene (Delrin) and polymethymethcrylate (Perspex) which are the commonly used insulators in pulse power systems. The electron and hole trapping parameters are calculated for PMMA and POM with an increase in surface potential decay of PMMA as compared to POM which is discussed on basis of length of the polymeric chain. The effect of surface roughness introduced on insulator

surface is also discussed.

Chapter 7 presents the summary and future scope of work in this area.

CHAPTER 2

LITERATURE SURVEY

2.1 Introduction

The high power pulse technology is a result of growing demand for high power source and an effective means of transferring this energy to the target. The use of switches is inevitable in high power pulse applications and differs from the conventional high voltage switchgears as these involve handling large values of peak power. The high voltage pulse techniques have undergone numerous changes from the time of Van-de-Graf generator to present age of Linear Induction Accelerators and Kilo Ampere Linear Injector. The increased application in the field of pulse power systems has put many constraints on the size, material selection and design considerations. The most important constraint in the operation of high voltage pulse power system is the insulation design as the insulation interface is the part that isolates components operating at different potentials.

At ORNL, performance problems were associated in the conventional acceleration tubes of the 25URC tandem accelerator limiting the voltage performance of the system [13]. The development and installation of a compressed insulator geometry tubes, with improved conditioning techniques has increased the voltage performance of the system. The NEC tubes in a compressed geometry increased the relative insulating strength of the tubes and the insulation ratio by 85% without any changes in the structure which improved the voltage performance of the system [14].

Pulse power systems employ different insulation mediums like vacuum, gas, liquid and solid at different stages of pulse power systems. However a combination of two or more dielectric media, one of them being solid is of considerable interest in study of pulse power

system. The 1 MV, 30kA electron beam accelerator employs nitrogen pressurized spark gaps enclosed by Delrin chamber as spark gap assembly setup in the Marx generator. This constitutes a potential point for surface discharge as a result of the triple point (metal-dielectric-gas) interface which serves a weak point leading to an earlier mission of electrons and breakdown at a reduced voltage. The entire Marx generator tank is filled with transformer oil to operate at higher voltages. The blumlein uses solid insulator supports between the inner and the intermediate conductor and between the intermediate and the outer conductor surrounded by transformer oil which forms a solid-liquid insulation interface. The SF_6 spark gap used for switching the blumlein output voltage to the REB diode is enclosed within a Perspex chamber which again forms a triple point [15].The REB diode chamber for flash x-ray and microwave generation uses a vacuum -solid interface [16].

Theses triple points create a weak link or points of charge emission, which can lead to flashover at lower voltage. Thus, surface flashover restricts the maximum operating field. Furthermore, the presence of dielectric leads to a modification in the electric field lines and hence leads to breakdown at a reduced voltage. Figure 2.1 shows the schematic of a composite dielectric system .In a composite dielectric system two conditions hold true namely a) continuity of tangential field strength and b) continuity of the normal component of electric flux density given by [17].

$$E_S = E_G \tag{2.1}$$

where subscripts S and G indicate solid and gaseous medium.

$$\varepsilon_S E_S = \varepsilon_G E_G \tag{2.2}$$

The limitation of the above equations is that it does not take into account the microscopic structure involving atoms and molecules which play a crucial role in proper design of composite

insulation system.

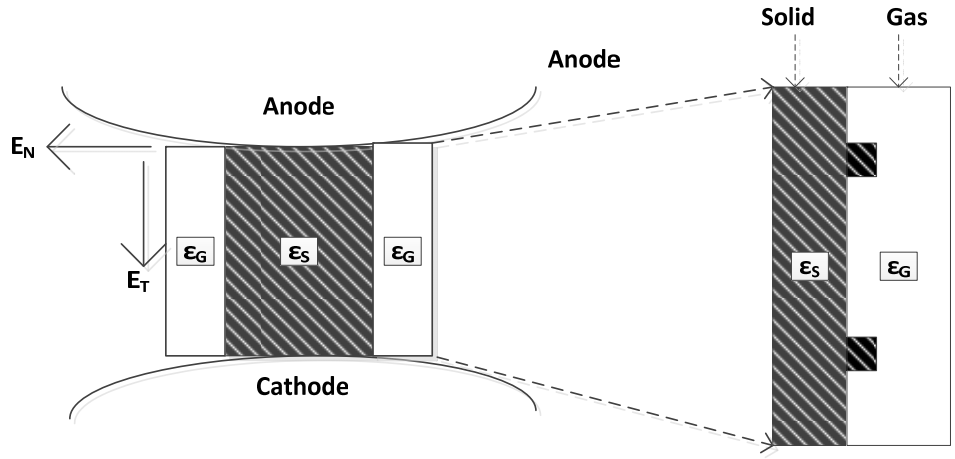

Figure 2.1 Schematic of a composite dielectric system (gas-solid interface)

(ε_S -permittivity of solid & ε_G- permittivity of gas, E_T-tangential component of applied field ,E_N-normal component of applied field)

A number of factors influence the breakdown voltage of spacer which include the material of the spacer, its geometrical configuration, its surface property and its surrounding environment like gas [18].The present studies are carried out related to high voltage pulsed power system where insulation system involves gaseous medium (surrounding the spark gap) and solid spacer (to act both as physical support and separator between two conductors at different potential). Since the major study involves the discharge along the gas-solid interface in nanosecond regime which are extremely relevant in KALI and gas insulated systems (GIS), the literature survey is mainly restricted (a) breakdown mechanism in gases under pulse voltages (b) breakdown mechanism in solids under pulse voltages (c) summary of the discharge mechanism along gas -solid interface and its applications along with the existing models of surface discharge along the gas-solid interface.

2.2 Gas breakdown

The breakdown strength in gases is mainly influenced by amplitude, duration of the applied voltage and the gas density [19]. The large number of molecules in the gaseous phase unlike vacuum inhibits charge motion and electrical conduction. The typical pattern for insulation strength shown in Figure 2.2 for a plane parallel electrode separated by one to few centimeters indicates that breakdown voltage strongly depends on the product of pressure and gap distance.

The gas switches are operated on the principle of ionization and breakdown in gases which involves transformation of the gas atoms into ions by detaching valence electrons from the former and transition of the gas molecules from a highly insulating (high resistivity) state to a highly conducting state[1].

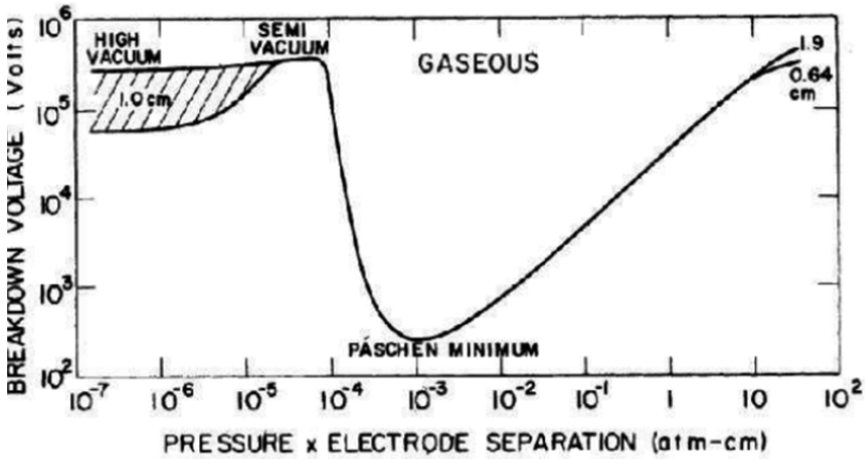

Figure 2.2 Breakdown Voltages in N_2 for cm length uniform field gaps [19]

The two most well-known mechanisms to explain breakdown in gases are Townsend's mechanism and Streamer mechanism. The presence of free electron is necessary to initiate the process of gas breakdown .These electrons are emitted either as a result of explosive electron emission from cathode or cosmic radiation in the atmosphere. These electrons on collision with a

neutral particle produce electron and positive ion. This process becomes complete when the electrons emitted initially reaches the anode .The other processes are [20, 21]

i)The emission of electrons as a result of positive ion striking the cathode.

ii)Excited atoms or molecules in the avalanches may emit photons which further leads to electron emission.

iii) The metastable atoms may diffuse back producing electron emission

The drawback of Townsend mechanism is that it cannot be applied to explain the breakdown mechanism beyond one atmospheric pressure as it considers current growth due to ionization only and does not take pressure and geometry of the gap into consideration.

The streamer discharge mechanism considers spark discharge from a single avalanche in which the space charge developed by the avalanche transforms the avalanche into a plasma streamer. The ionization takes place in the gas as explained by Townsend's mechanism. The electrons in the avalanche move very fast as compared to the positive ions .The positive ions are near the anode when the electrons reach the anode .This results in the formation of a positive space charge which enhances the field and gives rise to secondary avalanches. The positive space charge extends to the cathode resulting in the formation of a streamer.

The field produced by positive space charge is given by

$$E_r = 5.27 * 10^{-7} \frac{\propto exp \propto x}{(\frac{x}{p})} \tag{2.3}$$

where x is the distance to which the streamer travels in the gap, p is the pressure in Torr and α is Townsend's ionization coefficient.

2.3 Gas breakdown under pulse voltages

The breakdown in gases under pulse voltage conditions takes two important effects into consideration mainly the statistical time lag required for the initial electrons to be produced and

the other is formative time lag which is concerned with the subsequent process of steamer formation and propagation [1]. Breakdown in a gas gap under nanosecond pulse duration is explained on the basis of runaway electron model. Runaway electrons are electrons which gain sufficient energy from the field and encounter lesser collisions as it accelerates. An electron emitted from the cathode develops forming an electron avalanche in the gap. The ions emitted in the gap as a result of collision ionization are standstill as the drift velocity of ions is less than that of electrons. This forms a space charge field which distorts the main field. The avalanche can be considered as a localized group of electrons which bursts resulting in ejection of high velocity electrons ionizing the gas volume in its path and extending the main avalanche along a filamentary channel towards the anode. Once the avalanche touches the anode a conducting path is formed between cathode tip of avalanche and anode forming a highly conductive plasma channel which bridges the gap [22].

Further the application of Paschen's law does not hold true for nanosecond pulse in nitrogen, oxygen and air for the tested gap length. An increase in voltage pulse duration leads to reduction in the breakdown voltage and the phenomena cannot be explained on the basis of conventional avalanche to streamer theory [23].

Manokowski et al. [24] measured the breakdown strength of hydrogen,SF_6 in high pressure environment in sub nanosecond time regime and observed a field strength higher than that proposed by Martin et al.[25].The increase in breakdown strength with the application of negative polarity is attributed to the removal of space charge because of cathode field intensification which will lead to higher breakdown field to cause ionization in the gas gap unlike a positive polarity charged electrode where breakdown is caused by cathode directed streamer.

Fletcher [26] measured the values of formative time tags in the range of 0.5ns to 50ns as shown in Figure 2.3 and it was found to be a function of applied field for shorter gap lengths but was found to increase with decrease in gap lengths for longer times as a result of transition of single avalanche to a multi avalanche mechanism.

Mesayat et al. [27] considered that the electrons emitted from the cathode doesn't only lead to the complete formation of discharge channel and is assisted by photoelectrons from the cathode which is not considered in the two group breakdown model by Kundhart et al. [20].

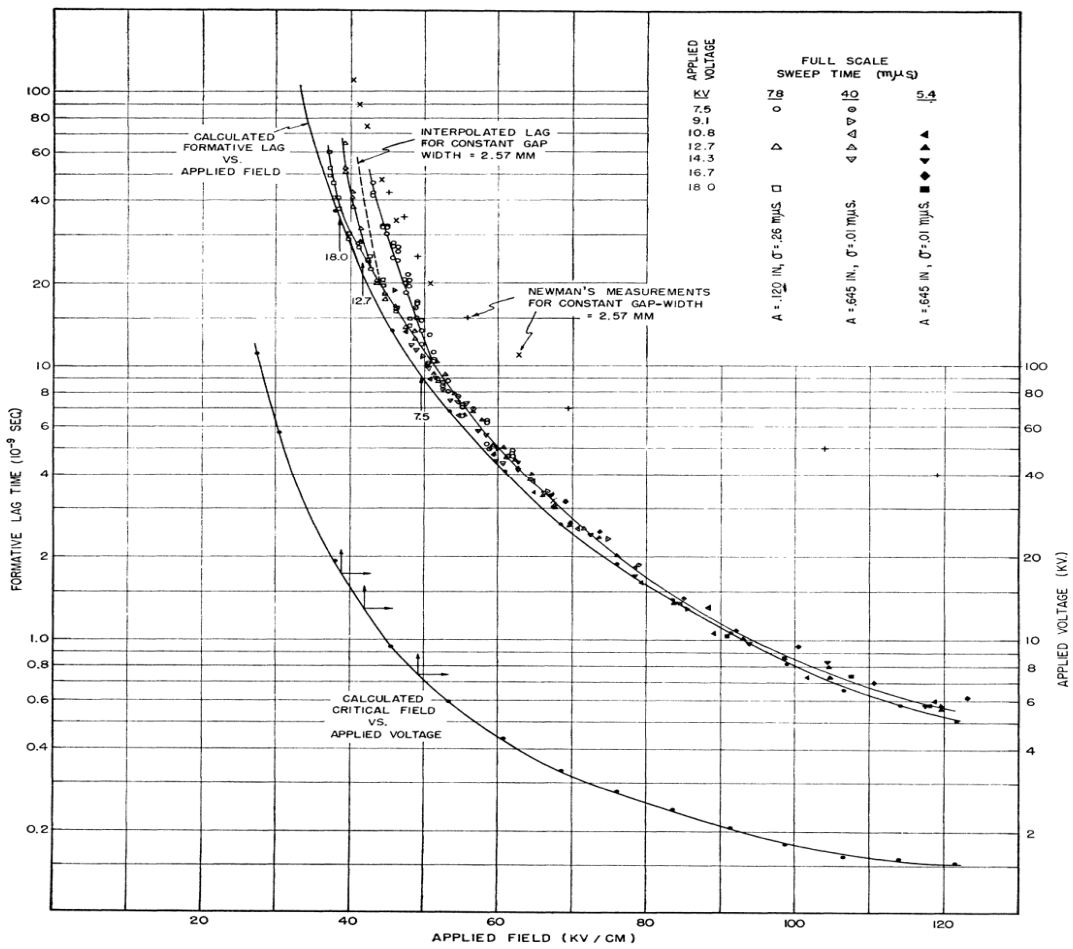

Figure 2.3 Measurements of the formative time lag as function of applied field for different gap-widths [17]

Koppitz [28] carried out the optical study on the spatial and temporal development of avalanches which involves a cathode directed streamer due to secondary electrons from the cathode and an anode directed streamer progresses causing further ionization in the gas gap. The material of electrodes strongly influence the statistical and formative time behavior and it is observed that graphite has the highest emission rate and the statistical distribution of time lag for graphite electrodes has least deviation which makes it useful to investigate the formative time lag[29].

The pulse rise time has a dominant effect on the propagating ionization wave front and a reduction in the rise time leads to an increase in the breakdown velocity with a source of high energy electrons producing pre ionization in the gas gap for an applied pulse of negative polarity [30].

Breakdown phenomena in a gas insulated gap shows streamer formation on the cathode surface which develops towards the anode and flashover takes place only several nanoseconds after the anode directed streamer reaches the anode in non-uniform field condition unlike in uniform field where a cathode directed streamer starts from the anode surface and propagates towards the cathode and breakdown takes place after a number of streamer processes [31].

The mechanism of repetitive breakdown in nitrogen under nanosecond pulses divides the breakdown process into four stages (a)creation of initial electrons at cathode by impact ionization or by cosmic and environmental radiation (b) the avalanche process which involves electron multiplication by collision ionization (c) transformation of conventional avalanche into streamer (d) heating of the plasma channel which leads to gap resistance drop and decrease in gap voltage which ultimately leads to breakdown[32].

Further the mechanism of repetitive breakdown in air is influenced by collision

detachment of negative ions which produces the initial 'seed' electrons for breakdown [33,34]. The memory effect of positive ions lasts for several hundred of microseconds whereas the effect of metastable species remains for hours which influence the discharge inception voltage under repetitive pulses [35].

Wang et al. [36] studied the behavior of nitrogen and hydrogen in a peaking switch at a pressure of 100 atm and a shorter rise time in nitrogen was observed as compared to hydrogen due to a higher breakdown field unlike hydrogen which had a better recovery characteristics.

The time dependent study of the arc resistances for nitrogen,SF_6,and argon shows a least value of arc resistance of 0.04Ω for SF_6 and a linear variation of the arc with breakdown voltage with the value of minimum arc resistance varying as an exponential function of maximum arc current [37].

The dependence of breakdown field on pressure in the range of 20-100atm and pulse stress time from 1to 5ns for nitrogen, hydrogen ,SF_6 and SF_6 -air mixture is due to the formative time lag which is much less than the pulse stress time at high pressures [38]. The use of hydrogen helps in rise time improvement and attaining better recovery characteristics as compared to nitrogen [39].

Manjunath et al. [40] carried out the breakdown study in compressed SF_6 environment under lightening (1.2/50μs) and switching impulse voltages (100/2500μs) with higher breakdown voltages for positive polarity as compared negative polarity impulse voltage. However saturation is observed in breakdown voltages at pressures beyond 0.3MPa with a slight variation of 10% in the breakdown data due to the use of brass electrodes as compared to the aluminum [41] and stainless steel electrodes [42].

Nam et al. [43] proposed an empirical relationship of breakdown strength in high

pressure SF_6 taking into account a modified d/r ratio (d_{eff}) and field enhancement factor (β) for non-uniform fields by modifying the relationship of breakdown strength in SF_6 in uniform fields [44] given by

$$E=88.5p+0.65\beta/d_{eff} \qquad (pd\leq 3\text{bar-cm}) \qquad (2.4)$$

$$E=68p+40\beta/d_{eff} \qquad (pd\geq 3\text{bar-cm}) \qquad (2.5)$$

and are in agreement with other experiments carried out in high pressure SF_6 gas environment within a pd range of 0.5-35.5bar cm which is very useful in a compact high pressure switch design [45-47].A few factors with influence the breakdown strength in gases in enlisted below-

2.3.1 Nature of gas and pressure

The nature of the gas and pressure affects the breakdown strength defined as the voltage per unit length .Sulpur hexaflouride (SF_6) possesses 16 times the breakdown strength of helium(He) at comparable densities and pressure owing to the nature of gas [19].

2.3.2 Time duration of applied voltage

The total time to breakdown is defined in two steps i.e the statistical time lag which involves the creation of an initiating electron and the formative time lag which considers the development of breakdown after initiating condition have been created. Figure 2.4 shows the breakdown field/density versus density time curve for different gases [48,49] and it is observed that a source of radiation in the gas gap provides initiating electron and leads to reduced breakdown strength as compared to un irradiated condition.

2.3.3 Electrode surface

The breakdown in gases takes place when the field exceeds the critical breakdown strength. The geometry of the electrode and gap pressure influences the initiation of electrons required to start

the breakdown process which finally leads to breakdown. The field non uniformity enhances the breakdown strength and leads to breakdown at reduced voltage [50].

2.3.4 Effect of particle

The presence of particle in gas insulated system leads to breakdown at reduced voltage [51].The particles immediately cross the gap when subjected to dc voltages and oscillates in the applied field in case of an alternating voltage and the activity increases with field ultimately leading to breakdown.

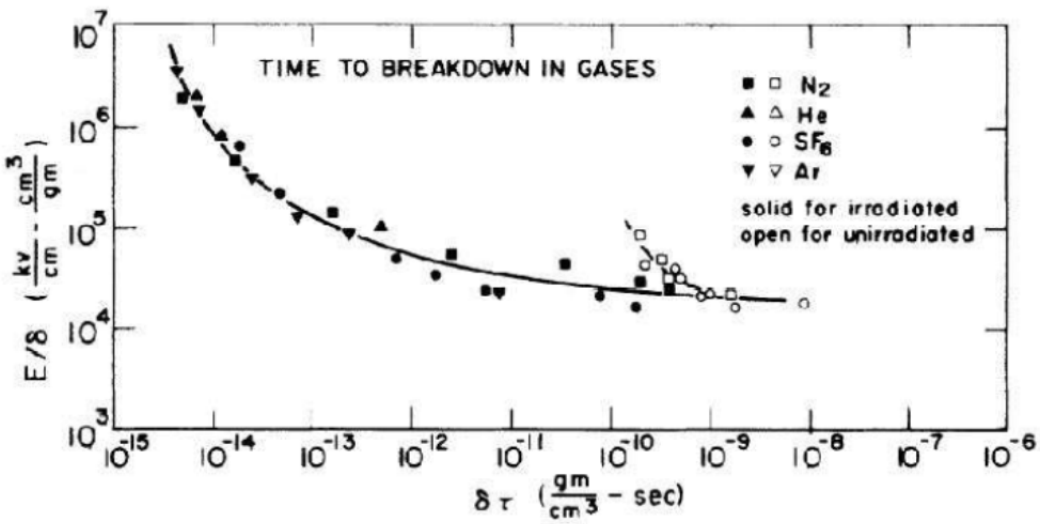

Figure.2.4 Time to breakdown in gases [48,49]

2.3.5 Role of insulators

The solid insulators form an important part in high voltage system. However the presence of solid insulators leads to the formation of triple point (electrode, gas, vacuum, liquid and solid dielectric) which leads to breakdown at reduced voltage. The micro discharge originate at the spacer electrode interface or at an imperfection on the spacer surface which leads to breakdown at reduced voltage [52]

2.4 Solid breakdown

Solid insulation forms an integral part of high voltage systems .However the breakdown mechanism in solids is not clearly understood. The breakdown mechanism in solids is irreversible unlike in gases and liquids which recover to the normal conducting state after a given time duration depending on pressure and gap distance. A number of mechanisms have been used to explain the breakdown in solids .However the mechanism of interest is the intrinsic and avalanche breakdown which occurs in the nanosecond regime as shown in Figure 2.5.

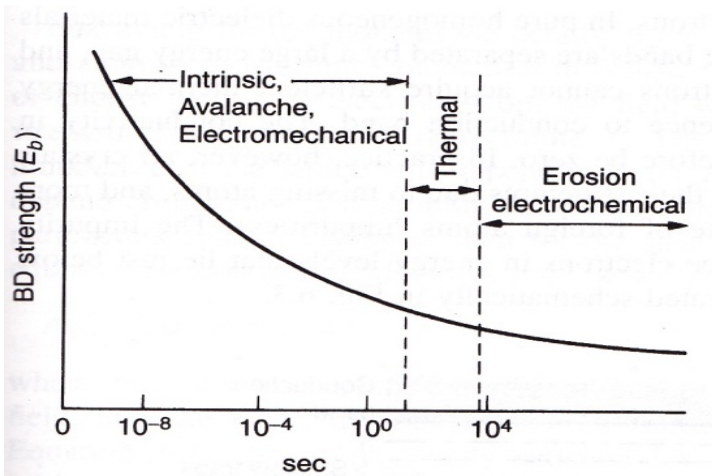

Figure 2.5 Mechanism of failure and variation in breakdown strength in solids with time of stressing [44]

1. Intrinsic breakdown is one in which electrons in the insulator gain sufficient energy to cross the band gap from valence band to conduction band and the duration is of the order of 10^{-8} sec. It follows from the establishment of conducting plasma through the gas or the liquid part of the composite insulation system along with the solid [53, 54]

2. Streamer breakdown occurs as electrons at the cathode dielectric interface on entering the conduction band of the dielectric drift towards the anode. An increase in the mean free path

between successive collisions leads to an increase in energy gain which leads to the production of an electron if the energy gain exceeds the ionization energy .This process leads to the formation of electron avalanche.

3. Electromechanical breakdown takes place when the electrostatic compression forces produced as a result of insulator surface charge exceeds the mechanical breakdown strength. The breakdown strength beyond which the dielectric becomes unstable leading to breakdown is critical breakdown strength (E_a) given by [55]

$$E_a = 0.6\sqrt{\frac{Y}{\varepsilon\varepsilon_r}} \tag{2.6}$$

where Y is the Young's modulus of the material and ε_r is the dielectric constant of the material.

The work carried out by different experiments make a basis of one of the above breakdown mechanisms to explain the physical phenomena.

An intrinsic theory of dielectric breakdown makes use of critical field as the basis of its model and considers collision ionization as the prime cause of breakdown in solids [56]

A relation between the critical field and time to breakdown is developed which considers recombination for the removal of charge carriers and drift of charge carriers towards the electrodes which affect the breakdown strength of a solid dielectric [57]. Another theory considers electron avalanche as the reason for breakdown and divides the breakdown process into the formative stage which involves energy deposition in the dielectric ,tree initiation stage in which there is a formation of ions in the gaseous phase ,tree growth stage in which energy is supplied from the field to the gas resulting in erosion of the dielectric and a return streamer stage in which the tree extends from one electrode to another resulting in the formation of breakdown channel[58].

2.5 Breakdown in solids under impulse voltage

The breakdown in a solid dielectric occurs within 1ns to 10μs after the application of the voltage pulse [59,60]. The breakdown study in polymethymethacrylate (PMMA) and polystyrene (PS) under pulse voltage shows bulk breakdown of solid dielectrics under nanosecond pulse duration whereas the phenomena of surface flashover is prominent in the microsecond pulse region along a solid -liquid interface .For a nanosecond pulse, delay time (t_d) for a flashover event to occur is inversely proportional to flashover field (E) given by

$$t_d \, \alpha (1/E^{1.4}) \tag{2.7}$$

The increase in breakdown voltage leads to an increase in peak current density according to Fowler Nordheim accelerating the creation of free radicals which finally leads to the formation of discharge channel [61].The effect of electrodes on solid dielectric breakdown under nanosecond time scale is analyzed and an increase in work function leads to an increase in the electric breakdown strength for solid dielectric breakdown and also proves that the emission of electrons takes place from the cathode under nanosecond time scale similar to dc,ac and microsecond duration pulses[62]. Figure 2.6 shows the average breakdown strength versus work function for polyethylene samples.

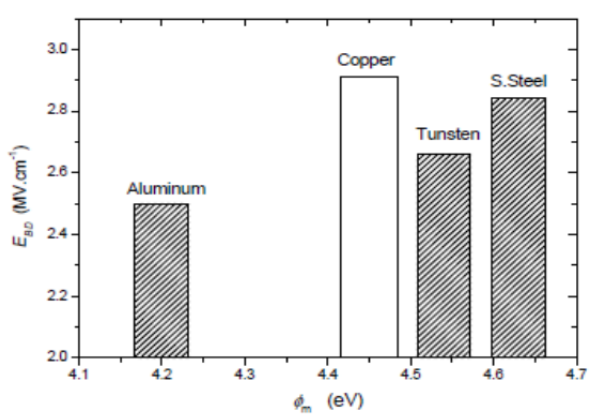

Figure 2.6 Average electrical breakdown strength versus work function for PE samples [62]

The analysis proposes electron impact ionization and electron multiplication as the possible mechanisms of solid breakdown in nanosecond time scale.

The propagation velocity of the breakdown channel in PMMA was found to be 80km/s which is attributed to the field enhancement at the tip of the point-plane electrode configuration which results in a high current density at the tip and electrons in the vicinity of the electrodes are pulled resulting in field ionization as in liquids [63,64].Figure 2.7 shows sequential records of the breakdown process for a positive point -plane electrode system with a 50 kV amplitude, 20ns rise time and 760ns duration pulse applied to the point electrode. The intrinsic breakdown strength of a solid dielectric under nanosecond pulse voltage results in difference in development of luminosity with applied voltage polarity. The application of negative polarity voltage initiates luminosity in the air column whereas positive polarity to the high voltage electrode initiates discharge development within the solid dielectric in a composite insulation system [65].

Breakdown in PMMA subjected to 2MV pulse voltage of rise time 20ns ,FWHM of 30ns and a fall time of 65ns when applied to a sample thickness of 0.16to 1.91cm shows the formation of partial discharge channels on the insulator surface at peak fields of 1.1 to 12 MV/cm .However the formation of a complete discharge channel from anode to cathode is responsible for solid breakdown with finally the occurrence of a gaseous discharge mechanism in the breakdown channels[66]. The dielectric strength of Perspex over a temperature range from 20ºC to 160ºC increases with rise time till values of rise time slightly higher than 100µs and then decreases with time falling close to the dc breakdown values is explained on the basis of space charge which reduces the field at the electrodes thereby increasing the electrical breakdown strength. The charge transport within the dielectric points towards an avalanche mechanism which may be responsible for the reduced breakdown strength close to dc values [67].

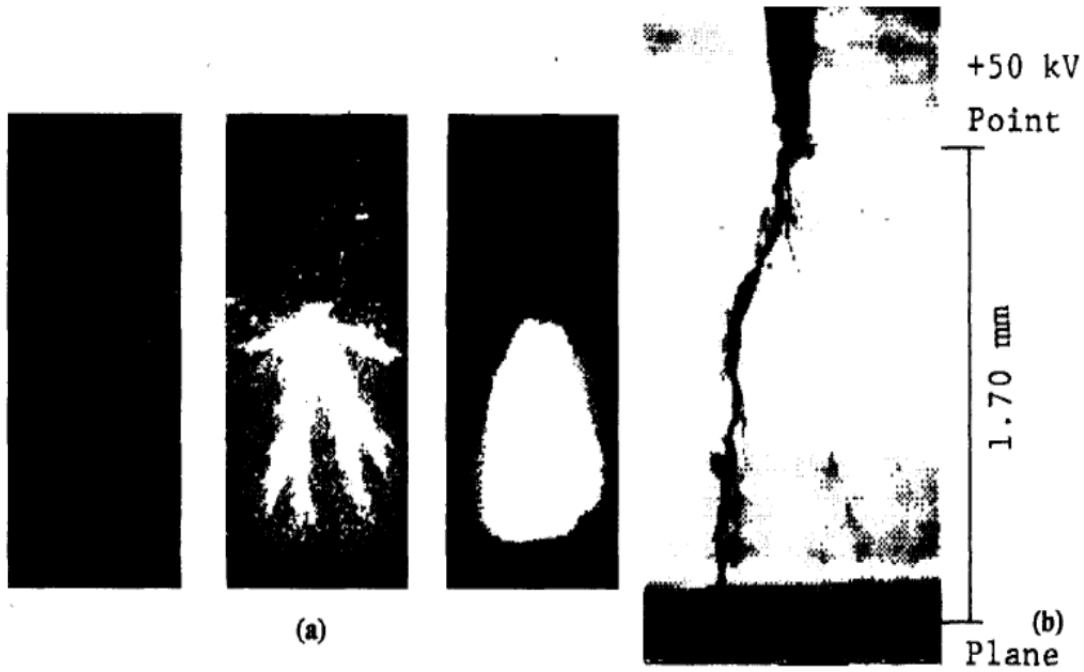

Figure 2.7 (a)The sequential records of breakdown process in PMMA obtained using an image converter camera, +50 kV point voltage, 1.70 mm gap, 10 ns exposure time, 40 ns between frames. (b) The corresponding breakdown channels viewed by an optical microscope. [63]

The effect of rise time and pulse width on the dielectric strength of polyethylene terephalate and polypropylene in the pulse width range of 0.2 to 5μs and rise time of 20 to 5μs with a pulse repetition rate of 500pps suggested streamer breakdown as the possible breakdown mechanism in air-solid and air-liquid composite insulation system. The existence of threshold voltage in polyethylene terephalate -fluorient for breakdown to occur for a number of pulses suggested thermal breakdown as the possible breakdown mechanism and heat so generated during inter pulse interval is retained by the system [68]. The measurement of pre-breakdown phenomena in air and solid argon using streak photography shows the development of cathode directed streamer from anode at 10^7 cm/s and breakdown initiation at the cathode in case of asymmetrically stressed solid dielectric placed in between the cathode anode gap as shown

below in Figure 2.8 [69].

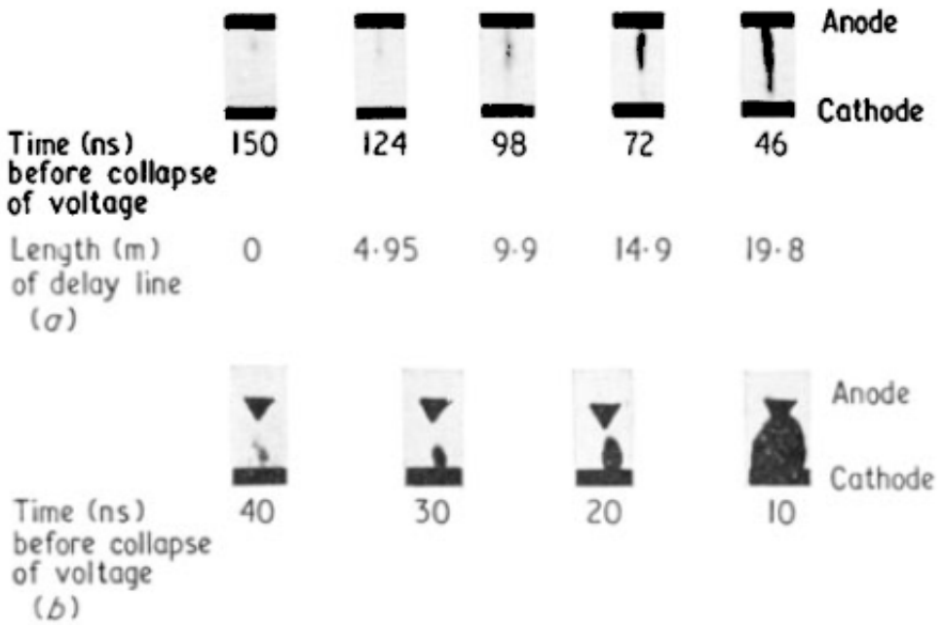

Figure 2.8 Photographs of pre-breakdown luminescence (a) in air at NTP between uniform field electrodes, separation 8 mm. (b) in solid argon between Point-Plane electrodes, separation 0.25 mm [69]

The variation in the breakdown probability of polymethylmethacrylate , polyethylene , polytetrafluroethylene and polypropylene using two parameter Weibull distribution [70-72] is given by the expression

$$F(E)=1-\exp((-E/E_{BD})^{8} \quad (2.8)$$

with a power exponent of 1/8.A reduction in the value of the exponent is observed in PMMA as compared to other samples due to the large number of pores present on the PMMA sample surface as shown in Figure 2.9 which leads to faster decrease in breakdown voltage of PMMA with gap length as compared to the other polymeric insulators[73].

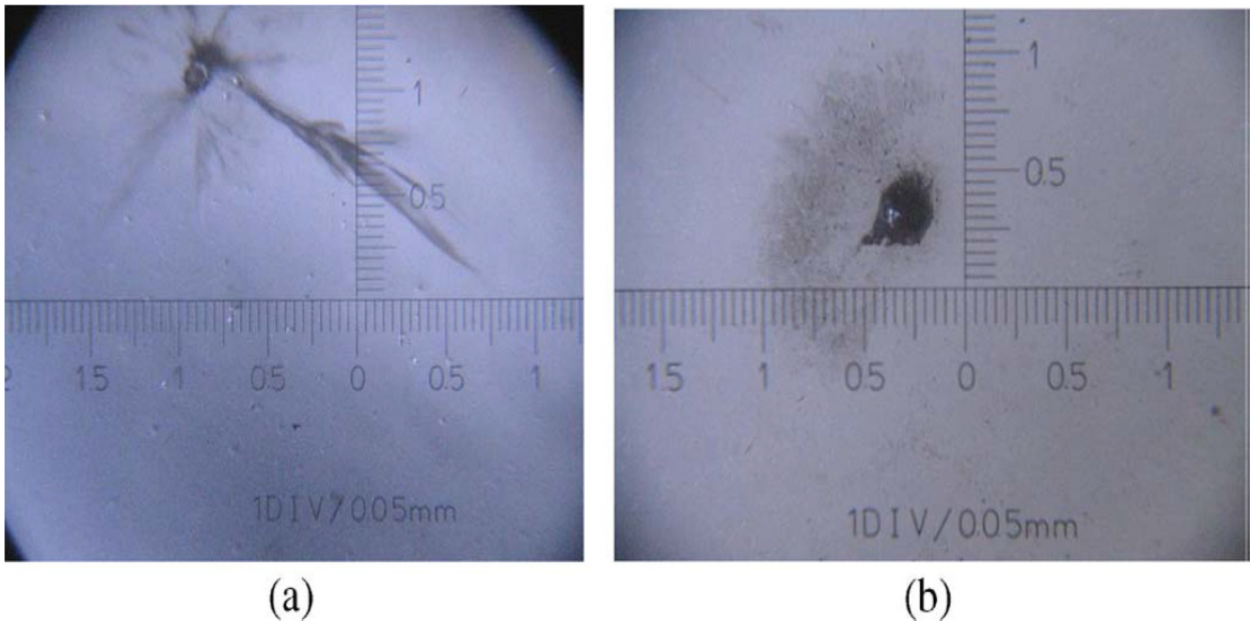

Figure 2.9 Enlarged photographs of the breakdown (a) PMMA and (b) PE samples.[73]

2.6 Gas-solid interface models

Flashover of insulator in gases is mainly determined by the dielectric constant of the insulator surface relative to the gas. The nature and dielectric constant of the insulator plays a major role in determining the flashover path [74]. The insulation is effective up to the breakdown threshold. Basically the breakdown process involves three stages: 1) primary electron generation to initiate the process, 2) exponential growth of the number of charge carriers, and 3) secondary electron generation to sustain the breakdown process. Interaction of material surface with the development of streamer is of prime importance as avalanches and streamers propagate along the surface of insulator leading to partial discharges and hence causing surface flashover of the insulator. Streamer propagation along an insulating surface takes places with an intrinsic propagation field and characteristic velocity depending on the type of the insulator material as shown in Figure 2.10[75, 76].

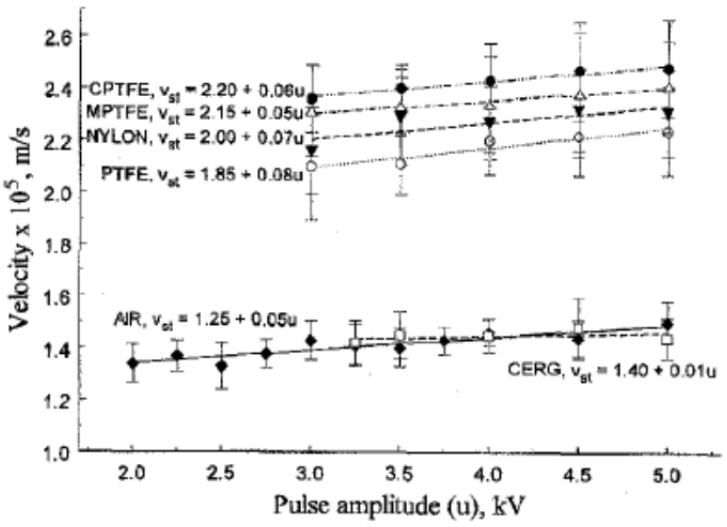

(a)

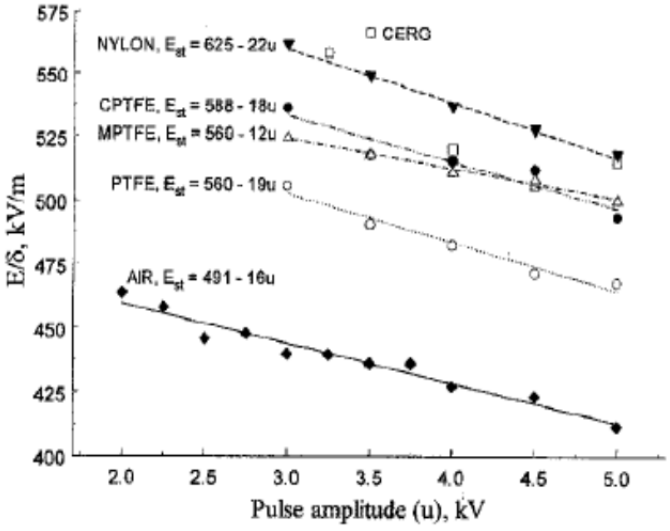

(b)

Figure 2.10 (a) Propagation velocities at traverse up to the cathode as a function of the pulse voltage amplitude,(b) Stability fields for propagation up to the cathode as a function of the pulse voltage amplitude, best fit equations shown for each material [75].

The accumulation of surface charge along the surface of the insulator affects the flashover characteristics [77] and ionized particles provided by gas micro discharges are the sources of the

surface charge accumulation [78]. Time–resolved optical and electrical study of the avalanche and streamer formation in uniform fields without space charge effects have already been carried out in nitrogen and air [79-81].

A study of the "swarm parameters" like electron velocity and ionization co-efficient has been carried out from these experiments. The breakdown process along a gas solid interface involves a number of interaction processes like electron photon processes at various points in the spacer and the surrounding gas volume. The surface flashover study of disc type spacers with a flat spacer end attached to a rounded electrode (type1) and a rounded spacer end attached to a flat sheath (type2) for positive, negative lightening impulse voltage, switching and ac voltages in compressed SF_6 environment gave a better flashover performance for a type 2 spacer electrode system due to the presence of shielding sheath which protrudes towards inner electrodes thereby preventing flashover. The space charge de concentration of the electric field lines at the electrodes leads to difference in calculated and experimental values at low pressures and decreases with increase in pressure [82].A cone type spacer leads to a higher breakdown strength as compared to disc type spacer in compressed SF_6 environment due to the reduction in field enhancement at the triple junction which delays the breakdown initiation and prevents the discharge development along the insulation resulting in breakdown in the gas gap which leads to an improvement in the voltage-time characteristics with the cone type spacer [83]. The study on the 50% flashover voltage on the surface of acrylic plates under impulse voltage with different creepage distances from 10-2.5cm (region A), 2.5cm-1cm (region B) and 1-0.4cm (region C) showed the development of positive leaders generating intermittent leader coronas in proceeding towards cathode which leads to flashover in region A unlike in region C where the primary positive streamer generated at cathode leads to flashover [84]. However polarity of the applied

impulse has a strong dependence on the development of discharge which consists of two surface distortion regions with creep age distances of 0.4 -1cm (region C) and 1-10cm (region A). The difference in the development of discharge in two regions lies in the fact that flashover in region C is caused by development of space charges whereas highly conductive negative leader is responsible for discharge in region A [85].

The study of the optical visible discharge paths of surface flashover along polythene, polymethy-methacrylate (PMMA) and polyvinylchloride surface under 1.3/50μs impulse voltages divided the discharge path into three regions as shown in Figure 2.11 (i) the discharges which leap out of HV triple junction (ii) the discharges which follow a certain length of insulator surface and then leap out (iii) the discharges which entirely follow the insulator surface. The discharges leaped out of the surface under positive impulse whereas discharges follow the surface of insulator under opposite polarity with material independent characteristics. The time to breakdown was least when discharge followed the insulator surface [86].

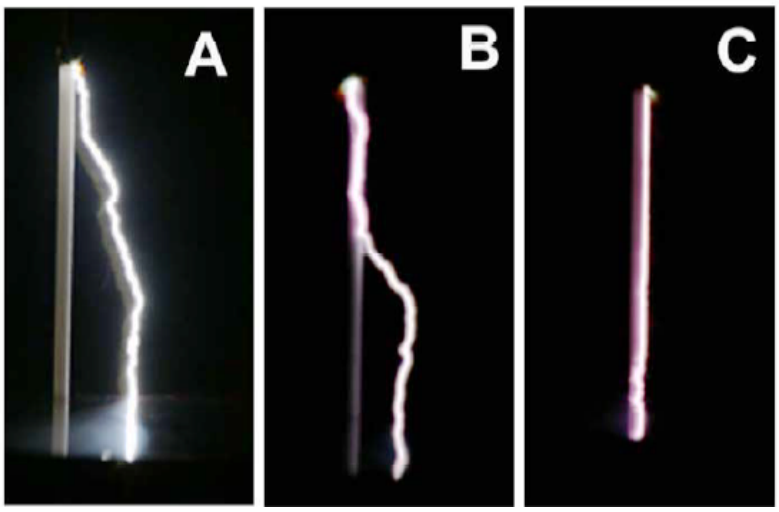

Figure 2.11 The 3 types of paths observed in the presence of the insulation rods [86].

The dielectric barrier discharge studies in the nanosecond regime finds tremendous applications in the field of sterilization, medicine [87] and biomedical treatment [88].The applied voltage pulse, pulse repetition frequency and air gap spacing does not change the mode of discharge in dielectric except for the decrease in discharge current with gap spacing which is attributed to greater energy deposition for an increased gap length and homogenous discharge as against filamentary discharge for an ac excitation pulse [89] as shown below in Figure 2.12.

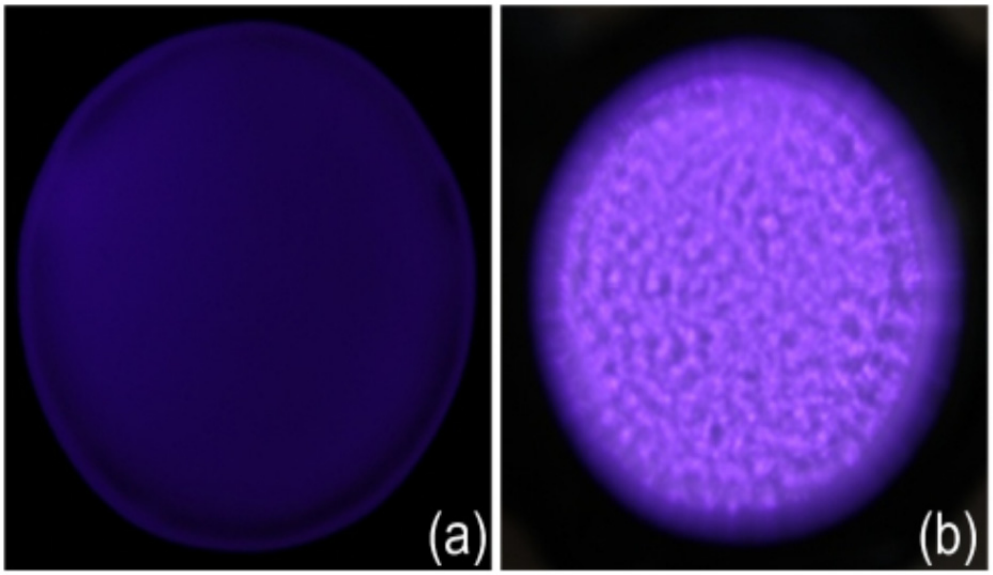

Figure 2.12 DBD images produced by high voltage nanosecond pulses (a) and ac power (b) (Exposure time: 0.5 s, ISO: 400, and air gap spacing: 2mm). [89]

The surface flashover of epoxy resin spacer in SF_6 under repetitive nanosecond pulses of rise time of 15ns and FWHM of 30-40ns shows decrease in flashover time delay and number of applied pulses with pulse repetition frequency (PRF) but leads to an increase in discharge current with PRF which indicates the presence of metastable species and residual ions which assist primary electron initiation. The increase in discharge current leads to a decrease in plasma resistance and an increase in area of plasma leads to brighter discharge images with PRF as

shown in Figure 2.13 [90].

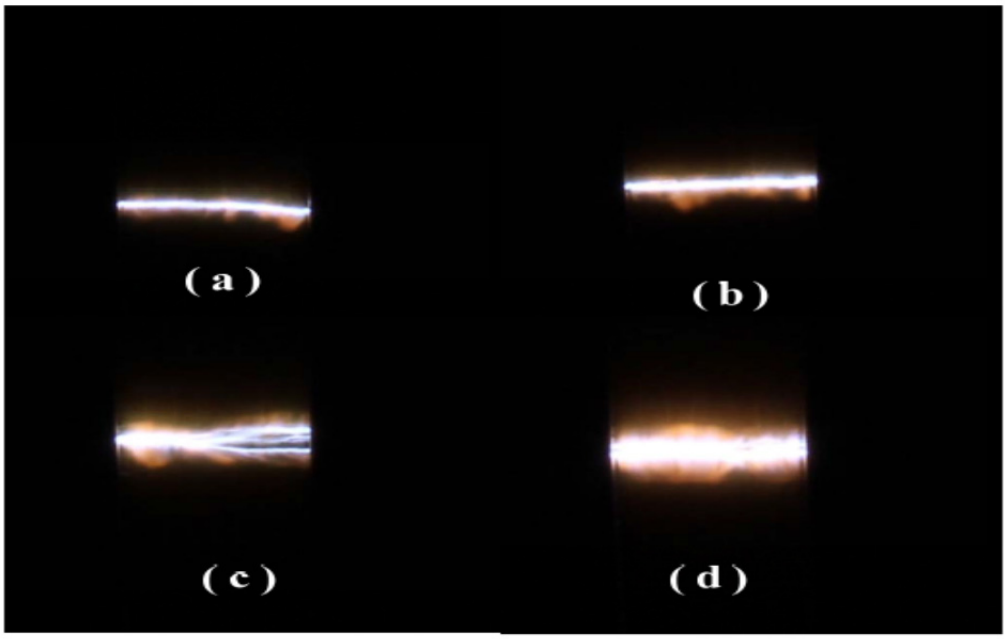

Figure 2.13 DBD Typical discharge images under 280 kPa. (a) 10 Hz, (b) 100 Hz, (c) 200 Hz, (d) 500 Hz.[90]

The spacer efficiency of polyterafluroethylene, polymethymethacrylate and nylon in SF_6 under positive and negative impulse voltages show spacer efficiency greater than 1 for pressures below 200kPA which is attributed to electron trapping by insulator surface, shielding effect of space charge and reduced area for secondary electron emission .However spacer efficiency less than 1 for pressures more than 200kPA results due to charge accumulation on insulator surface ,field enhancement at triple point and partial discharge which erode the insulator surface [91].

The pulsed flashover of lexan in nitrogen environment leads to the development of flashover path along the insulator surface in the presence of ultraviolet (UV) illumination and away from the surface in the absence of UV as shown in Figure 2.14 which is due to the presence of photoelectrons which helps in spark development close to the insulator surface. A decrease in

flashover delay time in humid nitrogen is due to the presence weakly bound electrons in moisture which is available for flashover initiation [92,93].

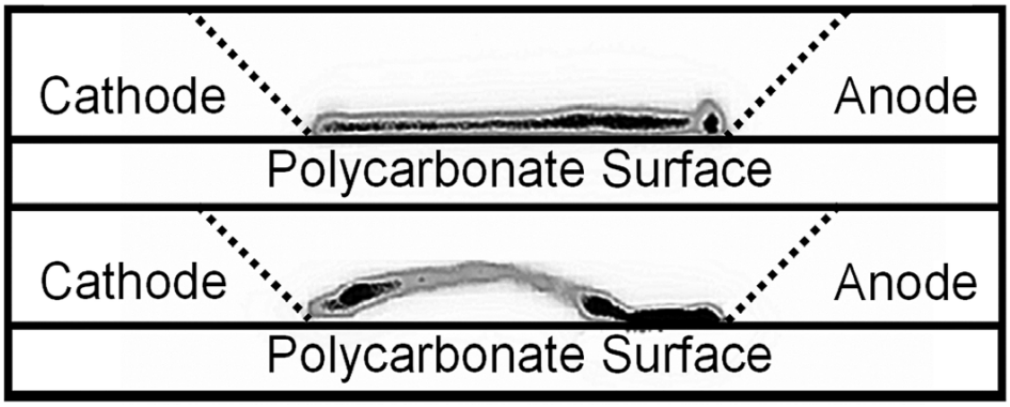

Figure 2.14 Side-on image of flashover in nitrogen. Discharge follows surface with UV illumination (top) and lifts off without illumination (bottom). Dielectric gap width = 7.8 mm, Vp = 25 kV, 30 ns optical gate time.[92]

However in the absence of UV the flashover path in air is close to the insulator surface and away from it in nitrogen environment mainly due to the presence of oxygen in air which has a lower excitation threshold leading to larger production of photoelectrons close to the insulator surface as show in Figure 2.15[94]

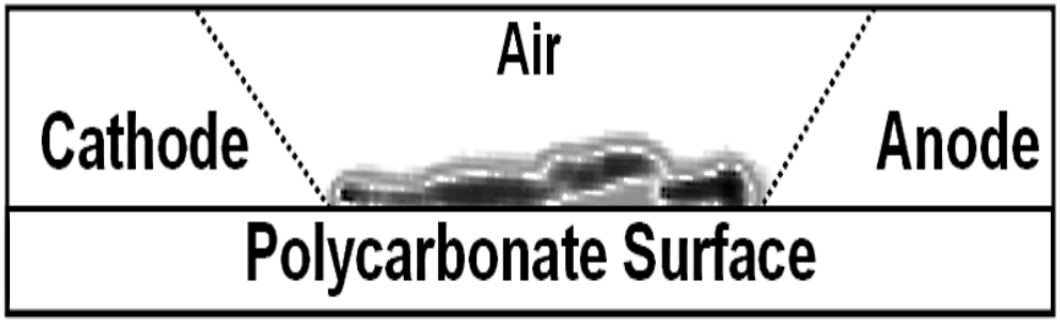

(a)

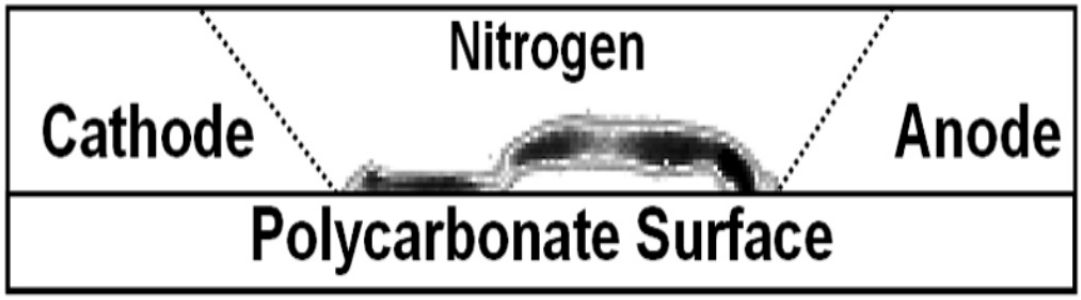

(b)

Figure 2.15 Side-on image of a flashover with voltage excitation from solid state pulser. Gap width = 5 mm, Vp = 32 kV(a) Air with ~200 ns exposure time (b)nitrogen with ~250 ns exposure time [94]

The streamer propagation study of magnesium fluoride in nitrogen ,oxygen and dry air using an ICCD camera shows streamer initiation at anode which is segmented in nitrogen environment unlike in oxygen where the streamer growth is blurry and diffused with self absorption of emission lines by oxygen molecules in Vacuum UV (VUV) range as shown in Figure 2.16[95].

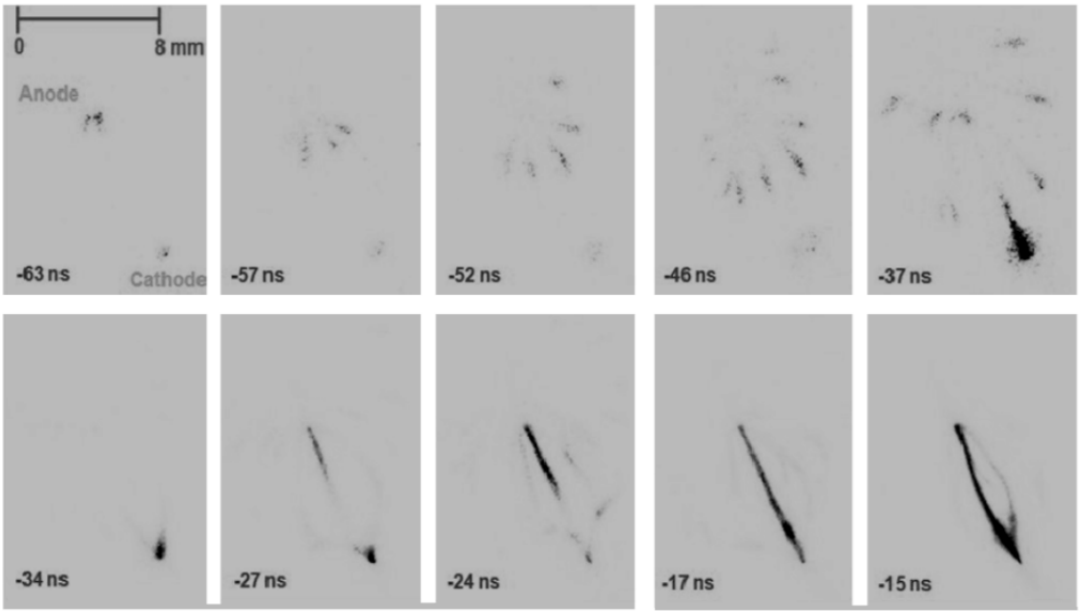

(a)

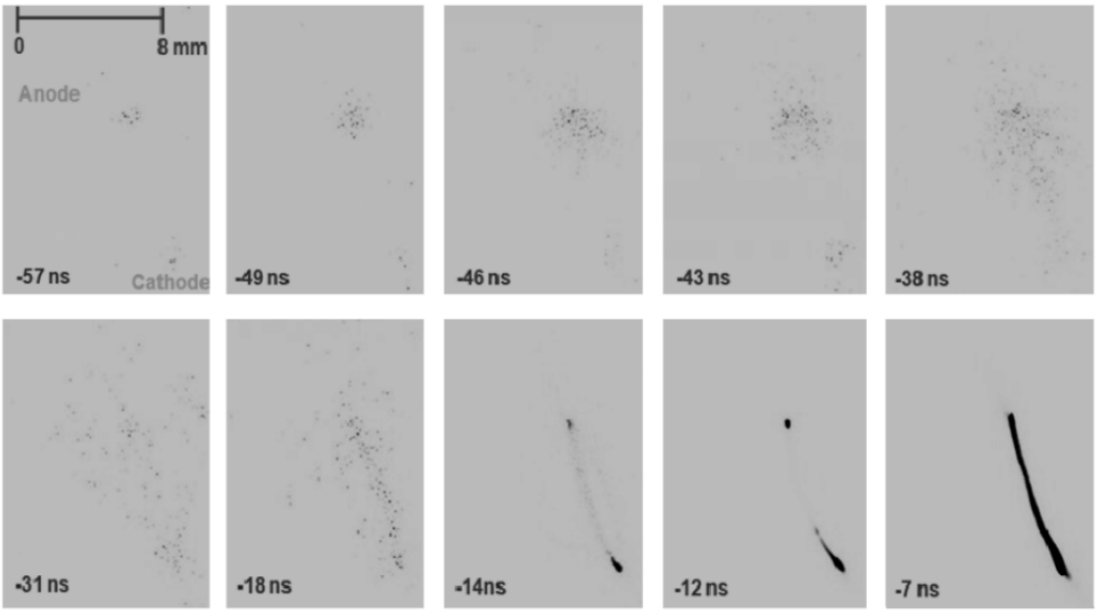

(b)

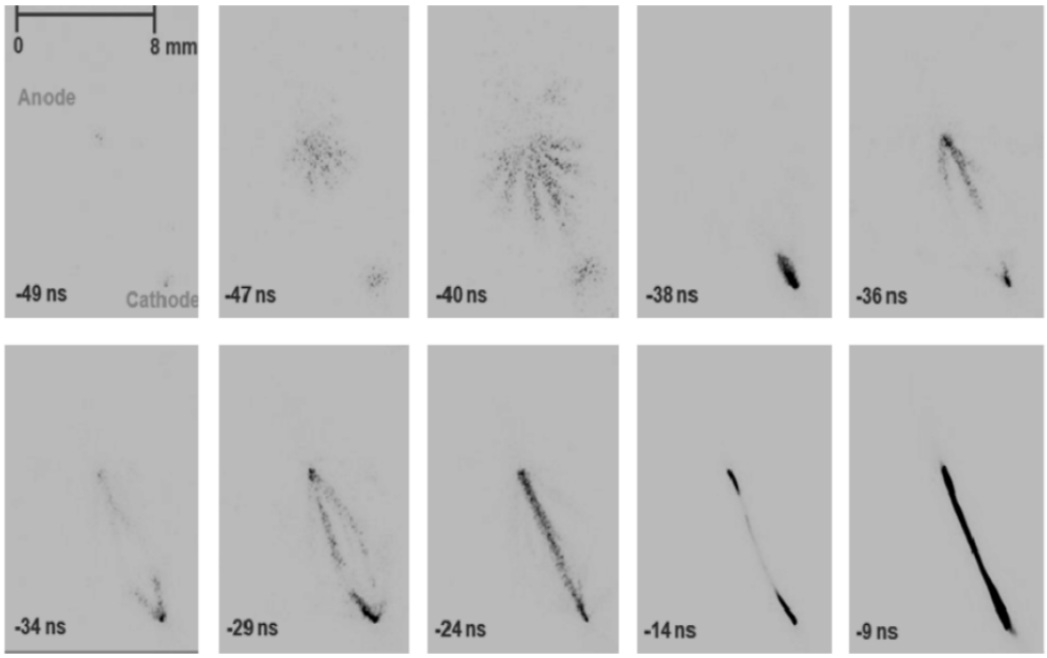

(c)

Figure 2.16 Streamer images captured from surface flashover, with 3 ns ICCD exposure (a) high purity nitrogen environment (b) high purity oxygen environment (c) dry air [95]

A number of interactions take place at the gas solid interface which is responsible for reduced breakdown strength at the interface and some of them are enumerated below and are shown in Figure 2.17[96].

i)field emission

ii)cosmic radiation

iii)photon initiation

iv)partial discharge

v)secondary electron generation along the insulator surface

vi)impact excitation

vii)surface charging

viii)volume charging

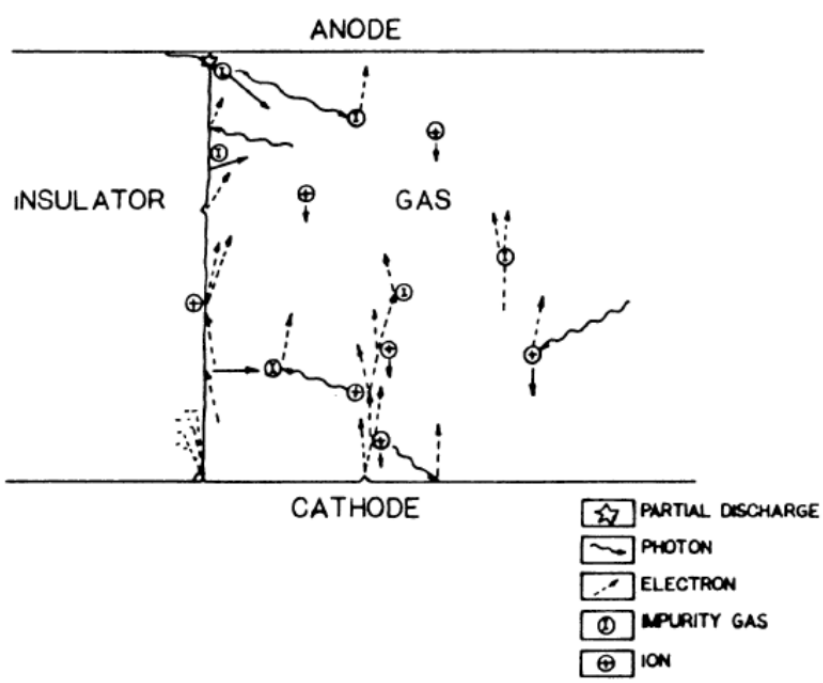

Figure 2.17 Physical processes responsible for insulator flashover in gases [96]

Some of the existing models which describe the discharge along gas -solid interface are described below in brief but each of these are suited for a particular set of experiments and does explain the physics of the process

Model-1: This model considers particle contamination as the dominant effect which leads to breakdown at a reduced voltage in compressed gas insulated system [97]. The particle modifies the electric field which leads to a modification in streamer formation in the gap. Breakdown was modeled by considering the growth of avalanche in the vicinity of electron. Breakdown was presumed to occur every time the critical avalanche size exceeded. Figure 2.18 shows the insulator and electrode geometry to study the discharge inception phenomena. The growth of the avalanche to 10^8 charges was considered as the criterion for discharge inception.

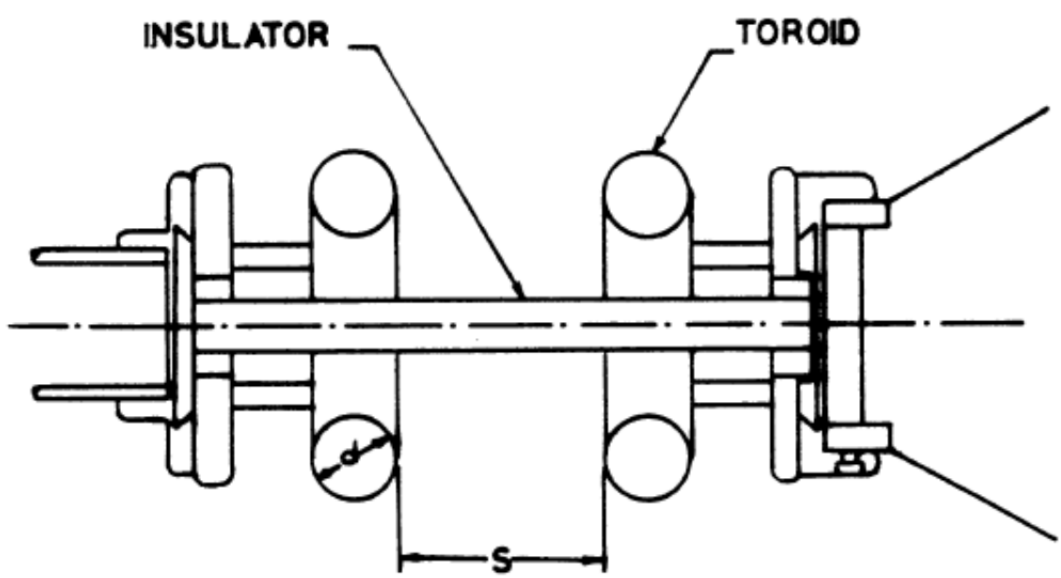

Figure 2.18 Rod-shaped insulator between toroidal electrodes as used to verify discharge initiation model based on peak stress [97].

The model employed a field solver and a numerical integration of

$$\int \alpha dx = 10^8 \quad (2.9)$$

where α is a function of the applied electric field and is the effective ionization coefficient of the gas. It failed to explain the physics behind the discharge process, role of insulator charging, the ionization processes along the insulator surface which is of considerable importance to the occurrence of a flashover event.

Model-2: The model considers the breakdown voltage of a spark gap near an insulating surface when the electron diffusion process is the dominant process which affects the breakdown. Breakdown was assumed to occur when the electron flux which is a product of electron velocity and number density reached a critical value .The effect of a solid insulator in not just to modify the electric field distribution but it also modifies the electron transport rates which affect the volumetric electron densities. A number of experiments were carried out for both cylindrical and flat insulator substrate and a minimum value of the breakdown voltage is observed with respect to the insulator and the axis of the inter electrode gap. This model does not consider the faster processes like electron avalanche and streamer which is very important in the sub-microsecond regime [98].

Model-3:A point -plane electrode system was used to study discharge along an insulating surface under impulse conditions as shown in Figure 2.19. The model describes the maximum length of the luminous discharge channel, radiating from a point electrode towards the grounded strip electrode with a flat insulating surface placed between the two electrodes. The tip of the discharge channel (leader) continued to propagate until the voltage drop in the leader channel reduced the leader tip potential to a value insufficient to supply the energy necessary for ionization, dissociation and heating of the gas in the path of the leader channel. This model does

not describe the discharge propagation in reference to the material which is very important when considering a flashover event of the dielectric but confines itself to the energy input to gas [99].

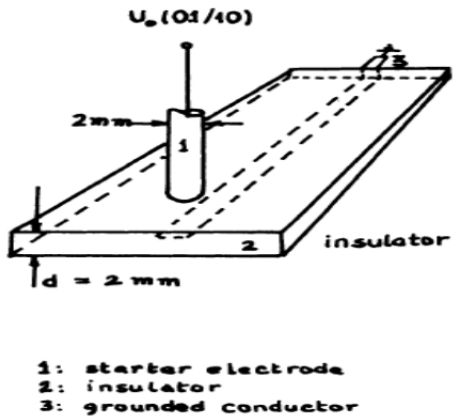

Figure 2.19 Test arrangement used in surface discharge studies of Niemeyer and Pinnekamp[97]

None of the above models clearly explains the discharge mechanism along the gas-solid interface.

2.7 Summary

The literature reviews the work carried out in the field of surface flashover of solid insulators mainly under pulse voltages in atmospheric air and compressed gas environment along with the breakdown mechanism in solid and gases and factors influencing their breakdown with an emphasis on studies related to pulse voltages. The understanding of the mechanism of discharge along gas-solid interface and the development of a solid -gas composite insulation is a step forward in the design of compact pulse power systems.

CHAPTER 3

ELECTROMAGNETIC PARTICLE-IN-CELL CODE FOR SIMULATION OF SURFACE DISCHARGE PROCESSES AND ITS ASSOCIATED ALGORITHMS

3.1 Introduction

The electromagnetic particle-in-cell code i.e. a finite-difference, time-domain (FD-TD) code for simulating plasma physics processes i.e. the processes that involve interaction between space charge and electromagnetic fields and simulation of the surface discharge processes has been developed and employed in the present study. The entire code comprises of the Maxwell's equation, Lorentz equation and the continuity equation. The Maxwell time dependent equations are solved by FD-TD algorithm to obtain electromagnetic fields. The Lorentz force equation is used to obtain the relativistic particle trajectories and the continuity equation is used to obtain the current and charge densities for Maxwell's equation. This approach is referred to as the electromagnetic particle–in–cell (PIC) technique which provides the solution of interaction between space charge and electromagnetic fields [100].

3.2 Finite difference time domain technique

The numerical calculation uses the finite-difference method. Time and three-dimensional space are divided into finite grids. From some known initial state, time is advanced by adding a single time step. At each new value of time, Maxwell's equations are solved throughout space to advance the electromagnetic fields in time. Using these new fields, the Lorentz equation is solved to advance the momenta and coordinates of all charged particles in the simulation. The continuity equation is solved to map charge and current densities onto the grid, which are then used as sources for Maxwell's equations on the next time step. This provides self-consistent interaction between the fields and particles. Figure 3.1 shows the layout of the particle-in-cell technique.

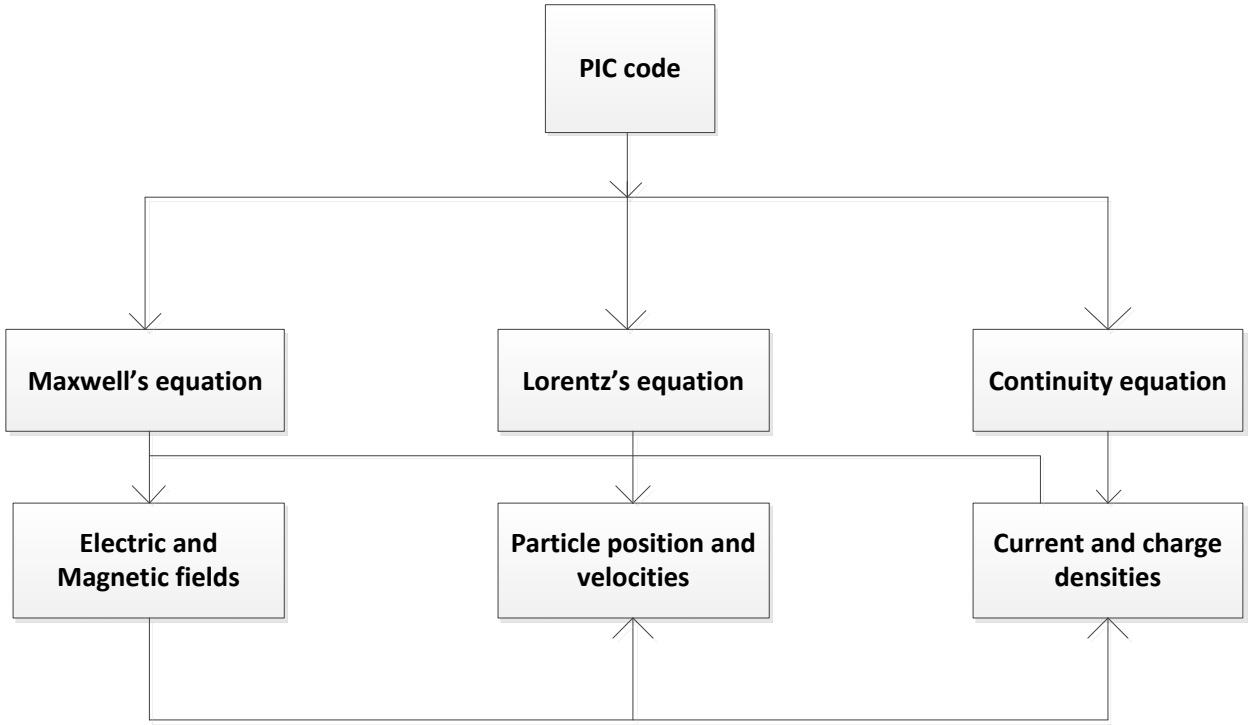

Figure 3.1 Layout of the particle-in-cell technique

The first order partial derivative, central difference approximation used in FDTD expansion, is given by Taylor series expansion.

$$\frac{\partial F(x)}{\partial x} = \frac{F(x+\left(\frac{\Delta x}{2}\right)) - F(x-\left(\frac{\Delta x}{2}\right))}{\Delta x} + O(x^2) \tag{3.1}$$

The 2nd and higher order derivatives are not usually computed and are treated as rounded up error of the order of $O(x^2)$.

The FDTD is a fully explicit solution technique which provides a direct solution of time dependent electromagnetic fields in a volumetric region. The advantages of FDTD technique over other numerical methods are

- It provides inherent modeling of inhomogeneous media
- Lossy ,non-linear and anisotropic media can be modeled

- Boundary conditions are inherently represented
- It is robust and provides an ease in implementation.

Some of the application areas of FDTD technique include antenna modeling and design, EM scattering, design of microwave circuits and non-linear device modeling. The important pillars of PIC technique namely the Maxwell's ,Lorentz and the continuity equations along with the FDTD technique is described in detailed in the subsequent sections which is used to model the surface discharge process.

3.3 Maxwell's equation

The Maxwell's equations are a set of four partial differential equations that describe the propagation and interaction of electric and magnetic fields.

The Maxwell equations are given by

$$\nabla . D = \rho \tag{3.2}$$

$$\nabla . B = 0 \tag{3.3}$$

$$\nabla X\ E = -\mu \frac{\partial H}{\partial t} - J_m \tag{3.4}$$

$$\nabla X\ H = -\varepsilon \frac{\partial E}{\partial t} + J_s \tag{3.5}$$

$$J_s = \sigma E \tag{3.6}$$

$$J_m = \rho H \tag{3.7}$$

where D=εE- Electric flux density

B=μH- Magnetic flux density

E=Electric field vector

B= Magnetic field vector

ε=Electric permittivity

μ=Magnetic permeability

J_S=Electric conduction current density

σ= Electric conductivity

$\boldsymbol{\rho}$=magnetic resistivity

Yee [101] introduced FDTD method to solve electromagnetic problems which uses simple central difference approximations to evaluate space and time derivatives in Maxwell's time dependent curl equations. The region being modeled is represented by two interleaved grids of discrete points as shown in Figure 3.2. In this diagram each electric field component is surrounded by four magnetic field vectors and vice versa.

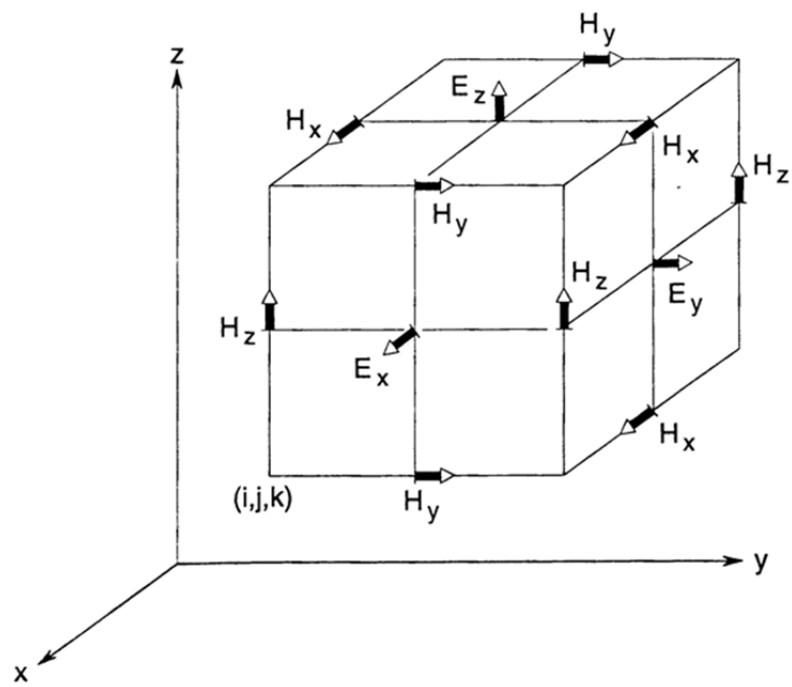

Figure 3.2 Yee's cell for electric and magnetic vectors

According to YEE notation a grid point in the region is expressed

$$(i, j, k) = (i\Delta x, j\Delta y, k\Delta z) \tag{3.7}$$

Thus, any function of space and time can be expressed as

$$A_m^n(i,j,k) = A_m(i\Delta x, j\Delta y, k\Delta z, n\Delta t) = A_m(x,y,z,t) \quad (3.8)$$

where

A=Vector electric field E or magnetic field H

m=Vector field component(x, y, z)

Δt=temporal increment

Δx=spatial x increment

Δy=spatial y increment

Δz=spatial z increment

n=time step

The central difference approximation evaluates the temporal derivative of electrical field in x-direction to the spatial derivative of magnetic field in y and z-directions resulting in six coupled scalar equations the resultant values of which gives the net electric and magnetic field acting on a particle at a given grid point. The field values so obtained are utilized for the calculation of particle positions and velocities using Lorentz equations.

3.4 Lorentz's equation

The particle–in-cell method uses computational particles (macro particles) to represent ions, electrons and neutral gas molecules. Force acting on the particles is given by Lorentz force

$$\vec{F} = q(\vec{E} + \vec{v}x\vec{B}) \quad (3.9)$$

Here q is the particle charge, $\vec{E}$ is the electric field, and $\vec{v}$ and $\vec{B}$ are the particle velocity and magnetic field, respectively. In case of non relativistic motion, the magnetic force of the wave (e (v/c)) H, is much less than electric force eE and hence is not taken into consideration [102]. The leap frog scheme is used to update the E and H fields alternately in the time domain. This scheme uses the value of E at time t to find the value of H at time 0.5Δt and this value of H is

utilized to calculate value of E at Δt thus allowing the applied electromagnetic wave to move ahead over the spatial grid as shown in Figure 3.3.

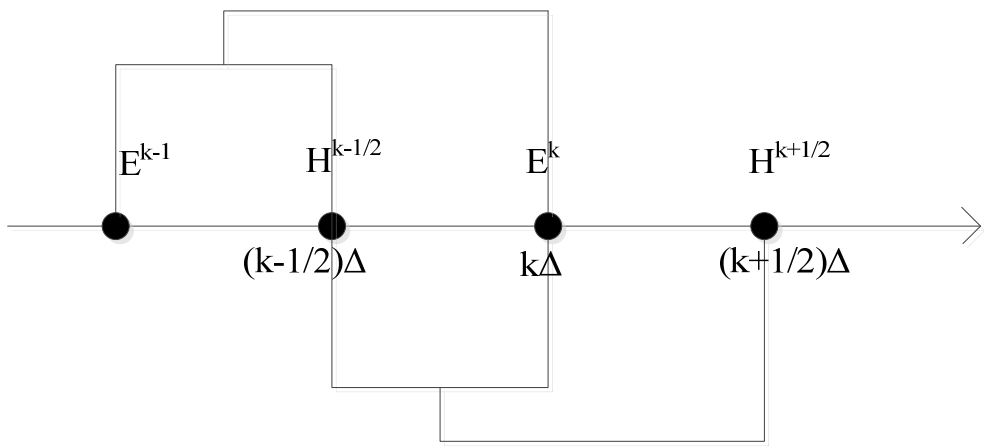

Figure 3.3 The leap –frog time marching scheme

The leap-frog algorithm is used to solve the particle motion as shown in Figure 3.4. The particle motion is described on the basis of two differential equations which are integrated separately for each particle.

$$m\frac{d\vec{v}}{dt} = \vec{F} \tag{3.10}$$

$$d\vec{x}/dt = \vec{v} \tag{3.11}$$

where $\vec{F}$ −electromagnetic force acting on the particle

$\vec{v}$-particle velocity

$\vec{x}$-particle position

m-particle mass

These equations are replaced by finite difference equations

$$m\frac{\vec{v}_{new}-\vec{v}_{old}}{\Delta t} = \vec{F}_{old} \tag{3.12}$$

$$\frac{\vec{x}_{new}-\vec{x}_{old}}{\Delta t} = \vec{v}_{new} \tag{3.13}$$

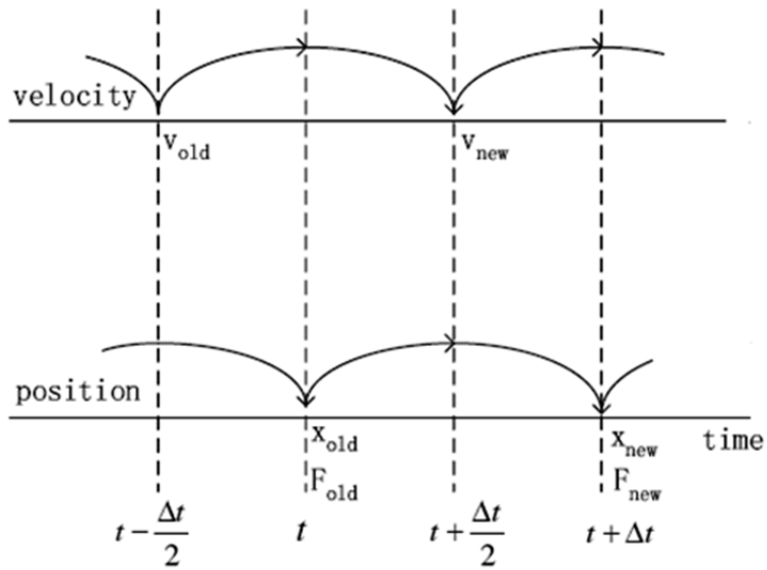

Figure 3.4 Leap-frog integration method shows time centering of force while advancement of velocity and of velocity while advancement of position

The Lorentz force equation provides the position and velocity at each grid point and helps in the traversal of the electromagnetic wave in the simulation volume. The continuity equations are then solved at each grid point to obtain charge and current densities which are used as source terms for the Maxwell's equation for calculation of field values for the next time step and the process is repeated.

3.5 Continuity equation

The continuity equation is solved to provide current and charge densities for Maxwell's equations. The simulation space is filled with gas of finite conductivity.The traversal of particles within the gas volume is based on the concept of mobility. Energetic electrons are considered to be the dominant source term in the density equations.The PIC algorithms considers that primaries in traversing through a gaseous medium produces low energy secondary electrons and

ions .The collision frequency of the electrons is high and hence the mean free path is short.The net velocity of each of these species produced during ionization is proportional to the electric field and the constant being the mobility term.

The process of ionization results in change in the background densities of electrons (n_e) ,positive ions(n_p) and negative ions(n_n). Negative ions(n_n)which is not considered in the present case since nitrogen is used as the background gas medium.The densities of these background species evolve according to the following equations.

$$\frac{dn_e}{dt} = Q_t + (\alpha_t - \beta_t)n_e - \alpha_{te}n_e n_p \tag{3.14}$$

$$\frac{dn_p}{dt} = Q_t + \alpha_t n_e - \alpha_{te}n_e n_p \tag{3.15}$$

where

Q_t-ionization rate for target species "t"

α_t-avalanche co-efficient

β_t-electron neutral attachment co-efficient

α_{te}-electron ion recombination co-efficient

3.5.1 Cross Section and Stopping Power

The ionization cross-section of electrons with the gas molecules specifies varying impact cross-sections with electrons of different energies. The impact cross-section can also be obtained from the stopping power using the expression

$$\sigma_{ion} = {\frac{dE}{dx}}\Big/{NW_{gas}} \tag{3.16}$$

where

$\frac{dE}{dx}$-electron stopping power

N-number density of the neutral gas

W_{gas}-energy needed to create an electron-ion pair

However in the present simulation the cross-section is taken as a function of electron energy (eV) [103].

3.5.2 Avalanche model

The avalanche co-efficient(α) is taken from the Longmire-Longley model .In this model ,p is the ratio of gas density to 1 atmosphere pressure ,|E| is the absolute value of the local electric field in V/m. The avalanche co-efficient α(|E|/p)is evaluated from the expression

$$\alpha\left(\frac{|E|}{p}\right) = A_1 p\left(\frac{\frac{|E|}{p}}{A_2}\right)^5 /(1 + A_3(\frac{\frac{|E|}{p}}{A_2})^{2.5}) \tag{3.17}$$

The co-efficient A_1, $A_2$and A_3 are modified depending on gases employed in the simulation volume. The values of A_1, $A_2$and A_3 are modified using the expression

$$\rho_r = \frac{\rho}{1.23kg/m^3} \tag{3.18}$$

where ρ is density of gas used in the simulation volume.

The values of A_1, $A_2$and A_3 used in the simulation are

A_1=5.38x10^8, A_2=2.82 x10^6, A_3=0.3

3.5.3 Recombination model

The recombination rate, $\alpha_e$of electrons to positive (m^3/s) is treated as a constant and its value at 1 atmospheric pressure is given by

$$\alpha_e(p) = R_e \tag{3.19}$$

R_e-1.0x10^{-12}

3.5.4 Mobility model

The mobility model used in the conventional code is based on Baum model. In this model, p is the ratio of gas density to 1 atmosphere pressure; |E| is the absolute value of the local electric field in V/m. The value of mobility is evaluated with the following expression.

$$\mu_e\,(|E|,p) = M_1/p(\frac{|E|}{p} + M_2)/(|E|/p + M_3)^{1/2} \tag{3.20}$$

where M_1,M_2 and M_3 are constants like A_1, $A_2$and A_3 whose values are different for different gases.

However the mobility expression used in the simulation is based on constant mobility model for electron and ions and is given by the following expression [104]

$$\mu_e = \frac{29}{p}\ (\mathrm{m^2/Vs}) \tag{3.21}$$

$$\mu_p = \frac{0.26}{p}(\mathrm{m^2/Vs}) \tag{3.22}$$

3.6 Numerical stability

The FDTD algorithms for Maxwell equations require that time increment Δt have a specific bound related to the spatial increments. This bound is necessary to avoid numerical instability, which can cause spurious results increasing without limit as the time increases. The bound on the time interval is given below

$$\Delta t = \frac{1}{\sqrt[c]{(1/\Delta x^2)+(1/\Delta y^2)+(1/\Delta z^2)}} \tag{3.23}$$

When Δx=Δy=Δz=Δ

$$\Delta t = \frac{\Delta}{\sqrt[c]{3}} \tag{3.24}$$

where c is the velocity of light. The above two equations state that the maximum allowable time step is determined by the smallest cell size, so that the electromagnetic wave cannot traverse across a grid in one time step. A generalized stability problem arises due to interaction between Yee's algorithm and augmenting algorithms used to model boundary conditions, lossy, dispersive, structured and unstructured meshing, non-linear or active materials.

3.7 The PIC computational cycle

The general computational cycle between electrons and electromagnetic fields is shown in the Figure 3.5.The cycle starts with some appropriate initial conditions on the particle positions and velocities. The particle quantities such as position and velocity (v_i,x_i) are known at the particle and may take on all the values in the phase space. The field quantities will be obtained on the

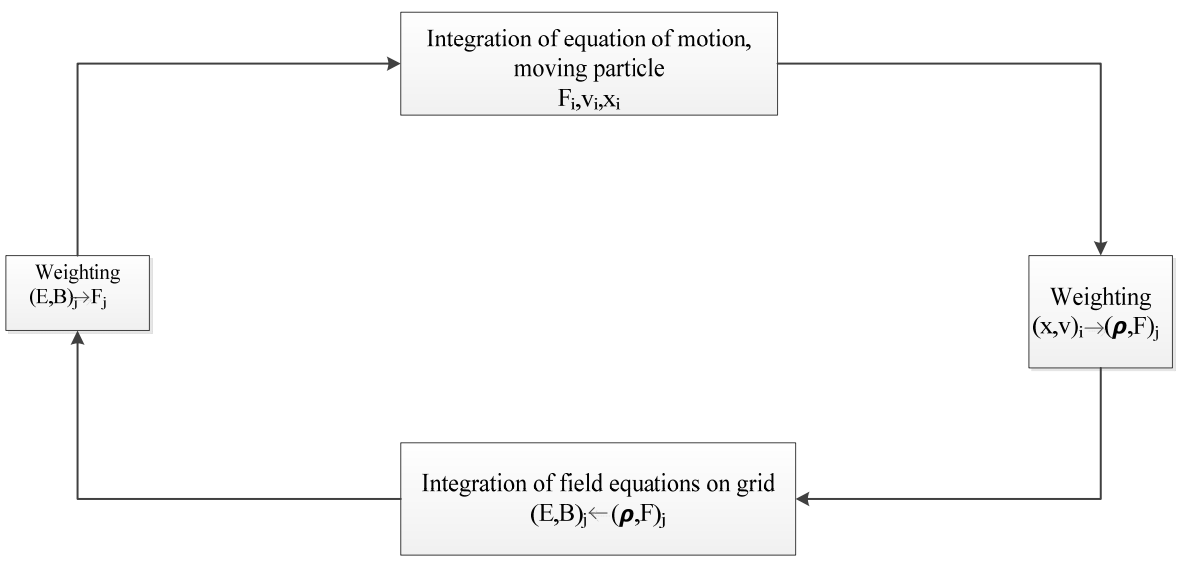

Figure 3.5 PIC processing cycle

spatial grid that is at discrete points. In order to calculate the field quantities on the grid, the charge and current densities must be known on the grid. This process of assigning particle charge and current on the grid is a kind of 'weighing' (ρ, F) which depends on the particle position. Once the charge and current densities are established on the grid, the electromagnetic

forces $(E,B)_j$ acting on the particle can be obtained through interpolating the grid fields and particle position and hence the electron moves forward[105-107].

3.8 Particle-in -cell simulations of discharge along gas-solid interface

The discharge along a gas-solid interface is of considerable hindrance in the reliable operation of high voltage pulse power systems specially laying importance into the insulation aspects of pressurized spark gaps and support insulators. A number of experimental studies have been carried out on the phenomenon pertaining to discharge along spacer surface in compressed gases but little has been reported on the physical mechanism of discharge along the interface [107-108].Partial discharges in voids in dielectric along the dielectric-gas interface involves a change from gas discharge like avalanche –streamer breakdown towards a spark like plasma [109].

Breakdown phenomenon has been explained on the basis of runaway electron model involving the interaction of space charge field due to a group of electrons ahead of the avalanche and the applied field [110].HV nanosecond discharges in gases at high pressure propagate as a fast ionization wave (FIW) with a typical velocity of 10^9-10^{10} cm/s[111]. Hence in order to gain an insight into the discharge process a PIC simulation code has been developed to understand the discharge mechanism along a gas-solid interface with a plain gas breakdown model under nanosecond pulse duration. Section 3.7.1 describes the development of the simulation model of an enclosed spark gap chamber .Section 3.7.2 emphasizes on the mechanism of discharge process in the cathode -anode gap with and without a dielectric followed by an analysis on the results in subsequent section 3.7.3.

3.8.1 Simulation method

Figure 3.6 shows the structure of electrodes (anode cathode (AK)) along with the insulator enclosed within a chamber. The diameter of cathode as well as the anode is 90mm and the

thickness is 26mm. The insulator placed in between the cathode and anode has a radius of 18mm and a thickness of 10mm. A dielectric hollow chamber sealed from either ends is used to create a pressurized chamber. The diameter of the cylinder which encloses the spark gap electrode arrangement is 232mm with a thickness of 10mm. The length of the entire simulation domain is 282mm and sufficient clearance is given between the inner interface and the electrodes so that there is no distortion of the electric field. A port forms the boundary of the simulation geometry that allows outgoing particles and waves to escape and incoming waves to enter. The entire simulation space is filled with nitrogen which is used as the background gas with the gas pressure in the chamber at 1 atmosphere. An FDTD based particle-in cell code is used in the modeling process which incorporate particles and automatically take the space charge effects into consideration.

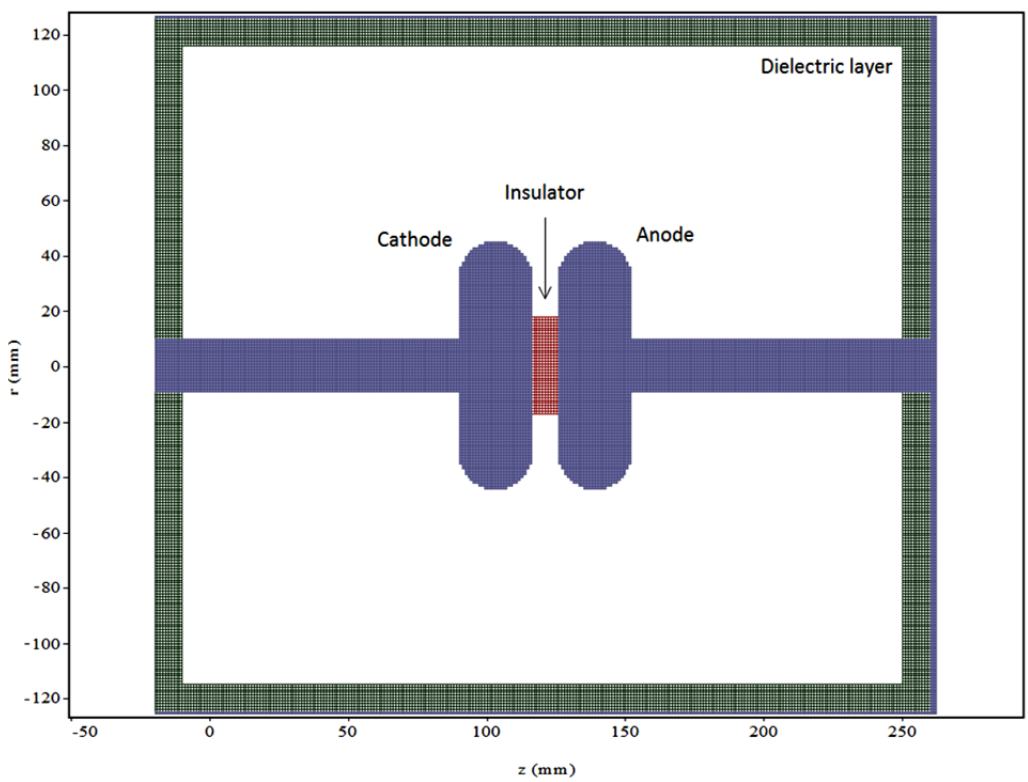

Figure 3.6 Schematic of cathode anode gap with the insulator

3.8.2 Mechanism of the simulation discharge model

The electrons emitted from the surface of cathode as a result of the explosive electron emission ionize the gas molecules in travelling towards the anode due to the electron mobility lead to the production of the positive ions and secondary electrons. The electrons emitted in the presence of dielectric, on striking the surface leads to emission of secondary electrons from voids present on the surface of the dielectric. The positive ions move towards the cathode under the applied electric field and on striking the cathode lead to the production of secondary electrons. SF_6 gas has greenhouse effect, so its use has to be minimized and nitrogen is used where gas handling plant is not needed unlike SF_6 gas to control the leakage in the atmosphere. The advantage of using nitrogen over argon and helium is that though both are non-attaching gases like nitrogen, they are not effective in slowing down electrons (slowing down of electrons enables them to be captured at low energies and hence they can be prevented from generating more electrons by electron impact ionization). The initial condition for the simulation is that both the electric and magnetic fields are zero at the start of the simulation and there is no net charge in the simulation space at the start. The simulations are carried out with explosive electron emission, neutral gas ionization and secondary electron emission models.

A. Explosive electron emission

Explosive electron emission [100] results from plasma formation on a material surface. Every surface has small micro protrusions and when exposed to high voltages, the electric field enhancement takes place at the protrusions which can cause significant high field emissions. The protrusions may dissipate due to joule heating leading to the formation of plasma on the material surface. The explosive electron emission plays a significant role for long duration high voltage pulses and is widely used for the production of high power pulsed electron beams, microwaves [112] and x-rays [113]. The electron emission occurs when the applied field exceeds threshold

field and follows the Child Langmuir law. The simulation is based upon the application of Gauss's law to half cells; the emitted electrons per unit area can be represented by [100]

$$\frac{dq}{dA} = \varepsilon_0 f\left(E_c - E_r\right) - \rho dx \tag{3.25}$$

where $\varepsilon_0$is permittivity of free space , f is plasma formation rate E_c is threshold field ,E_r is the residual charge field, ρ is the existing charge density and dx is the cell height.

B. Neutral gas ionization model

The electrons emitted from the surface of cathode produce electron-ion pairs on collision with the gas molecules. The mean free path between successive collisions is very small at high pressure and electrons with sufficiently high energy can only reach the anode. In our model the charged particles are created due to ionization of the background gas. The ionization cross-section of electrons with the gas molecules is not constant but is taken as a function of electron energy [103]. The impact ionization coefficient, recombination coefficient and electron and ion mobilities which are empirically determined functions of E/p are also included in the model. The electron and ion mobility are based on constant mobility model given by equations 3.21 and 3.22 respectively.

C. Secondary emission

The secondary emission takes place when positive ions impact the cathode leading to the production of secondary electrons. The secondary emission coefficient depends upon the primary particle energy, angle of incidence of particles and upon material properties. The equation governing secondary emission is given by [100]

$$\frac{dq_s}{dq_P dE_s d\theta_s \sin\theta_s d\theta_s} = \frac{1}{2\pi}\delta\left(E_P\theta_P, f\left(\frac{E_s}{E_P}\right)\right) \tag{3.26}$$

where is product of two functions of primary polar angle Θ_p and primary energy E_p , E_s is the

energy of emitted particle ,$f(E_p/E_s)$is the energy distribution function, $\sin \Theta_s \, d\Theta_s$ is the spherical angle distribution function.

D. Analysis on the effect of dielectric between the electrodes

A dielectric can be characterized by a conductivity σ in parallel to a frequency dependent dielectric displacement "conductivity" jωε. The presence of dielectric between spark gap electrodes can be analyzed as follows.

Let V be the voltage applied between the spark gap electrodes ,E is the applied field, l is the gap length ,R is the resistance between the electrodes, A is the cross-sectional area and σ is the conductivity

$$V = El = IR$$

$$E = \frac{I}{\sigma A}$$

$$\vec{J_1} = \sigma \vec{E} \tag{3.27}$$

The analysis of a solid dielectric gas interface can be considered in terms of two parallel dielectrics between two parallel plates one of which is a gas and the other is an insulator and hence forms the case of a capacitor. The capacitive current is given by

$$I_c = \frac{dq}{dt} = C\frac{dV}{dt}$$

$$I_c = A\varepsilon_0\varepsilon_r \frac{dE}{dt}$$

$$J = \varepsilon_0\varepsilon_r \frac{dE}{dt}$$

For a frequency dependent case electric field will be given by

$$E = E_m e^{jwt}$$

Using the relation $J = \varepsilon_0 \varepsilon_r \frac{dE}{dt}$, we have

$$\vec{J_2} = jw\varepsilon_0 \varepsilon_r \vec{E} \tag{3.28}$$

Hence the total current density is given by

$$\vec{J} = \vec{J_1} + \vec{J_2}$$

The presence of dielectric in the AK gap causes avalanche and streamer formation along the insulator surface and the effect is mainly dominated by the electric field through the dielectric constant given by

$$\vec{J} = (\sigma + jw\varepsilon_0 \varepsilon_r)\vec{E} \tag{3.29}$$

where J is the current density ,ε is the permittivity of the dielectric, ε_0 is permittivity of free space, σ is the gas conductivity and E is the applied electric field

3.8.3 Results and discussion

The study is carried out on the variations in electron momentum in the phase space, charge density, ionization co-efficient, drift velocity and temporal variation of charge in the simulation volume with and without a dielectric in the cathode-anode gap. The phase profile of electrons shown in Figure 3.7 and 3.8 shows the motion pattern of electrons at different time steps of 1.3ns, 1.7ns and 2ns in the initial stages of discharge with and without a dielectric spacer. It can be observed that in the presence of spacer the emitted electrons are directed towards the surface of spacer leading to a decrease in momentum when compared to the plain gas gap conditions. The electrons basically hop and move along the surface of the insulator towards the anode.

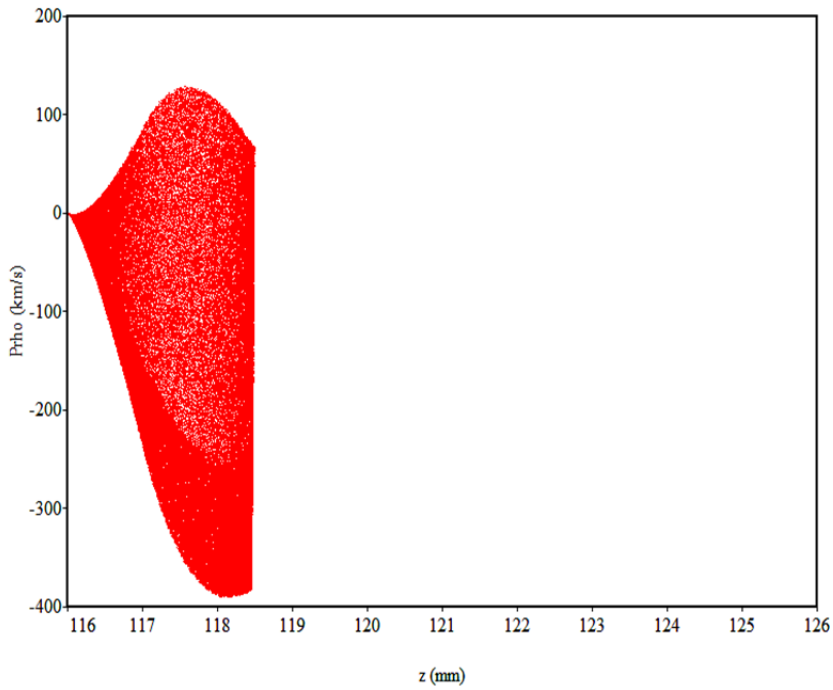

(a) Phase profile of electrons along AK at 1.3ns.

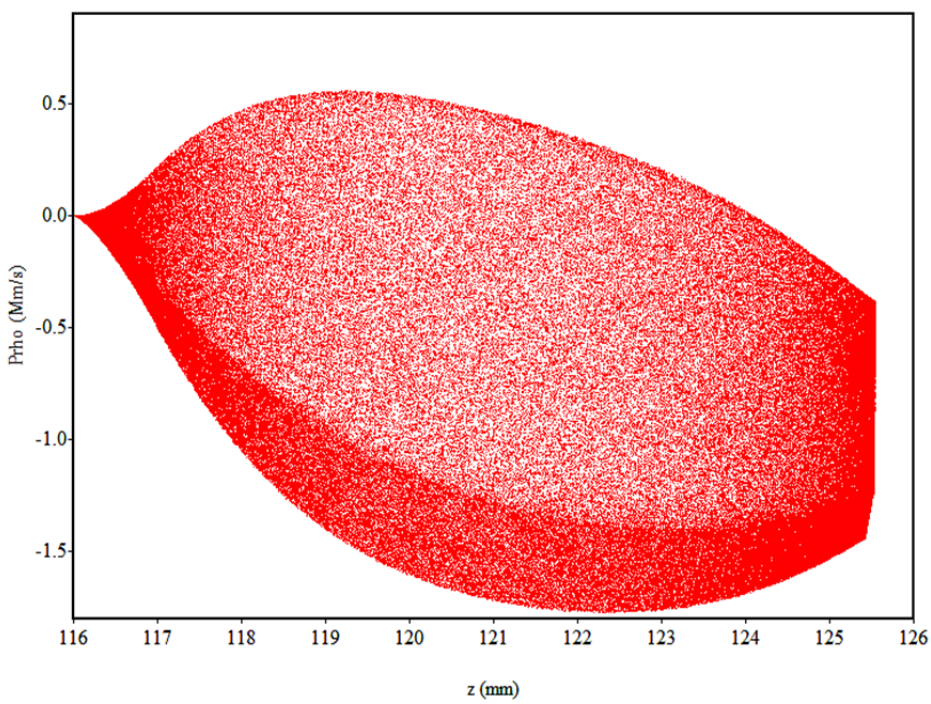

(b) Phase profile of electrons along AK gap at 1.7ns.

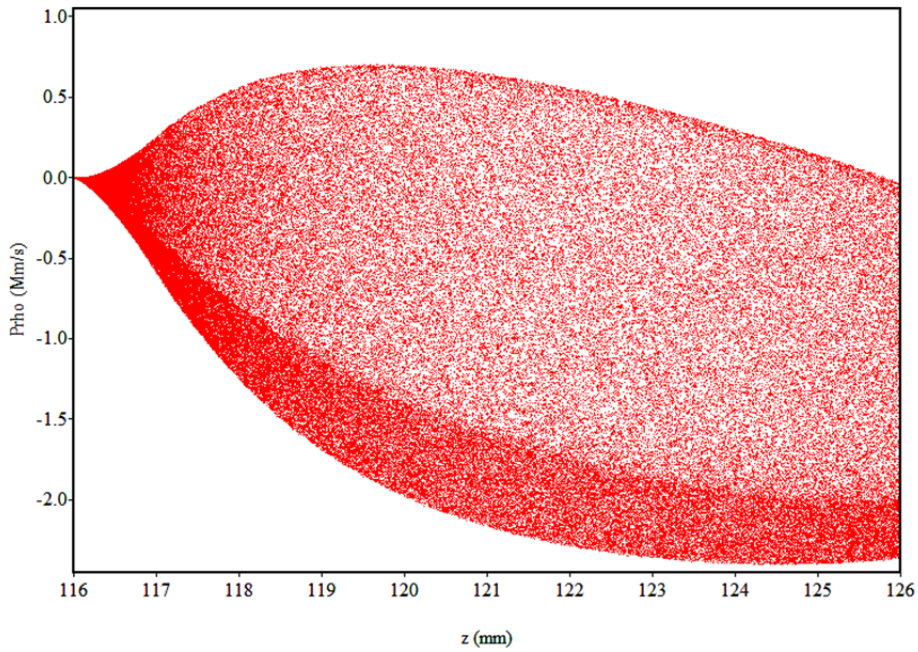

(c) Phase profile of electrons along AK gap at 2ns.

Figure 3.7.Profile of phase space with dielectric

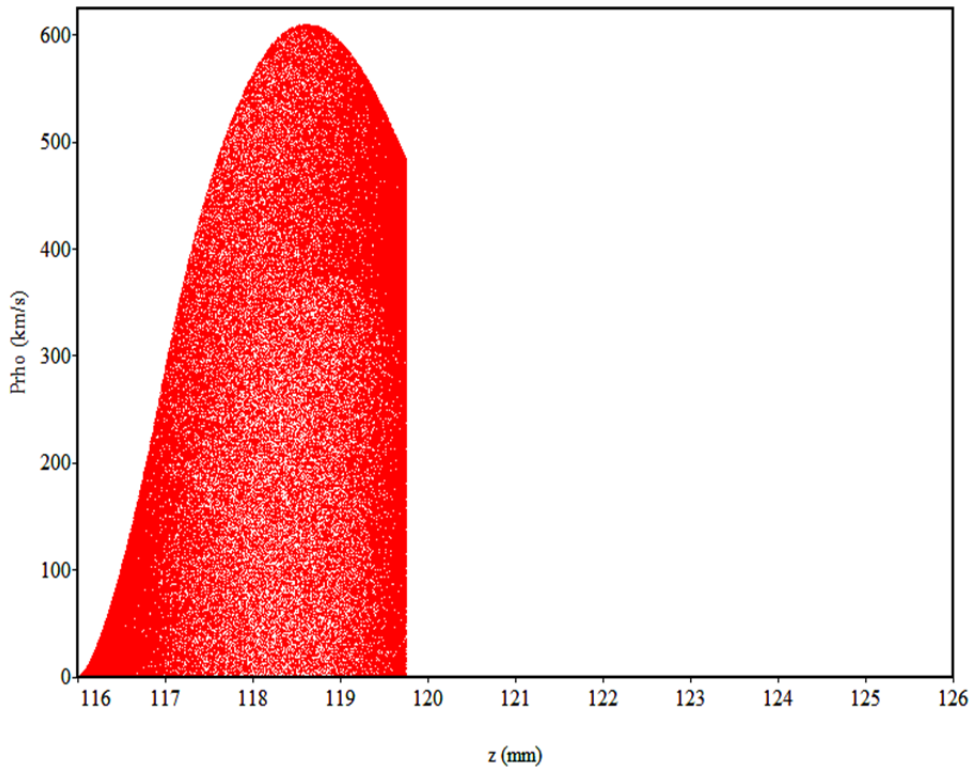

(a) Phase profile of electrons along AK gap at 1.3ns.

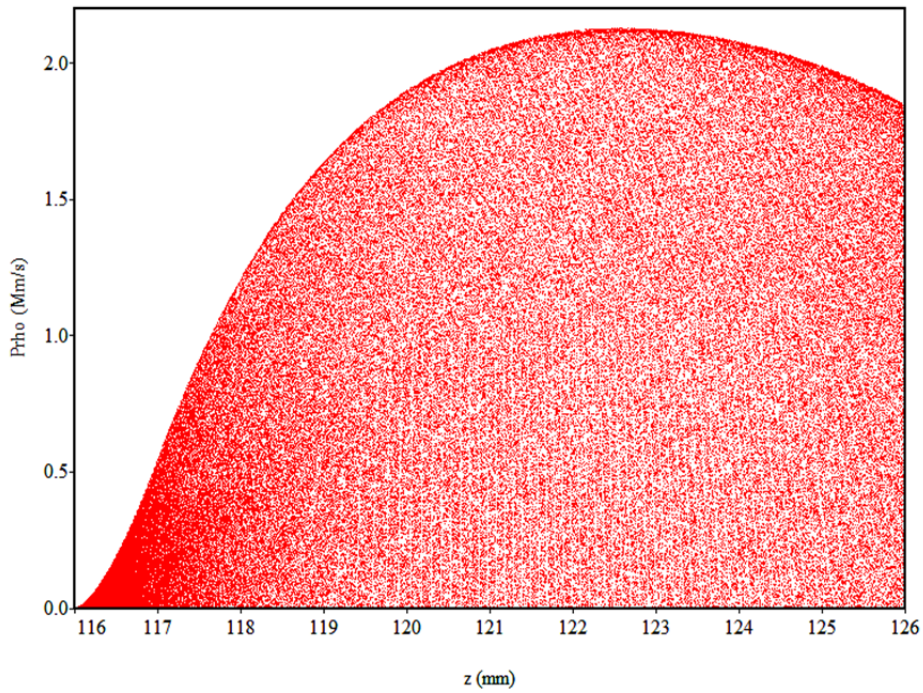

(b) Phase profile of electrons along AK gap at 1.7ns.

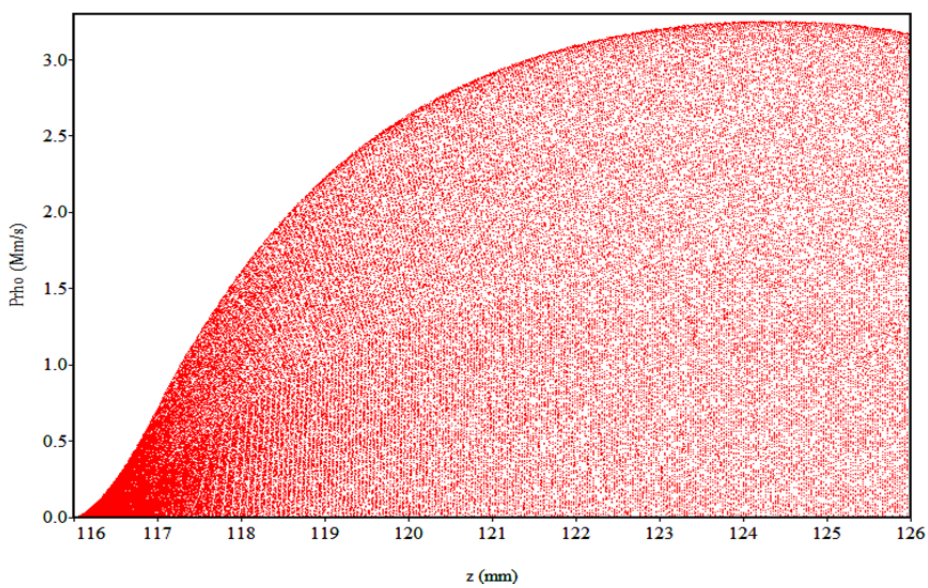

(c) Phase profile of electrons along AK gap at 2ns.

Figure 3.8 Profile of phase space without dielectric

However in case of the plain gas gap conditions the electrons show a directed nature as seen in Figure 3.8 .Even no such reduction in the momentum of electrons is observed in the plane gas gap conditions.

Figure 3.9 shows the charge density profile in the gas gap with and without insulator at different durations of the applied pulse.

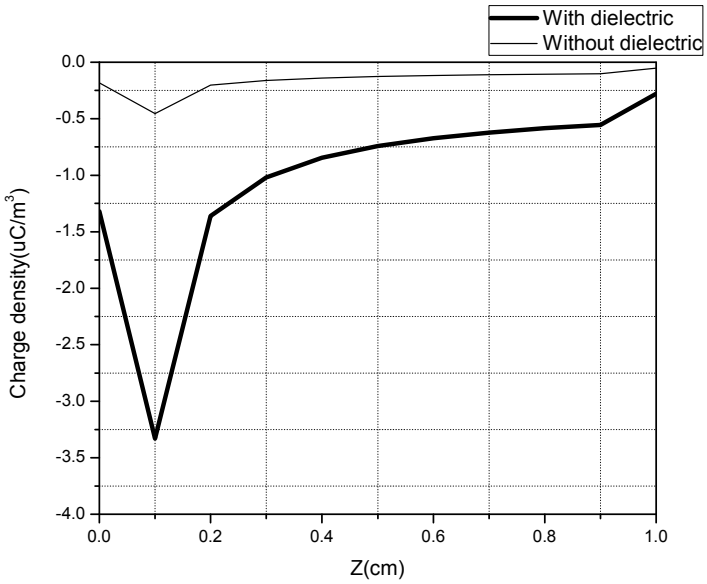

(a) Charge density profile with and without dielectric at 25ns

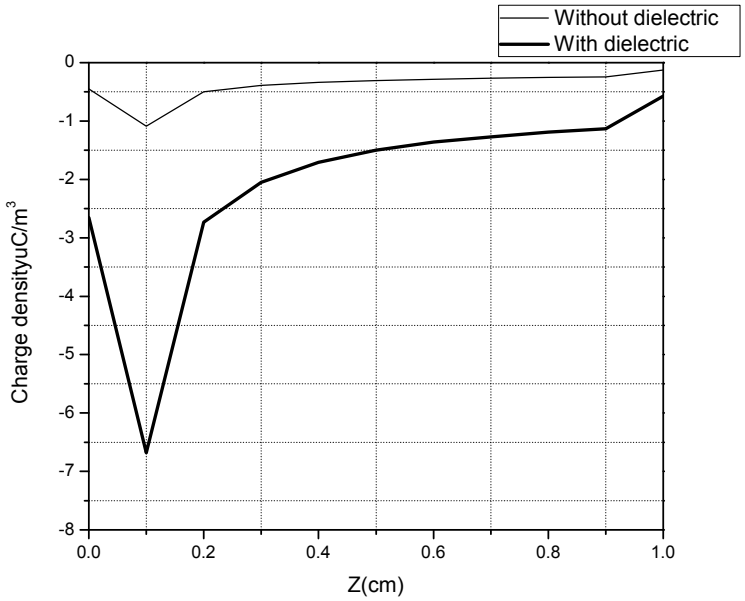

(b) Charge density profile with and without dielectric at 50ns

Figure 3.9 Charge density profiles along normalized z-axis

An increase in the charge density along the insulator surface implies secondary electron emission along the surface which travels along with the primaries towards the cathode leading to a higher

value of field distortion along the insulator surface which in turn reduces the breakdown voltage. A peak charge density of nearly 6.5μC/m^3 is obtained along the insulator surface. The variations in the profile of charge density are found to be similar to the results carried out by Srivastava in which charge on the insulator surface was measured by means of capacitive probes [114].

The particle statistics in the gas with and without an insulator is shown in Figure 3.10.

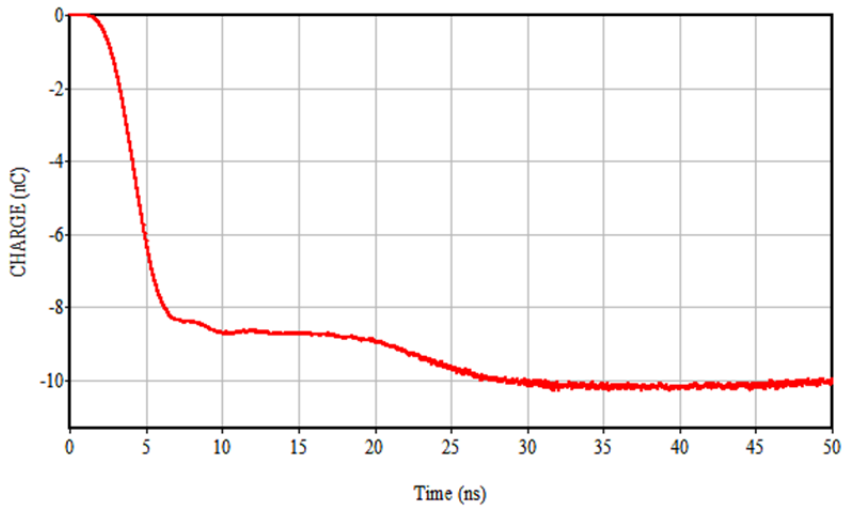

(a) Without dielectric

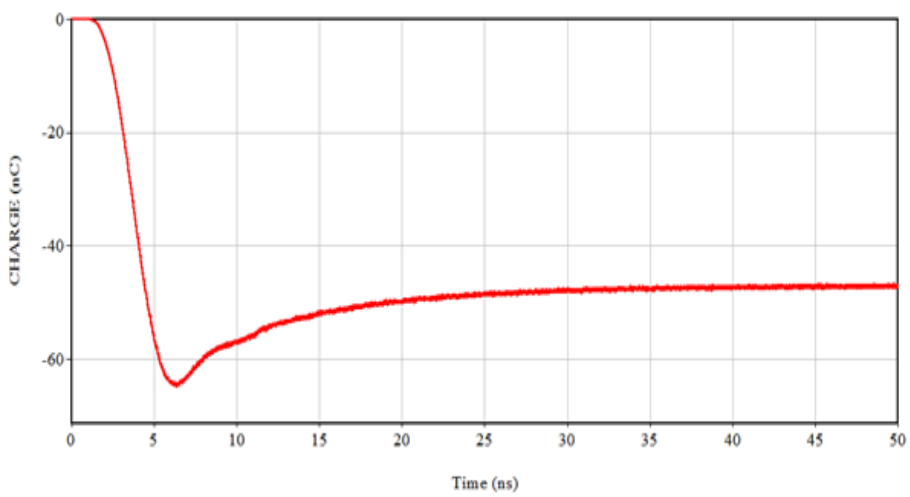

(b) With dielectric

Figure 3.10 Particle statistics in the simulation volume

The presence of an insulator leads to an increase in the net charge along the AK gap pointing towards the generation of secondary electrons along the insulator surface and hence an increased

ionization in the gas gap.

The comparison of velocity versus electron density profile for dielectric and non-dielectric case is shown in Figure 3.11. An increase in the number density of the electrons along the insulator surface at the same velocity indicates the presence of a low pressure region close to the insulator surface which gives a lesser opposition to the flow of electrons and positive ions and also a reduced recombination with the neutral gas molecules.

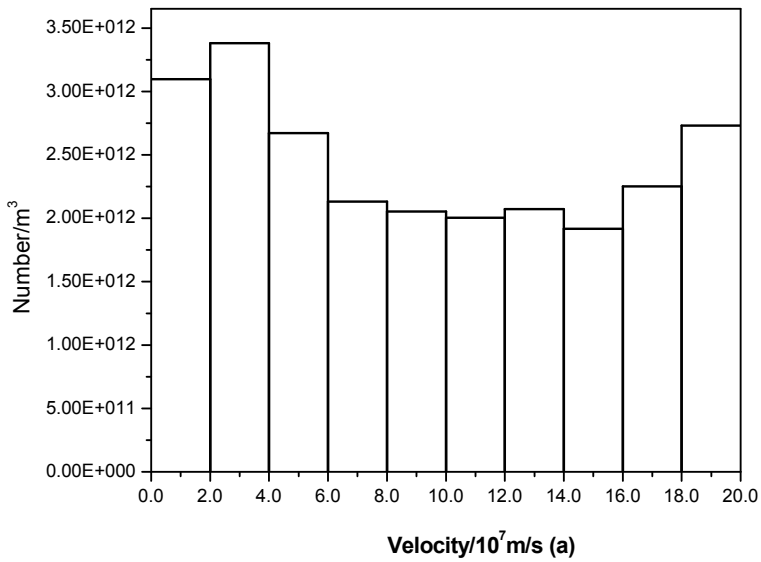

(a) With dielectric

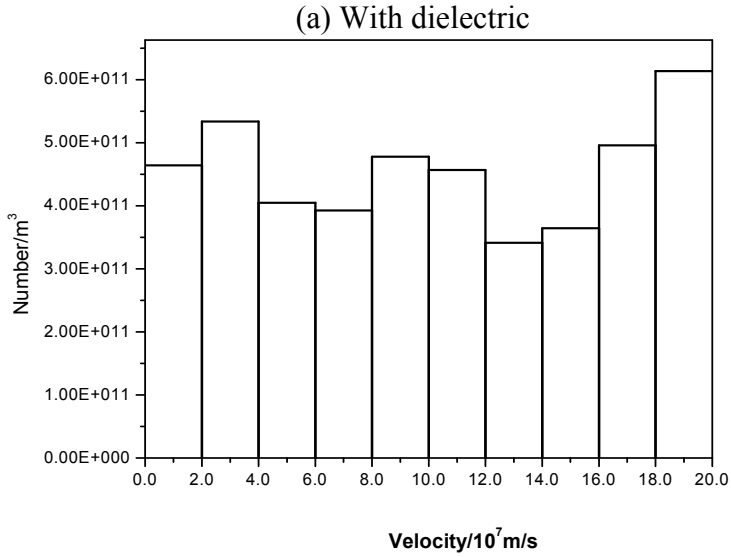

(b) Without dielectric

Figure 3.11 Histograms of velocities

The peak value of electron number densities is 3.38 x10^{12} m^{-3} in the presence of dielectric as compared to 6.14 x10^{11} m^{-3} in a plain gas gap condition in a velocity range from 0-20 x10^{7} m/s which highlights secondary electron emission along the insulator surface as a dominant factor for insulator flashover.

The variation of pressure along the AK gap is calculated using equation 3.30 and is shown in Figure 3.12

$$P=n_T K_B T \tag{3.30}$$

where n_T is the number density of gas molecules ,K_B is the Boltzmann's constant and T is the temperature. However along the gas gap the pressure is same throughout which leads to a reduced number of electrons along the gap as generated electrons and ions are constantly swept away by the gas molecules before they reach the anode. This also indicates the movement of secondary and subsidiary avalanches along the insulator surface as proposed by Jaksts and Cross[115].

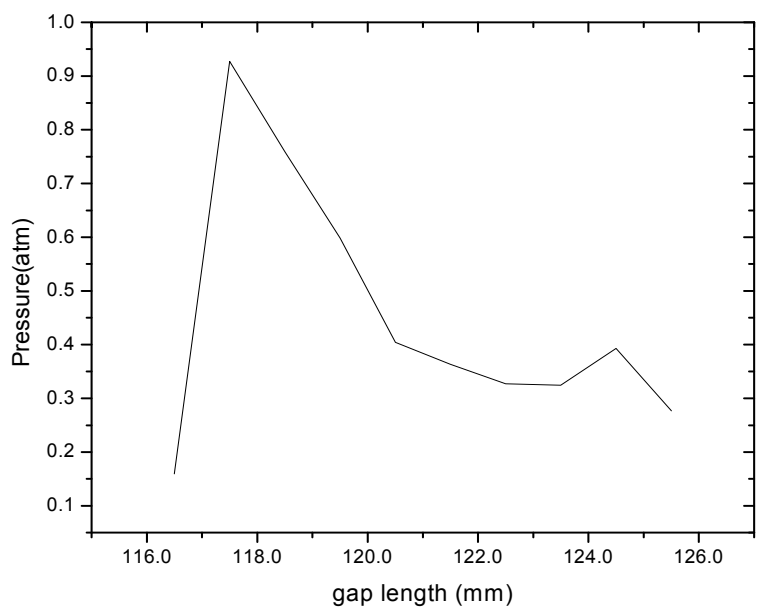

Figure 3.12 Pressure profile along the AK gap

The results of drift velocity (Ve) and ionization co-efficient (α/p) as a function of E/p in nitrogen

gas with and without the dielectric are shown in figure 3.13 and 3.14. Suppression in ionization growth and drift velocity is observed in an insulator bridged gap. This is as a result of enhancement of electric field near the cathode triple junction. Most of the electrons in an avalanche are created in the half of the gap towards anode. Therefore the majority of electrons are produced in a reduced electric field which leads to the reduction in the drift velocity and the ionization coefficient. The results obtained are in agreement with experimental results obtained by Mahajan [116].

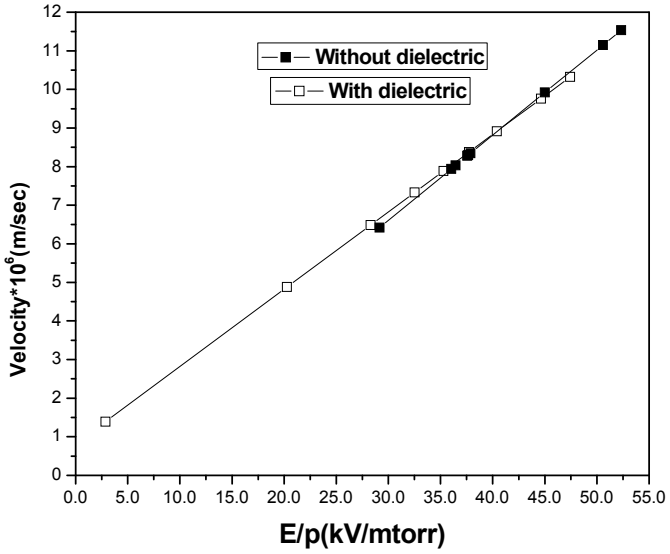

Figure 3.13 Drift velocity (Ve) vs E/p

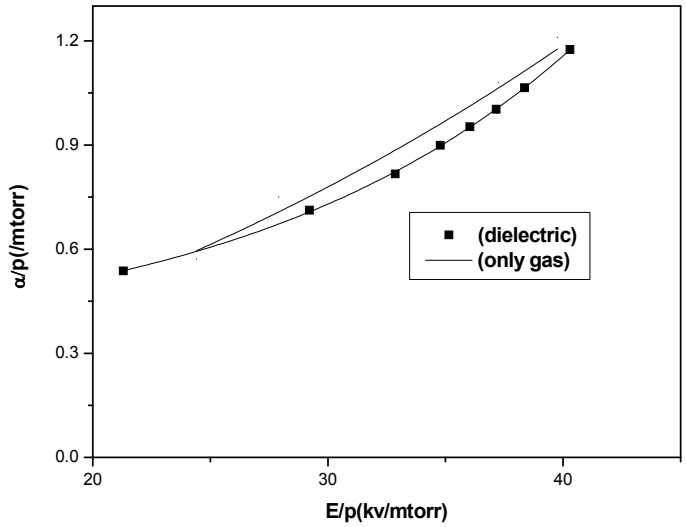

Figure 3.14 α/p vs E/p

Figure 3.15 and 3.16 shows the voltage profile of a plain gas gap and an insulator bridged gap respectively.

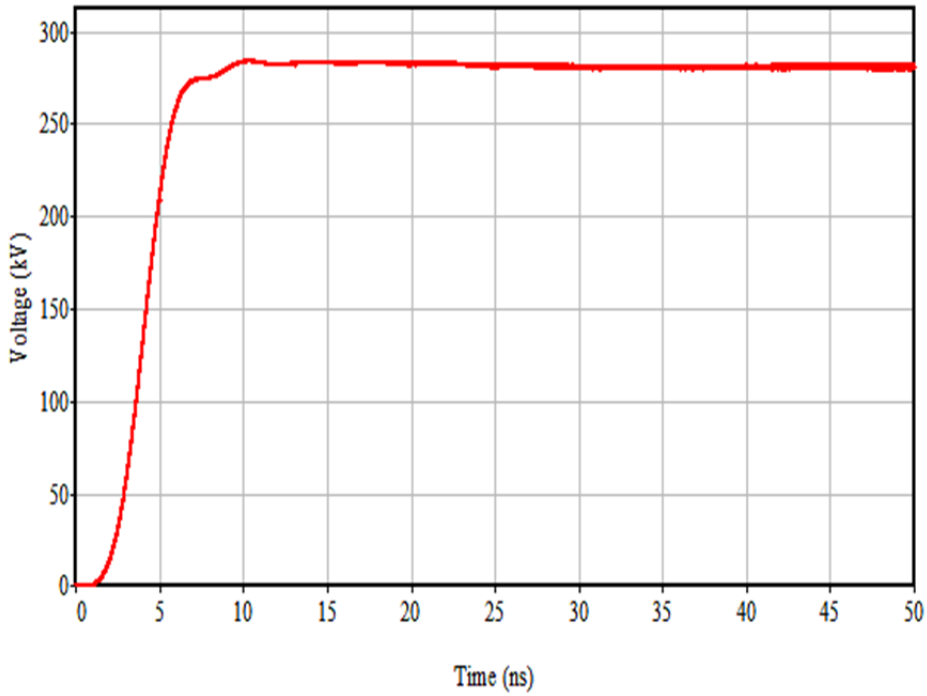

Figure 3.15 Voltage profile in a plain gas gap

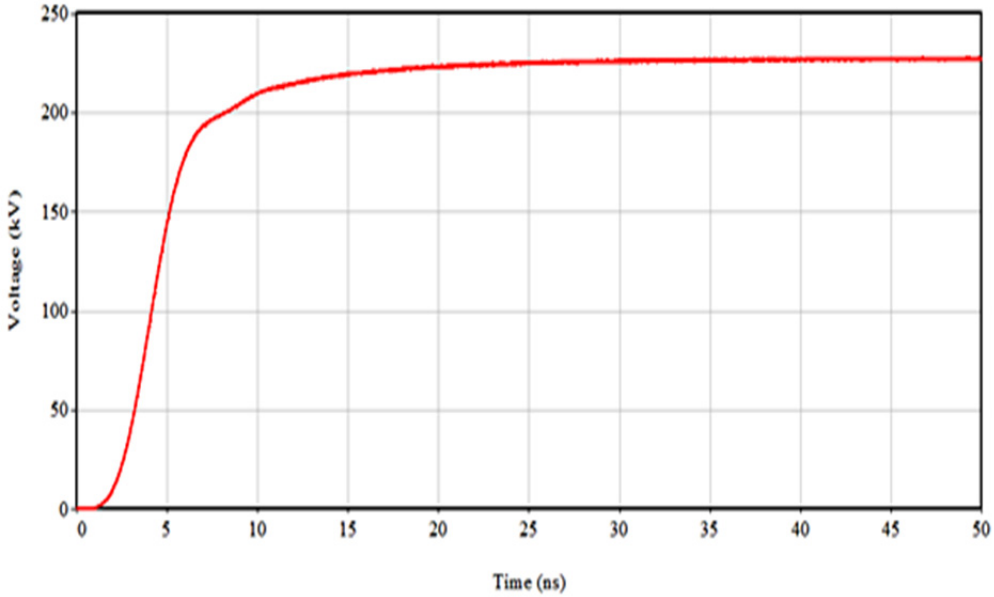

Figure 3.16 Voltage profile in an insulator bridged gas gap

A reduction in the output voltage in an insulator bridged gas gap can be explained on the basis of modification of space charge distribution along the insulator surface. As the electron avalanches propagate near the insulator surface, it produces image charges within the solid dielectric. Therefore the local electric field is modified by image charges within the dielectric. Thus the net effect is reduction in the electric field at the head of the avalanche and hence a reduced voltage in an insulator bridged gap unlike the plain gas gap. The spacer efficiency which is defined as a ratio of flashover voltage in an insulator bridged gap to the voltage plain gas gap condition is 81%. The results are found to be in agreement with the experimental results carried out by Laghari for the determination of spacer efficiency [107].

Figure 3.17 and 3.18 shows current density profile in an insulator bridged gap and a plain gas gap respectively. The current density profile follows the applied voltage which indicates that emission from cathode depends on the applied voltage.

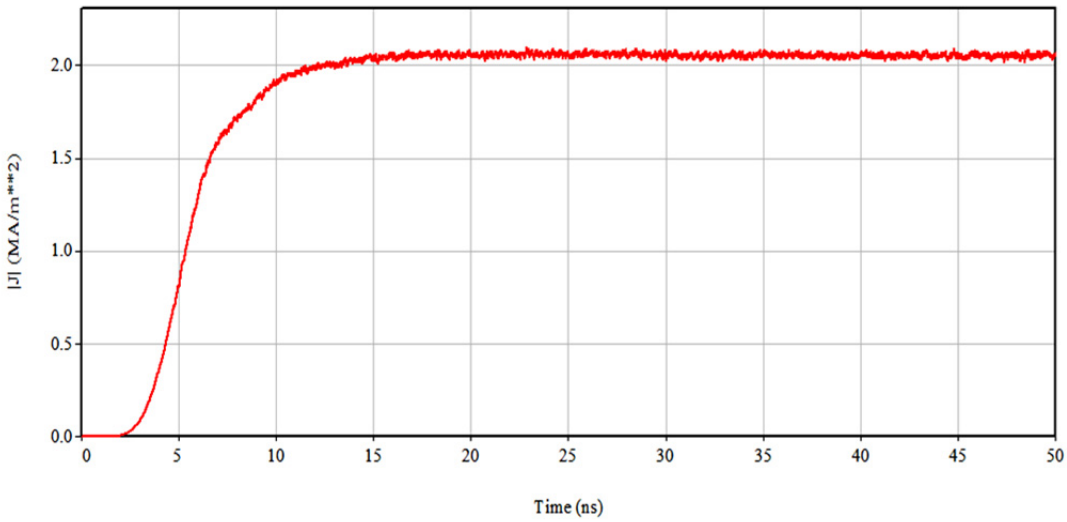

Figure 3.17 Current density profile in an insulator bridged gap

A reduction in the value of the current density in case of an insulator bridged gas gap can be

attributed to the higher resistivity offered by the insulator unlike the plain gas gap whose resistivity is lower than that of the insulator.

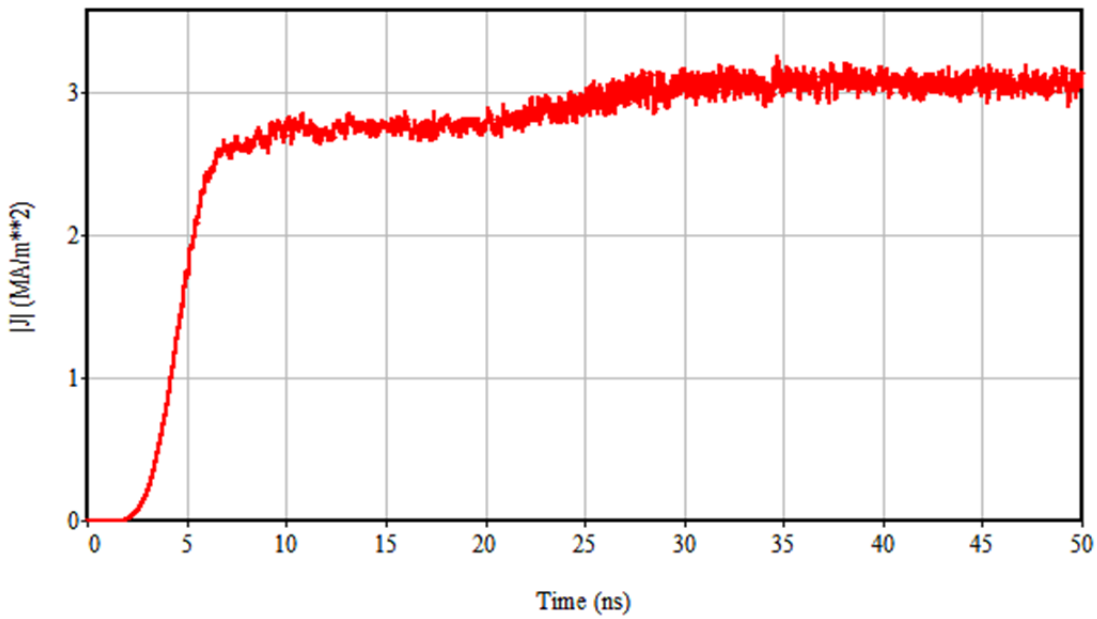

Figure 3.18 Current density profile in a plain gas gap

3.8.4 SUMMARY

An FDTD based particle –in cell code based on the models of explosive electron emission, secondary emission and gas ionization is developed to study the discharge along the gas-solid interface. A reduction in the momentum of electron along the dielectric -gas interface takes place when compared to the plain gas gap. A spacer efficiency of nearly 81% is observed in an insulator bridged gap .An increase in the net charge in the simulation volume in the presence of an insulator highlights the secondary electron emission along the insulator surface as the dominant mechanism of breakdown in an insulator bridged gap.

The reduction in the drift velocity and ionization coefficient indicates the suppression of avalanches along the insulator surface and results are found to be in close agreement with the

existing experimental data. Further studies are carried out in chapter 4 to analyze the effect of changes in the spacer geometry and its surface conditions on spacer efficiency.

CHAPTER 4

EFFECT OF SPACER SURFACE AND GEOMETRY USING PIC SIMULATION

4.1 Introduction

Particle-in-cell simulations of non-uniform electrode geometry in pressurized gases give a corona discharge which changes to a glow discharge as the pressure is reduced [117].The presence of an insulator in the AK gap leads to field enhancement and breakdown at a reduced voltage. The design of insulators forms a major part in high voltage systems and the development of arc along the insulator surface is of prime importance in the design of suspension insulator[118].The spacer play a critical role in blumlein pulse forming line (PFL) based high voltage pulse power systems. Blumlein consists of two PFL one between the outer and intermediate conductor and the other between the inner and intermediate conductor [119-120]. The advantage of blumlein PFL is that it reduces the voltage requirements on the charging system. However it consists of support insulators between the conductors the design of which is of considerable importance for reliable operation at high voltages. The presence of spacer in compressed gases significantly reduces the breakdown voltage and increases the speed of propagation of electrons between the electrodes [121].The discharge can start at any point on the surface of the spacer [108] and the high speed photographic study shows a consistent growth of charge carriers along the spacer surface that helps in discharge development [122].

The present chapter involves the study on the impact of spacer geometry and its surface on discharge along a solid -gas interface which is placed between the spark gap electrodes. Section 4.2 describes the modeling technique and the construction of different spacer geometries required for discharge analysis between the spark gap electrodes. Section 4.3 shows the effect of spacer geometry on particle statistics of charge carriers, avalanche growth, voltage and field

profile in the gap and also emphasizes on the variation of charge with voltage for different spacer geometries. Section 4.4 studies the effect of protrusions introduced on insulator surface on discharge along insulator gas interface.

4.2 Simulation model

The model used in the present work is based on 3D FDTD based PIC code which incorporate particles and automatically takes into account the space charge effects [100]. The insulator geometry placed in between the cathode and anode is modified for varying shapes. The electrodes are made of stainless steel with epoxy as the insulator material. The physiochemical processes taking place in the AK gap is described as follows. Nitrogen is used as the background gas at 1 atmospheric pressure with an AK gap distance of 20 mm. The simulations are carried out with explosive electron emission, neutral gas ionization and secondary electron emission models. The electrons emitted from the surface of the cathode strike the neutral gas molecules leading to the production of positive ions and secondary electrons. The ionization cross-section of electrons with the neutral gas molecules is computed as a function of electron energy [103].

The insulator geometry placed in the AK gap is as shown in Figures. 4.1 to 4.4. Two types of conical insulators are used as shown in Figures. 4.1 and 4.2. The spacer angle 'Ɵ' is measured between the inclined surface and line normal to the electrode. The angle is positive when narrow end is connected to the anode and is negative otherwise [123]. A doubled sided frustum geometry is used as shown in Figures 4.3 which is a combination of the geometries used in Figures 4.1 and 4.2. A bush bar shaped geometry similar to the one used in suspension insulators is placed between the spark gap electrodes as shown in Figure 4.4. A plain cylindrical geometry is introduced in Figure 4.5 which is used for comparison with remaining spacer geometries. A voltage pulse with a rise time of 5 ns and pulse duration of 50 ns (FWHM) is used as the input

pulse .

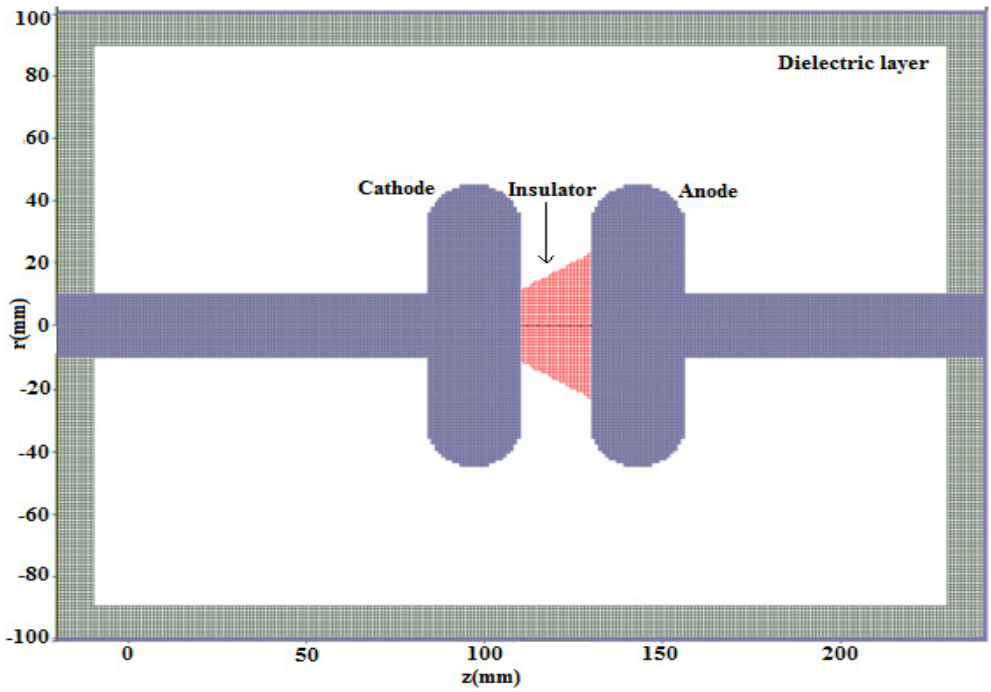

Figure 4.1 Negative Angled geometry

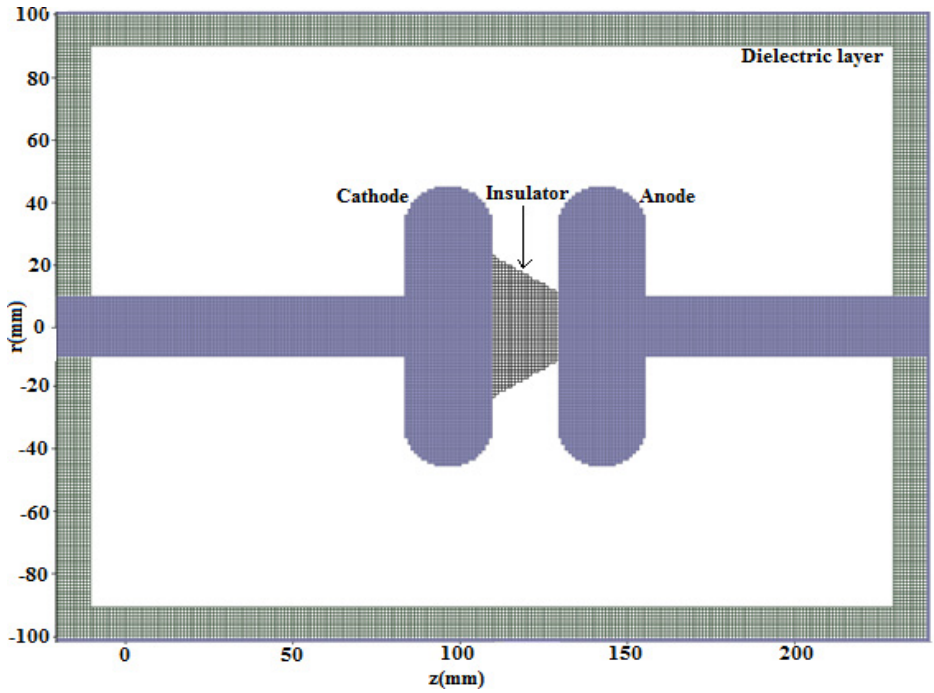

Figure 4.2 Positive Angled geometry

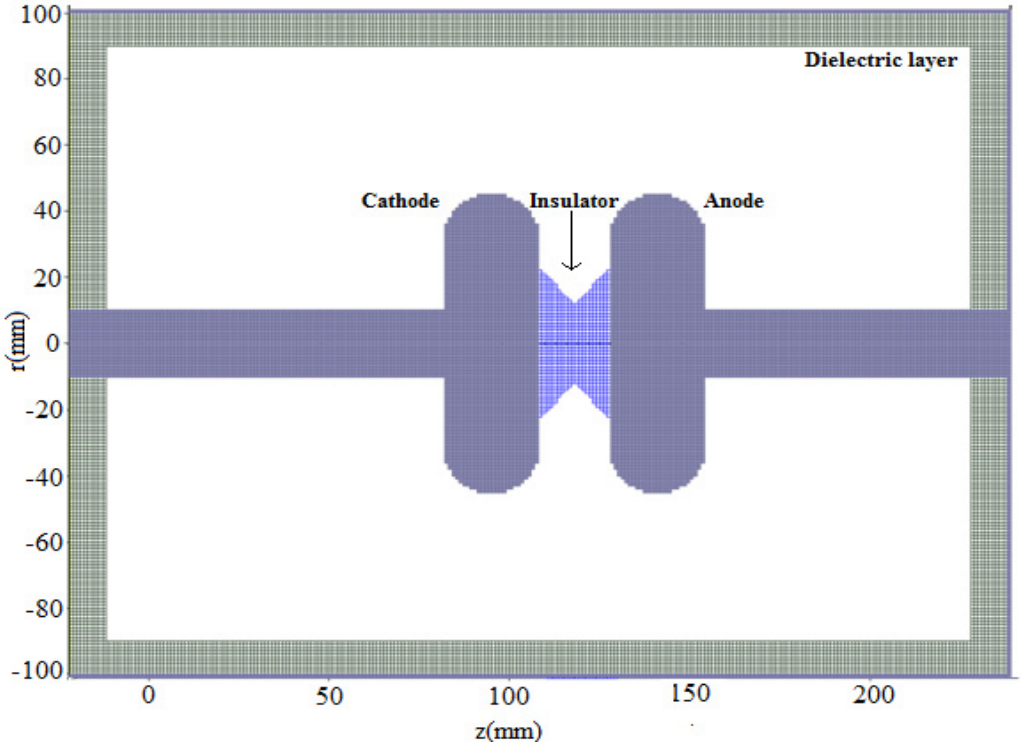

Figure 4.3 Double sided frustum geometry

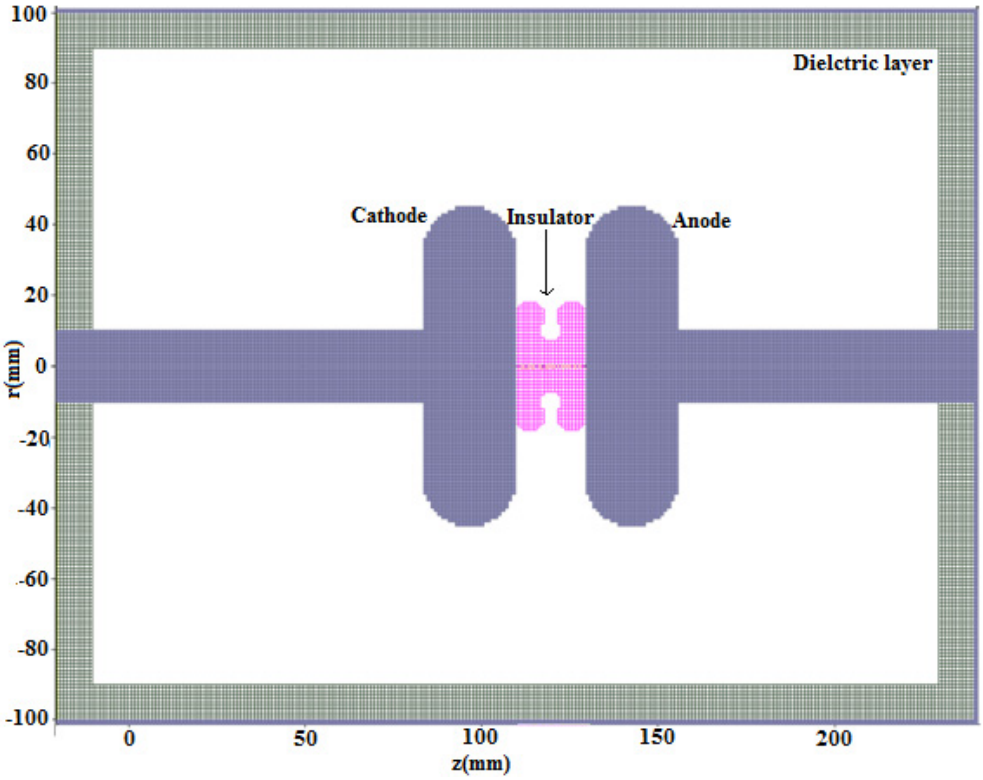

Figure 4.4 Bush bar geometry

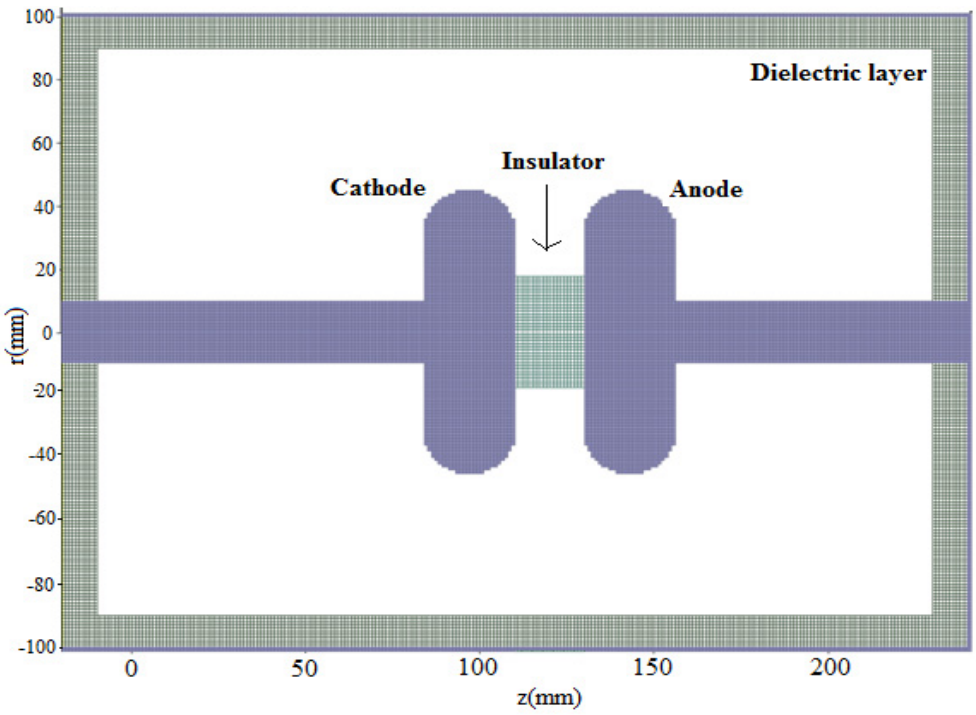

Figure 4.5 Cylindrical geometry

4.3 Results and discussion

4.3.1 Effect on particle statistics

The Figure 4.6 shows the particle statistics for the different spacer geometries placed in the AK gap. It is observed that for spacer geometry shown in Figures 4.1 and 4.4 the electrons emitted from the surface of the cathode encounter obstruction in the path of the motion of electrons towards the anode due to the spacer profile and hence less ionization takes place in the gap and along the surface of the insulator leading to a very low net charge buildup in the gap. However the positive angled spacer geometry provides no hindrance in the path of the motion of electrons like the plain cylindrical geometry leading to earlier ionization and higher emission of secondary electrons from the surface of the insulator leading to an increase in the net charge in the gap. The double sided frustum geometry behaves like a positive angled spacer till middle of the gap leading to net increase in charge. As the mid gap is reached the space charge so formed aids in

further ionization leading to highest net charge unlike all the remaining geometries.

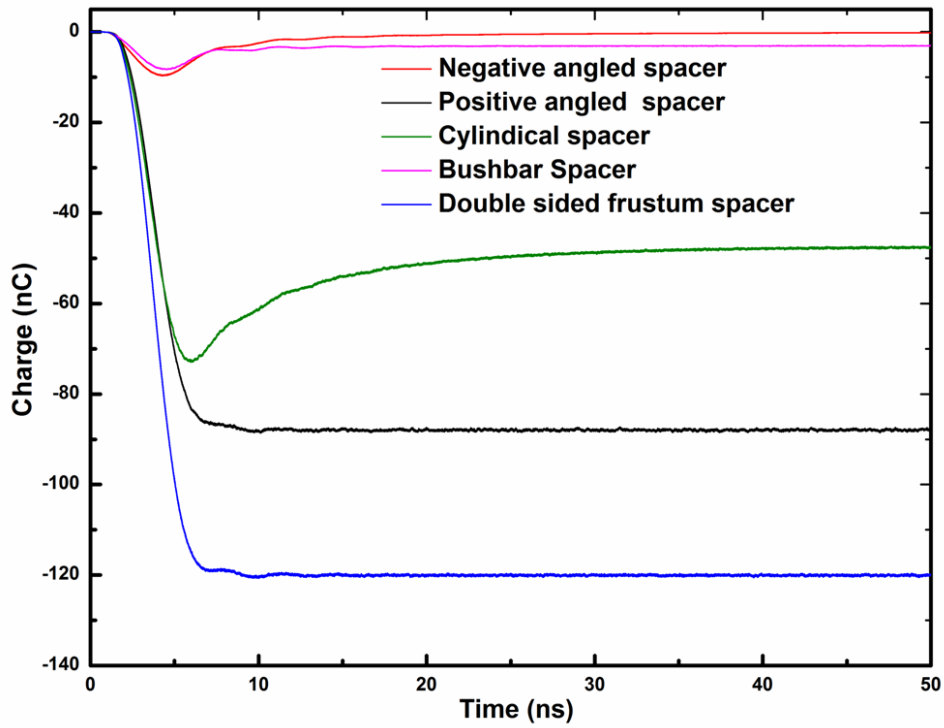

Figure 4.6 Charge in the gap for different spacer geometries

4.3.2 Effect on avalanche growth

The Figure 4.7 shows the avalanche growth in gases along the surface of insulator based on Longmire –Longley model of breakdown in gases as described in detail in chapter 3 which is modified to take nitrogen into consideration. It is observed that the avalanche growth in the gap follows the spacer profile. In the case of a plain gas gap, there is a continuous rise in the avalanche growth, whereas in the case of cylindrical insulator, the avalanche growth is suppressed. For the remaining geometries the growth follows the electric field leading to the variation in the discharge voltage. The bush bar spacer has hollow profile in the middle of the gap as shown in Figure 4.4 which leads to increased ionization in that region and a dip in ionization near the cathode and anode regions because of the reduced volume of the gas gap. The

presence of dip at centre in case of double sided frustum spacer like the bush bar spacer leads to a rise in avalanche growth at centre near 10mm. However as the half of the gap is reached more ionization takes places along the insulator surface than in the gas volume leading to suppression in the avalanche growth near the anode.

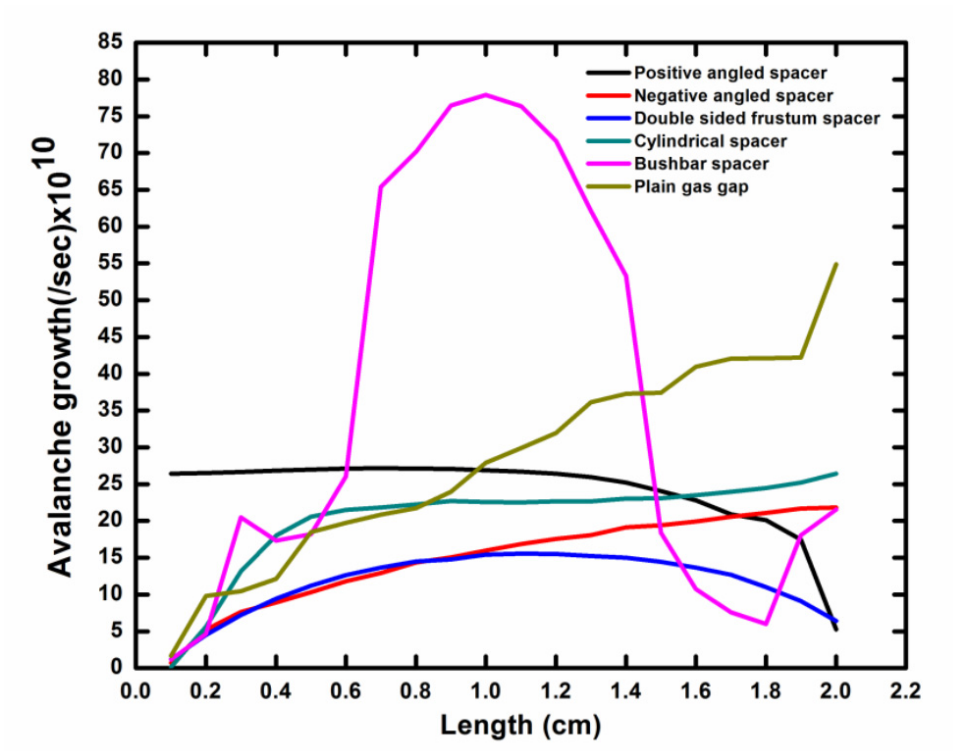

Figure 4.7 Avalanche growths in the gap for different spacer geometries

4.3.3 Effect on voltage profile

The Figure 4.8 shows the voltage profile of different insulator geometries. It is clearly observed that a maximum voltage of nearly 400kV is observed in case of the negative angled spacer and bush bar spacer. The negative angled spacers and the bush bar spacers provide a longer tracking path for electrons emitted from the surface of the cathode towards anode, and in the process reducing the secondary electron emission from insulator surface, ultimately leading to a net decrease in net charge in the gap as shown in Figure 4.6. The positive angled spacer geometry

provides a path of low pressure close to the insulator surface like the cylindrical insulator which aids in earlier ionization and secondary electron emission from the insulator surface and leads to net increase in net charge in the gap as shown in Figure 4.6 thereby leading to a reduced voltage of 323 kV. This is close to the plain cylindrical geometry which has a voltage of 354 kV as shown in Figure 4.8. However a low voltage of 297 kV is observed in case of double sided frustum geometry. This is because of the fact that half of the geometry is similar to positive angled spacer resulting in earlier ionization and secondary electron emission takes place along the insulator surface. When the half of the gap is reached the energy acquired by the electrons is high enough to strike the insulator surface leading to the faster insulator charging which creates a high value of net charge of 120nC in the gap and resulting in a lowest discharge voltage of nearly 300 kV as shown in Figure 4.8. Spacer efficiency is defined as the voltage along an insulator bridged gap to the voltage across plain gas gap condition [107] is calculated for different spacer geometries. Table 4.1 shows a comparison of spacer efficiency for the above geometrical configurations. The highest spacer efficiency is observed in bush bar and negative angled spacer geometries and hence can be very useful as support insulators in blumlein PFL.

Table 4.1 Comparison of spacer efficiency for the different geometrical configurations

S.No	Spacer geometry	Spacer efficiency
1.	Negative angled spacer	97%
2.	Positive angled spacer	78.8%
3.	Bush bar spacer	97%
4.	Double sided frustum spacer	72%
5.	Cylindrical spacer	86%

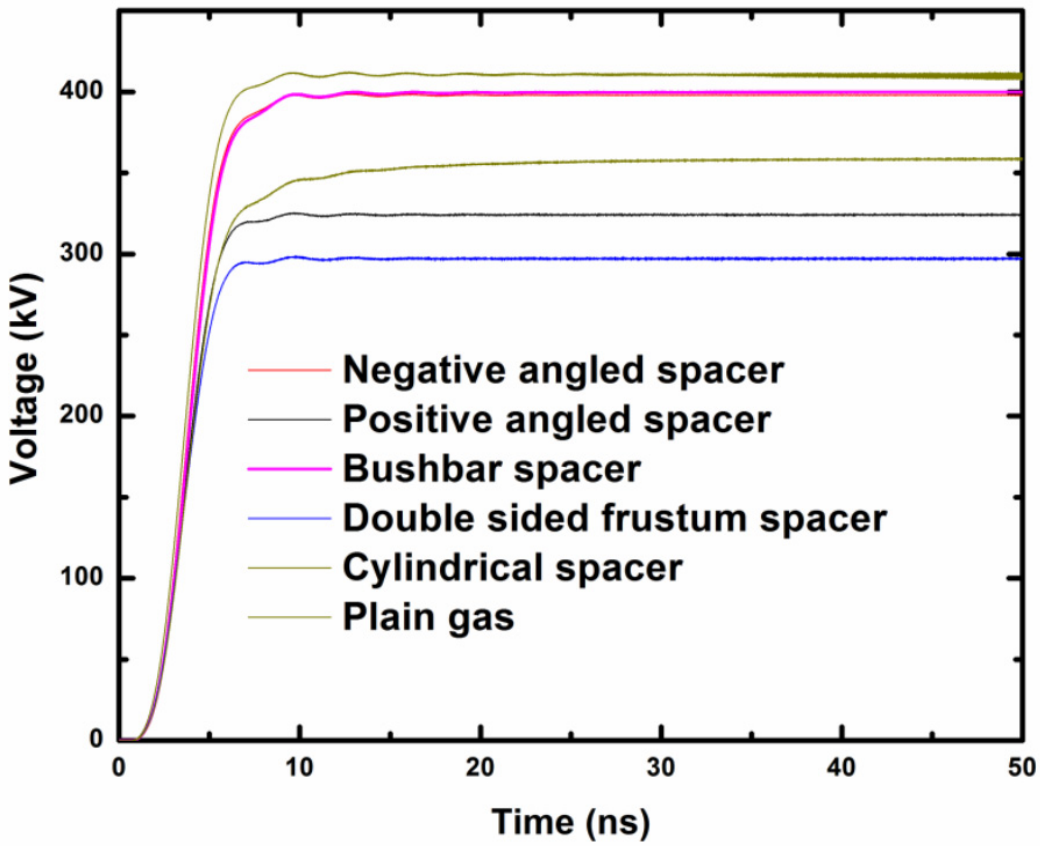

Figure 4.8 Voltage profile in the gap for different spacer geometries

4.3.4 Effect on electric field variation in the gap

Further study has been carried out to analyze the variation of electric field profile in the gap for different spacer geometries and is shown in Figure 4.9.The electric field in the gap follows avalanche growth profile which governs the mechanism of the discharge process for different spacer profiles. The double sided frustum spacer has highest field at cathode among all the spacer profiles. The field near the centre is maximum (174 kV/cm) with reduced values at both the electrode ends. The bush bar spacer and negative angled spacer with highest spacer efficiencies has reduced field enhancement at cathode which grows towards the anode leading to highest discharge voltage in both the spacer profiles. The electric field for plain cylindrical

geometry has a continuous growth along the gap. The electric field near the cathode for negative angled spacer shows a slight dip as observed in Figure 4.9 which leads to lesser field enhancement near the cathode and hence a higher discharge voltage. The positive angled spacer has higher field enhancement at cathode as compared to a plain and negative angled spacer but the field growth along the gap is less as compared to the plain and negative angled geometry and hence reduced discharge voltage in the gap.

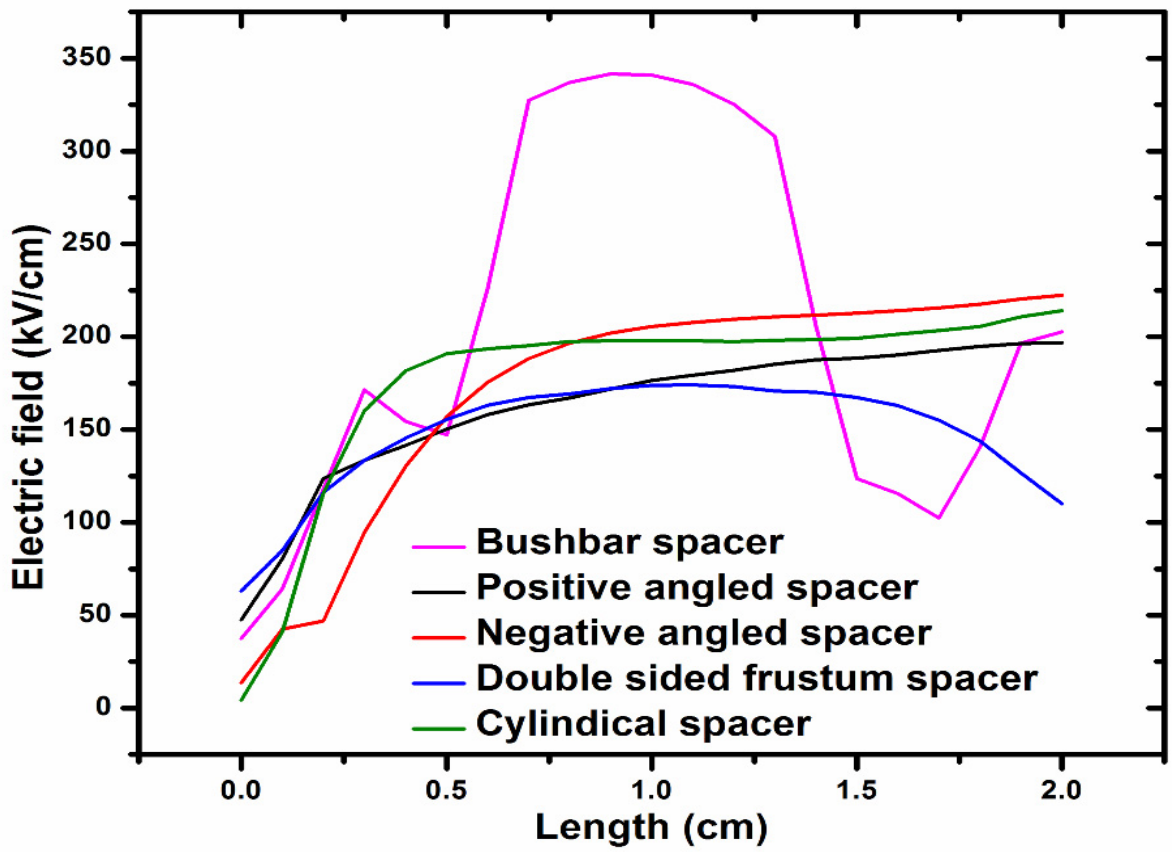

Figure 4.9 Field profile in the gap for different spacer geometries

4.3.5 Effect on variation in particle statistics with discharge voltage

The Figure 4.10 shows the charge as a function of voltage profile for a bush bar spacer. The triple point in case of bush bar geometry is hidden and the geometry of the spacer leads to

discontinuity in the path of the electrons. Moreover due to a large space charge the electric field at the cathode reduces after 10-15ns .This leads to reduction in the emission from the triple point which is responsible for the decrease in the charge with the buildup of voltage.

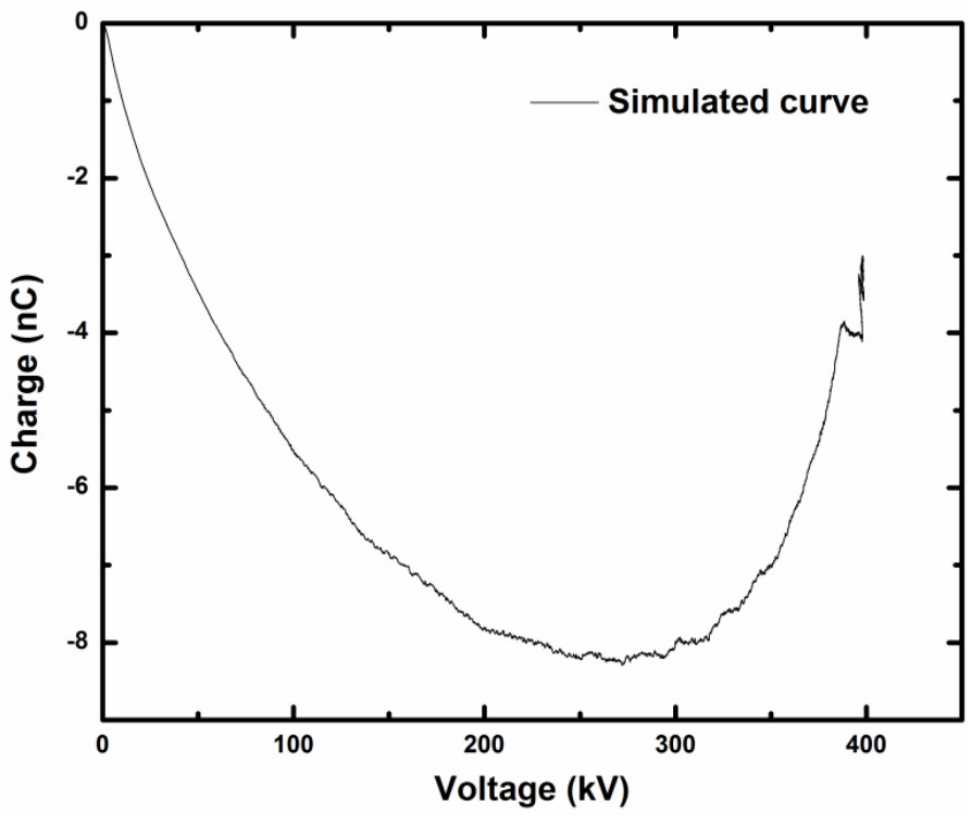

Figure 4.10 Charge vs voltage for bush bar spacer

There is no discontinuity in the path for electron movement in case of positive angled spacer and the exposed triple point aids in earlier ionization that leads to a net increase in charge with voltage as shown in Figure 4.11. The negative angled spacer profile leads to a very few electrons reaching the anode and the electrons does not gain enough energy before colliding with the insulator in the intermediate path which leads to less net charge . The path followed by electrons is close to the plain gas gap and in the process recombine with positive ions leading to complete decay in the charge as shown in Figure 4.12.

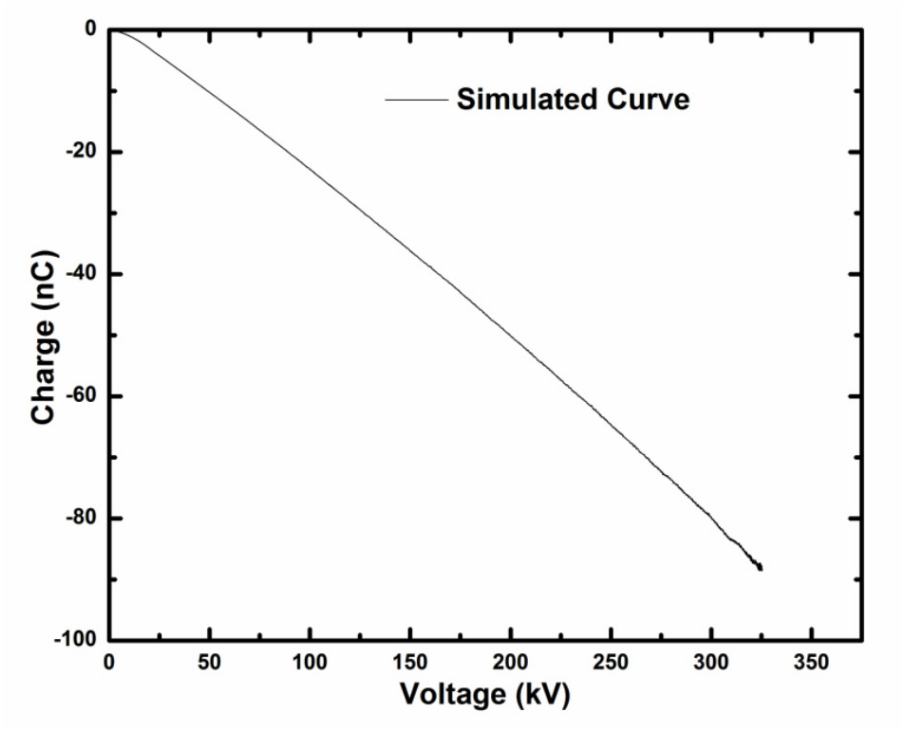

Figure 4.11 Charge vs voltage for positive angled spacer

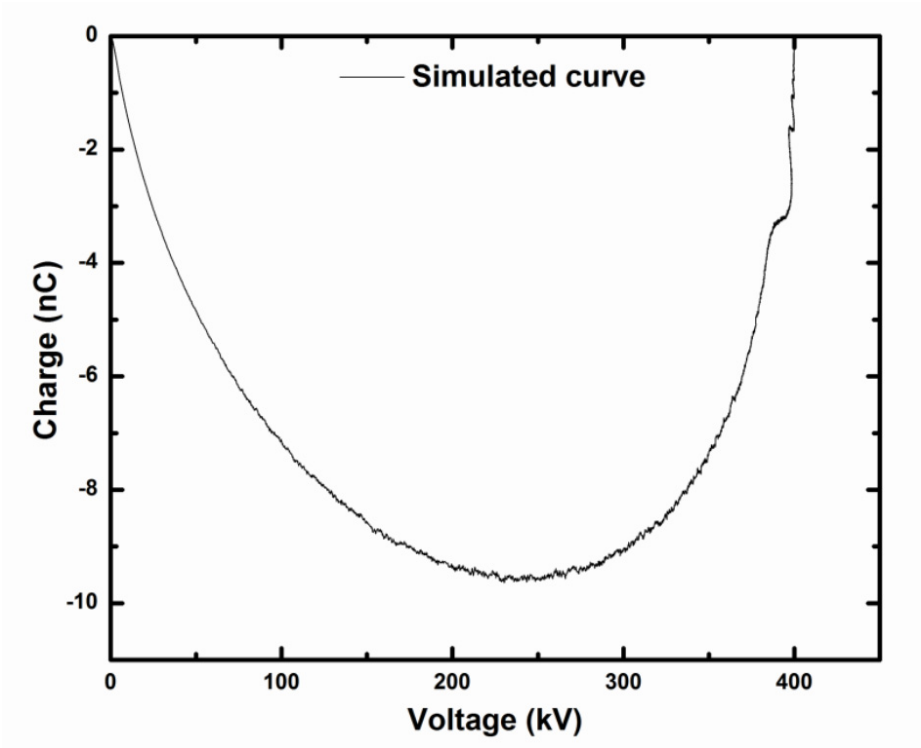

Figure 4.12 Charge vs voltage for negative angled spacer

The double sided frustum geometry aids maximum charge accumulation due to exposed triple point and secondary electron emission along the insulator surface. This geometry has discontinuity in the movement of electrons but this discontinuity increases the electron emission because a large area of insulator is exposed to the electrons emitted from triple point. This leads to the high net charge in the gap with voltage as shown in Figure 4.13.

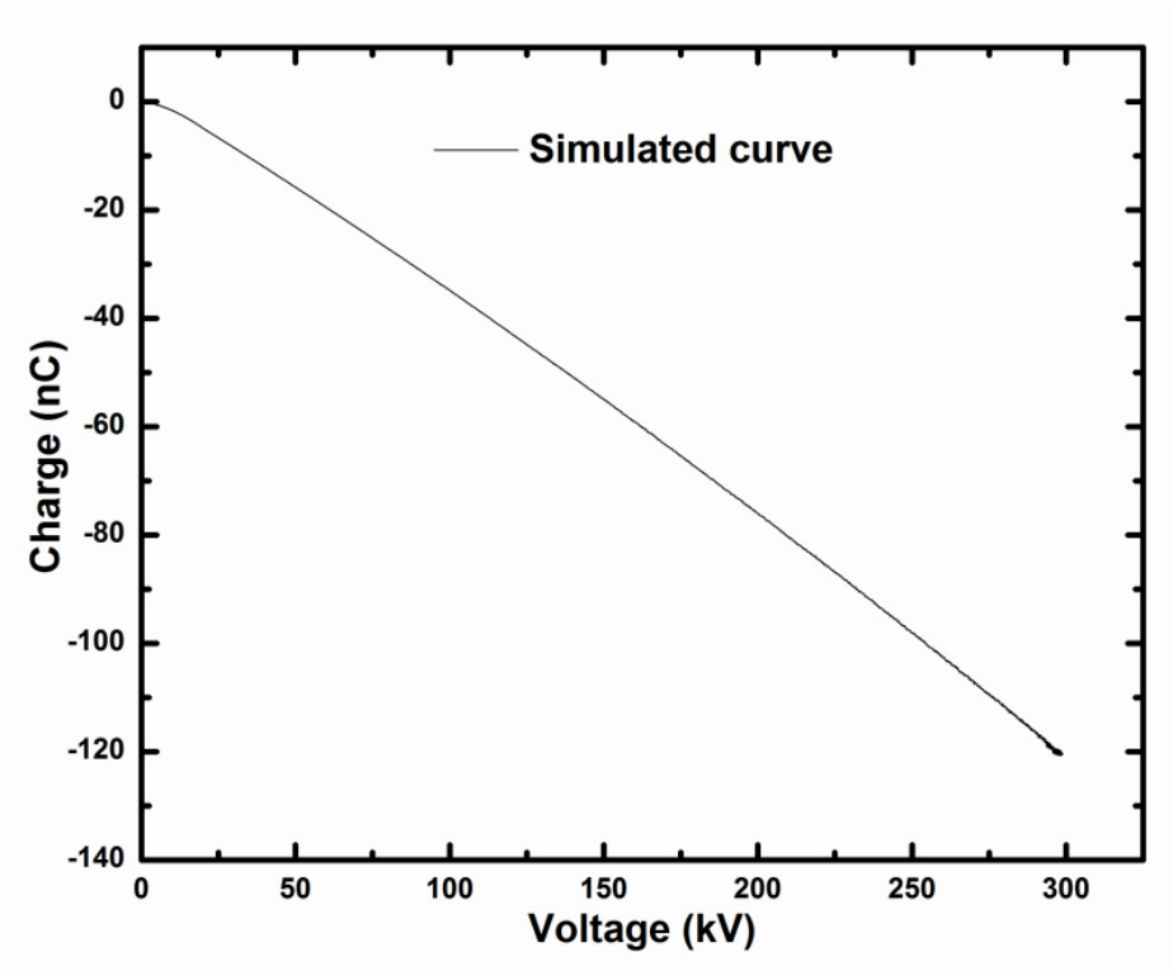

Figure 4.13 Charge vs voltage for double sided frustum geometry

The plain cylindrical spacer follows the charge profile close to the positive angled geometry but the slight less exposed triple point gives less electron emission and the space charge build up leads to slight decrease in net charge after a voltage of nearly 325 kV as shown in Figure 4.14

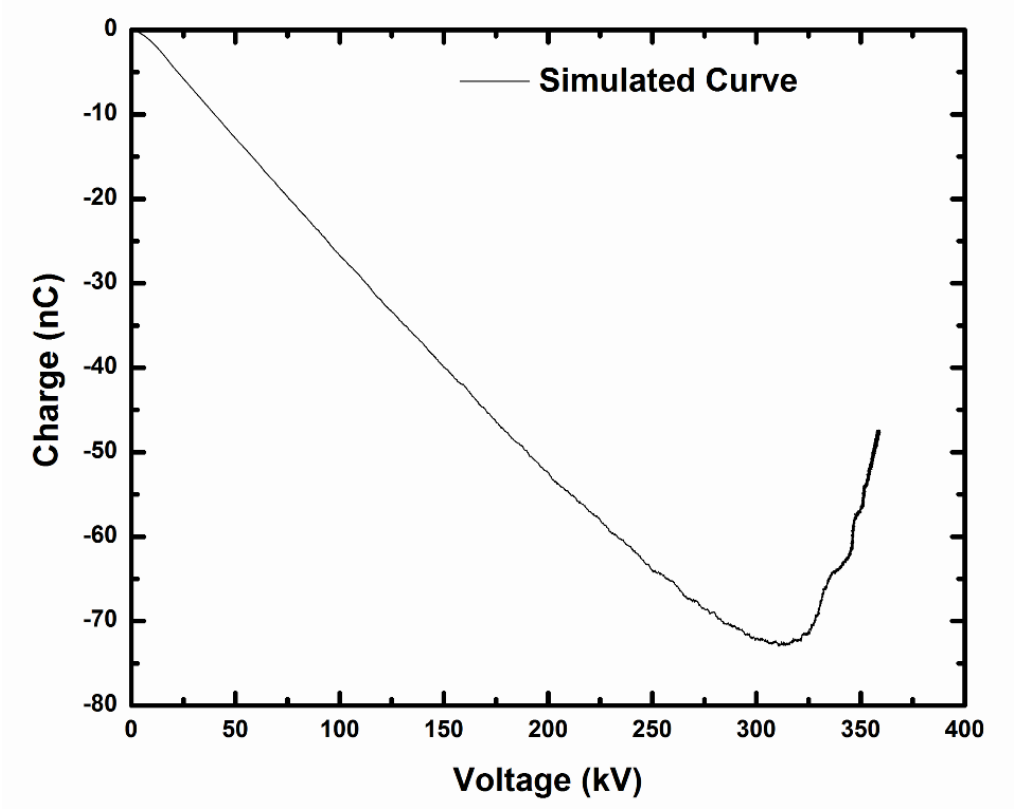

Figure 4.14 Charge vs voltage for plain cylindrical geometry

4.4 Effect of protrusions on insulator surface

The simulation is carried out with teeth on the surface of the insulator which acts as protrusions as shown in Figure 4.15.The simulation mechanism of the discharge process in the AK gap is same as employed for the study of different spacer geometries. The magnified view of a portion of the teeth construction arrangement on the insulator surface is highlighted within the Figure 4.15. A protrusion (teeth) of 1mm with void creation in the subsequent 1mm is introduced along the entire insulator surface. It is observed that for 1 mm teeth height at regular intervals of 1 mm along the surface of the insulator, there is an increase in discharge voltage to 383 kV from 354 kV for a plain cylindrical insulator as shown in Figure 4.8. The presence of teeth along the surface of the insulator leads to a longer tracking path and hence less area of the insulator is exposed to secondary electron emission leading to a higher discharge voltage.

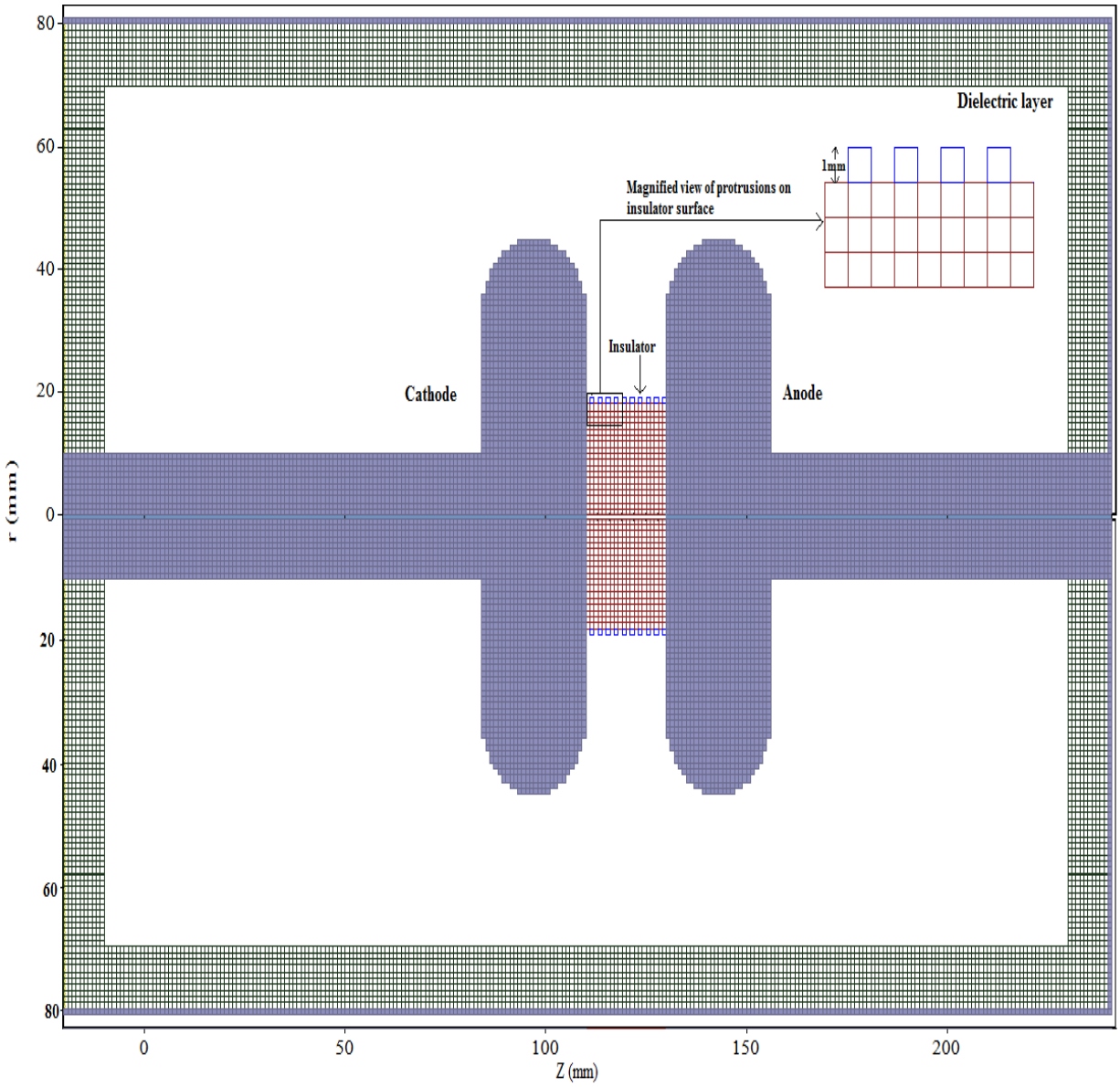

Figure 4.15 Cylindrical spacer with teeth (protrusions) on its surface

However if the teeth height is further increased from 1 mm to 2 and 3 mm the breakdown voltage increases to nearly 400 kV as shown in Figure 4.16 and remains constant because the ionization mainly occurs in the gas and the teeth height further hides the triple point which leads to suppression in secondary electron emission along the insulator surface. This is also justified with field profile in the AK gap due to the increase in teeth height along the insulator surface.

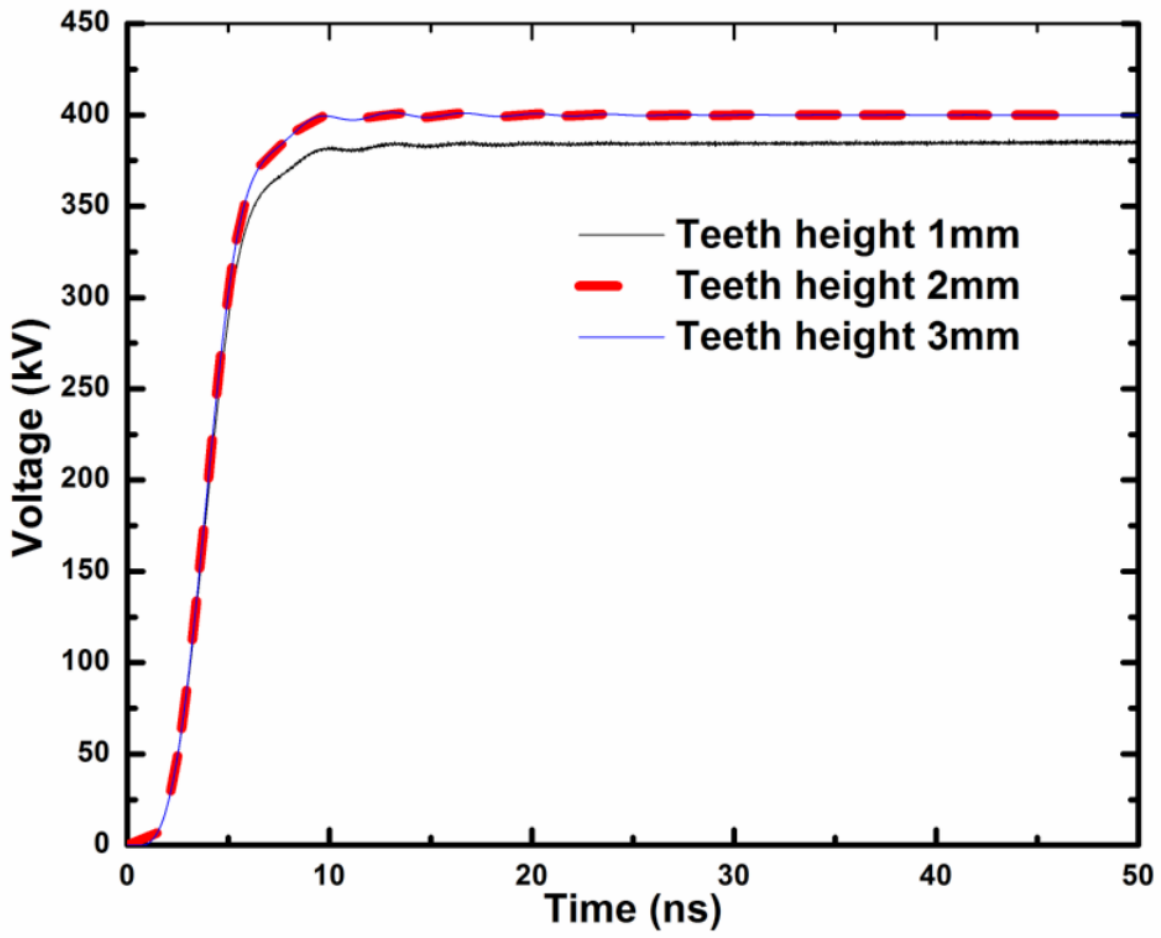

Figure 4.16 Effect of teeth height on discharge voltage

Figure 4.17 shows the effect of teeth height on the electric field profile in the gap in the z-direction as shown in figure 4.15.The field enhancement at 2mm from cathode is highest at a teeth height of 1 mm and slightly reduces for 2mm and further decreases for a 3mm protrusions on the surface of the insulator. The presence of teeth along the surface of the insulator leads to an increase in effective flashover length. The discharge which is initiated along the gap follows a path of least resistance. The surface with protrusions contains fine grooves which are randomly oriented thus not allowing a single preferred path for discharge unlike a plain surface. The increase in the teeth height also provides cavities where electrons and other ionization products get trapped thereby hindering ionization .This leads to an increased field value in the middle of

the gap from 5mm to 19mm for a teeth height from 1mm to 2 and 3mm and field stabilization for protrusions of 2 and 3mm as a result of trapping of the charge carriers.

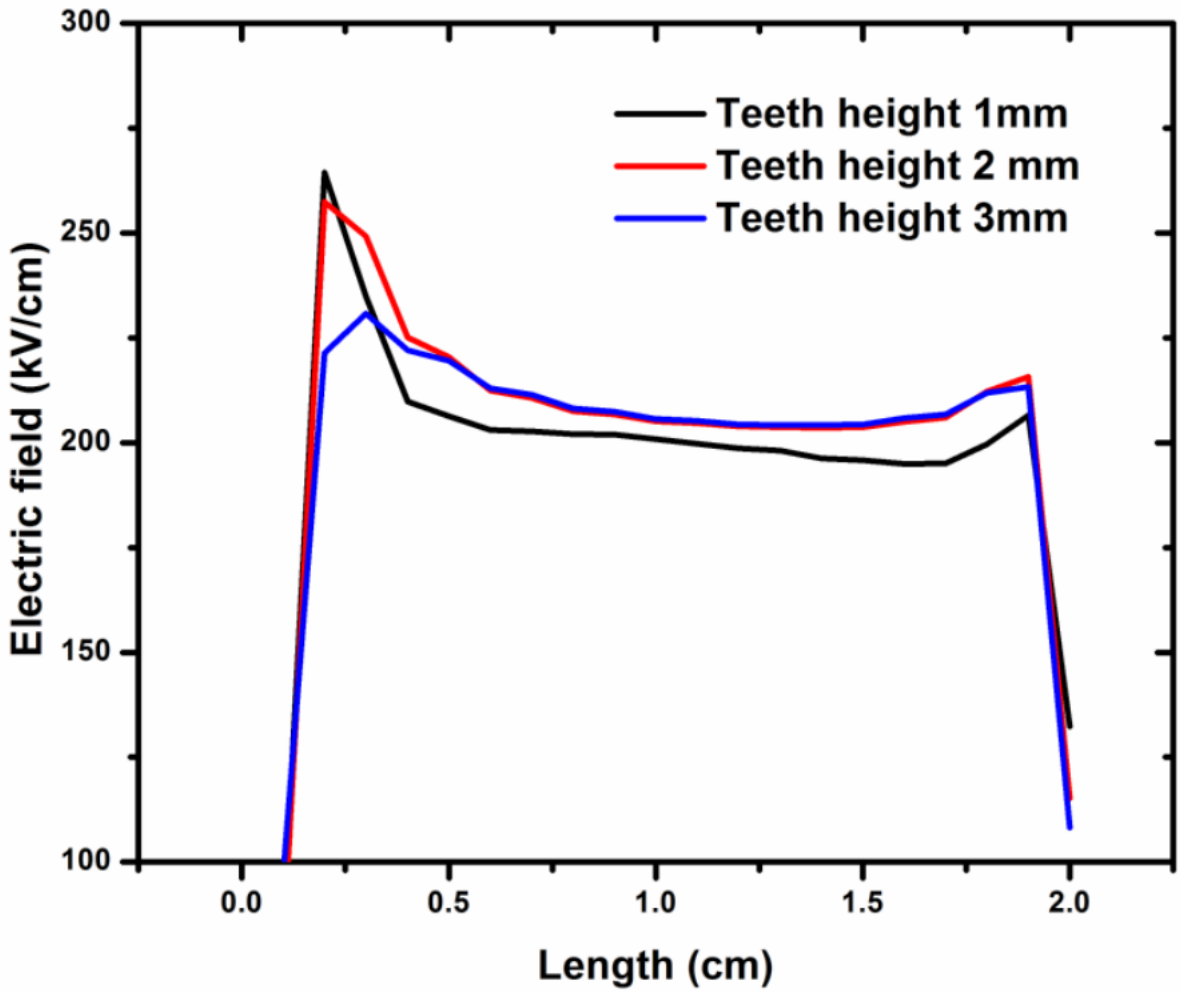

Figure 4.17 Effect of teeth height on field profile in the gap

4.5 Conclusion

The effect of spacer profile and surface effects on discharge voltage in gases is studied using FDTD based PIC code. The negative angled spacer and bush bar spacer geometry gives a highest spacer efficiency of 97% and are useful in designing system subjected to high pulsed voltage like blumlein pulse forming line. The protrusions along the surface of the insulator leads to an increase in the discharge voltage which remains constant after a certain teeth height where the

dominant role is played by ionization in the gas rather than secondary electron emission along the insulator surface. The reduction in field enhancement at a distance of 2mm from cathode leads to increase in voltage with teeth height.

Further a Marx generator based on a pulse forming network is developed which is described in chapter 5 along with a high pressure spark gap switch which serves as a test setup for surface flashover studies.

CHAPTER 5

DEVELOPMENT OF COMPACT MARX GENERATOR BASED ON PFN AS A PULSAR FOR THE HIGH PRESSURE SURFACE FLASHOVER STUDIES

5.1 Introduction

Pulsed power sources are widely used in various experimental and research studies for the generation of intense electron beams used to generate high power microwaves [112,124] and flash x-rays [113]. The pulsed power systems also finds applications in surface flashover study of insulators [125] and radiated field studies using antennas [126,127].The major advantage of compact Marx generator is that the output pulse duration, shape, amplitude, polarity can be altered by choosing appropriate design parameters thereby eliminating the use of any other pulse conditioning system [128].High power rectangle pulse is very useful because of the improved quality of the electron beam. However spark gap switches are preferred in Marx generators unlike the solid state switches because of limitation in their operation for nanosecond pulse generation [129].

Some of the salient features of this Marx generator are as: i) for ultra wide band systems (UWB) energy requirement is the range of ten of joules and hence PFN Marx generators are useful. ii) The presence of peaking capacitor at the output of the Marx generator provides a very short rise time and hence a very high intensity of far field radiations in case of an antenna load. iii) The number of energy transfer stages and the number of large components which do not store energy are minimized and hence this approach is useful as compared to a conventional Marx generator. Spark gap triggering is enhanced by the ultra violet illuminations as switches are placed in the line of sight. This provides a Z shaped discharge path resulting in magnetic field cancellation and also reduction in the circuit inductance. This chapter describes the design and

development of PFN based compact Marx generator which is subsequently utilized as a pulsar for surface flashover studies. Further a peaking capacitor was development which improved the rise time of the output voltage waveform.

5.2 Marx Generator Design

The input parameters of the Marx generator would be the output load impedance, required full width half maximum (FWHM) of the pulse, output voltage or output energy. The pulse characteristics of the Marx generator are given below:

i) Output voltage across matched load (V_o): 300 kV

ii) Output energy (E): 64 J

iii) Output pulse duration (FWHM):150 ns

iv) Load impedance: 180 Ω to 200 Ω

v) Maximum charging voltage (V_c): 30 kV

The grounding resistors basically prevent the damage of the charging supply system. The output pulse voltage of the Marx generator is given by equation (1).

$$V_o = nV_c / 2 \tag{5.1}$$

Where, V_o = Marx output voltage

Vc = Marx charging voltage

n = number of stages

Figure 5.1 shows the schematic of Marx generator. The Marx generator is discharged through the load by closing the switch 'S'.As the switch 'S' is closed there is a disturbance at the load end and a reflected voltage of 'E' travels away from the load end .Here V_0 is Marx output voltage ,SG is the spark gap and V_C is the Marx generator charging voltage. Here 'ZL' is the load impedance and R_C and R_G are the charging and grounding resistors respectively.

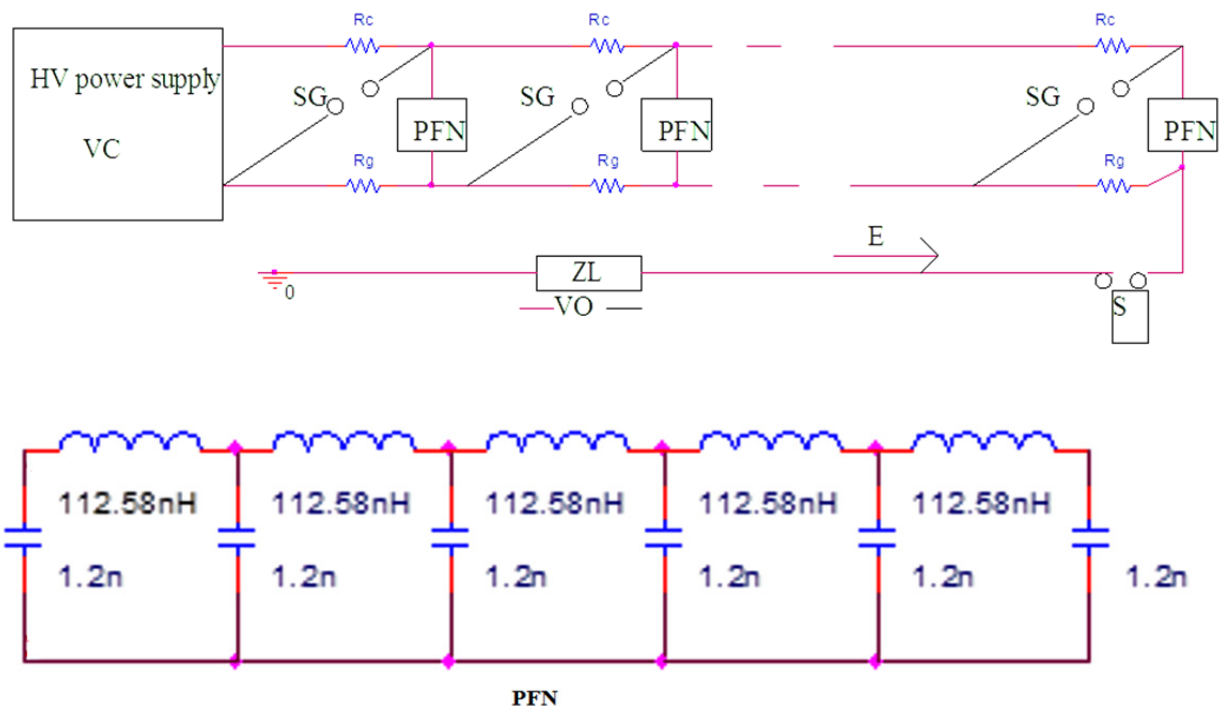

Figure 5.1Schematic of Marx generator

5.2.1 Calculation of capacitance

The Marx generator is operated at matched load for maximum energy transfer. The total energy input to the capacitors just before erection is equal to the output pulse energy at the matched load neglecting the energy loss in the connecting wires and spark gaps. The energy per PFN module is $0.5NCV_c^2$ where N is the number of elements in PFN, C is capacitance of each PFN element and V_c is the charging voltage. However the total stored energy is given by $0.5nNCV_c^2$ where, n is the total number of stages. Thus,

$$E = 0.5nNCV_c^2 = 64J$$

The value of capacitance obtained from above is 7.11nF. Hence six 1200 pF, 30 kV oil filled capacitors are connected in a PFN configuration which gives a total capacitance of 7.2nF. The energy obtained with the above capacitance value is slightly higher than calculated value and

hence we choose the following capacitors for the PFN configuration.

5.2.2 Calculation of inductance

The Marx generator is operated in the self-breakdown mode. The equivalent circuit of the Marx generator after erection is shown in Figure 5.2. In order to find the circuit inductance and hence characteristic impedance of the PFN module, two stages of the Marx generator was tested with a non-inductive load of 10 Ω. From the waveform shown in Figure 5.3, the erected inductance is calculated by using the time period of oscillation. The source impedance is then calculated from the erected inductance and erected capacitance.

$$T_{period} = 2\pi\sqrt{L_{eq}C_{eq}} \tag{5.2}$$

Where, L_{eq} and C_{eq} are the equivalent inductance and capacitance of two stages.

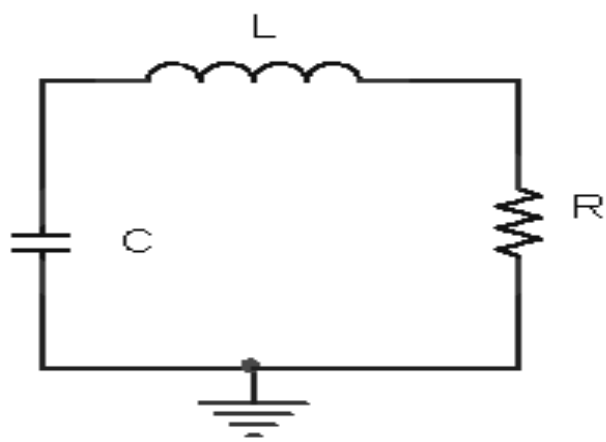

Figure 5.2 Equivalent circuit of the PFN based Marx generator after its erection.

The characteristic impedance is given in equation (5.3).

$$R = \sqrt{\frac{L}{C}} \tag{5.3}$$

The total capacitance (C) is given by the series combination of all the capacitors. The total inductance (L) obtained is $nL_{eq}/2$. The total value of inductance obtained from the equation 5.2 is

11.25 μH.

Figure 5.3 Inductance measurement waveform (Time-200ns/div)

5.2.3 Output energy of the Marx generator

The Marx generator has 20 stages with six 1200 pF 30 kV oil filled energy storage capacitors per stage placed inside a stainless steel (SS) chamber filled with compressed nitrogen to operate at higher voltages. The total energy drawn from the system is 64 J and is calculated by equation 5.4

$$E = V_o I_o T_o \tag{5.4}$$

Where, V_o is the Marx output voltage on matched load, I_o is the Marx output current and T_o is the output pulse duration**.**

5.3 Design of PFN based Marx generator

The Marx generator is constructed in the form of a complete co-axial geometry, which can minimize circuit inductance. The Marx generator is erected by a sequential triggering of each spark gap switch. Triggering complexity is avoided by arranging the switches in an optical line of sight so that the ultraviolet (UV) radiation from the first gap photo triggers the second gap and so forth. They are 20 stages staked one upon the other in vertical towering shape as shown in

Figure5.4. Each PFN module consists of six capacitors connected in parallel by means of copper strips. Charging resistors of 100 Ω each made of nichrome wire wound on flat FRP strip former and potted using epoxy resins to provide electrical insulations. These resistors are required for charging the PFN module capacitors and to isolate the modules during erection. Each spark gap is made of stainless steel having an 18 mm diameter and 62 mm lengths and is firmly mounted on the capacitor connecting plates to reduce the inductance. Energy storage castor oil capacitors are used since ceramic capacitors have a very poor reliability when used for high current discharge applications. Each stage consists of six capacitors each of 1200 pF and 30 kV connected in parallel in a PFN configuration across the charging and grounding resistors. The capacitors are mounted on a Perspex sheet .The output of the last stage of the Marx generator is connected to peaking gap electrode as shown in Figure5.5 enclosed by a peaking capacitor. The entire assembly is placed inside a stainless steel chamber of 0.6 m inner diameter and length of 1.5 m pressurized with nitrogen and the output of the other peaking gap electrode is connected to the load along with voltage and current measurements as shown in Figure5.6.The voltage divider consists of a tube of aqueous copper sulphate solution acting as a high voltage arm and a 1 Ω lower voltage arm made of low inductance commercial carbon resistors. The aqueous copper sulphate resistor was chosen for its proven ability to withstand large electric fields. The solution has the advantage of being readily shaped by varying the container shapes, providing good contacts and being self- healing in the event of a voltage breakdown. The voltage divider is calibrated using a cable pulsar that consists of a high voltage charged cable as pulse forming line (PFL) coupled to a cable as pulse transmission line through an air spark gap of nanosecond rise time and delivers a rectangular voltage pulse onto the load and a commercial high voltage probe. The copper sulphate column resistance can also be measured by an LCR meter. Table 5.1 shows

the parameters of the PFN based Marx generator.

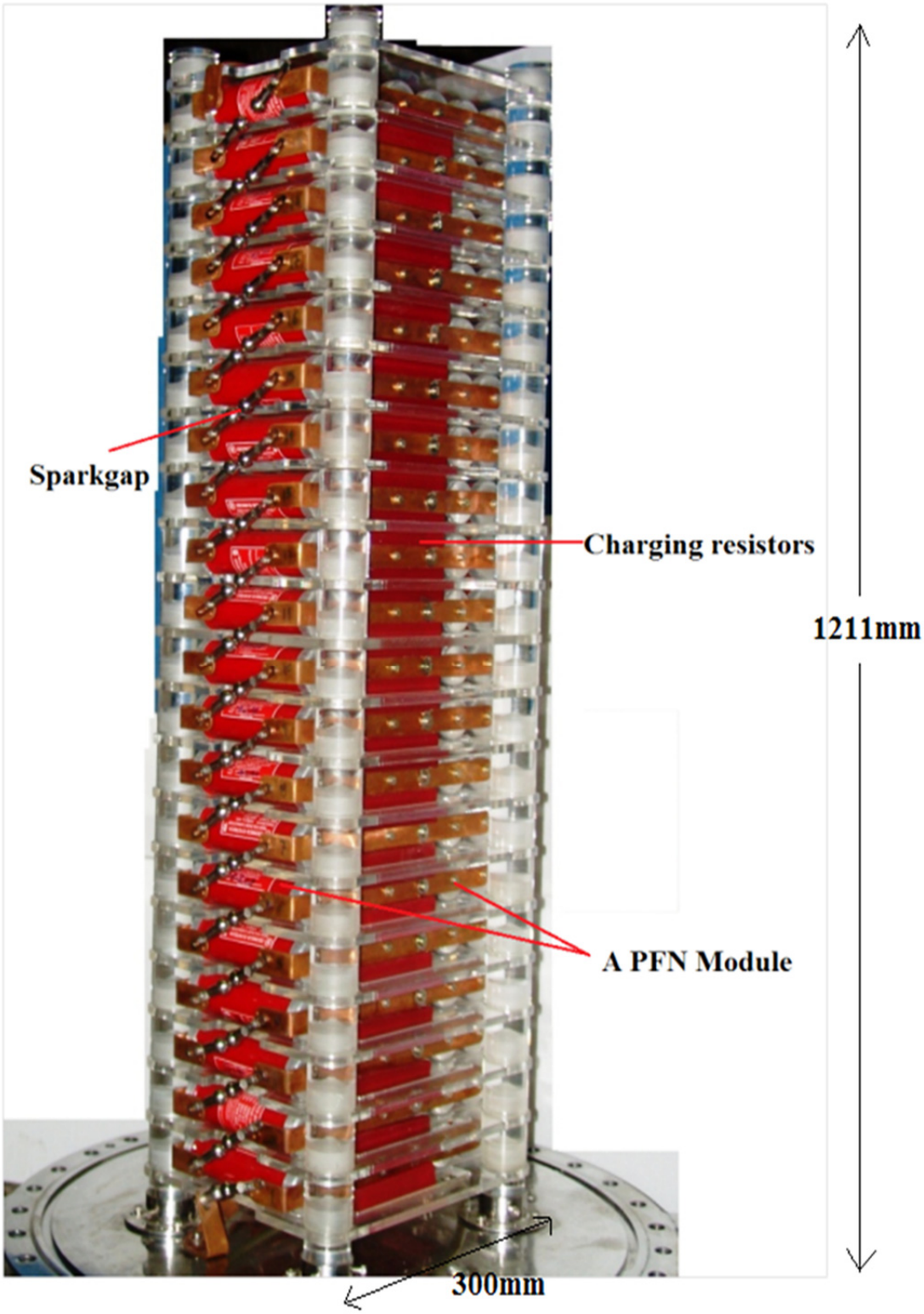

Figure 5.4 300 kV compact Marx Generator based on PFN.

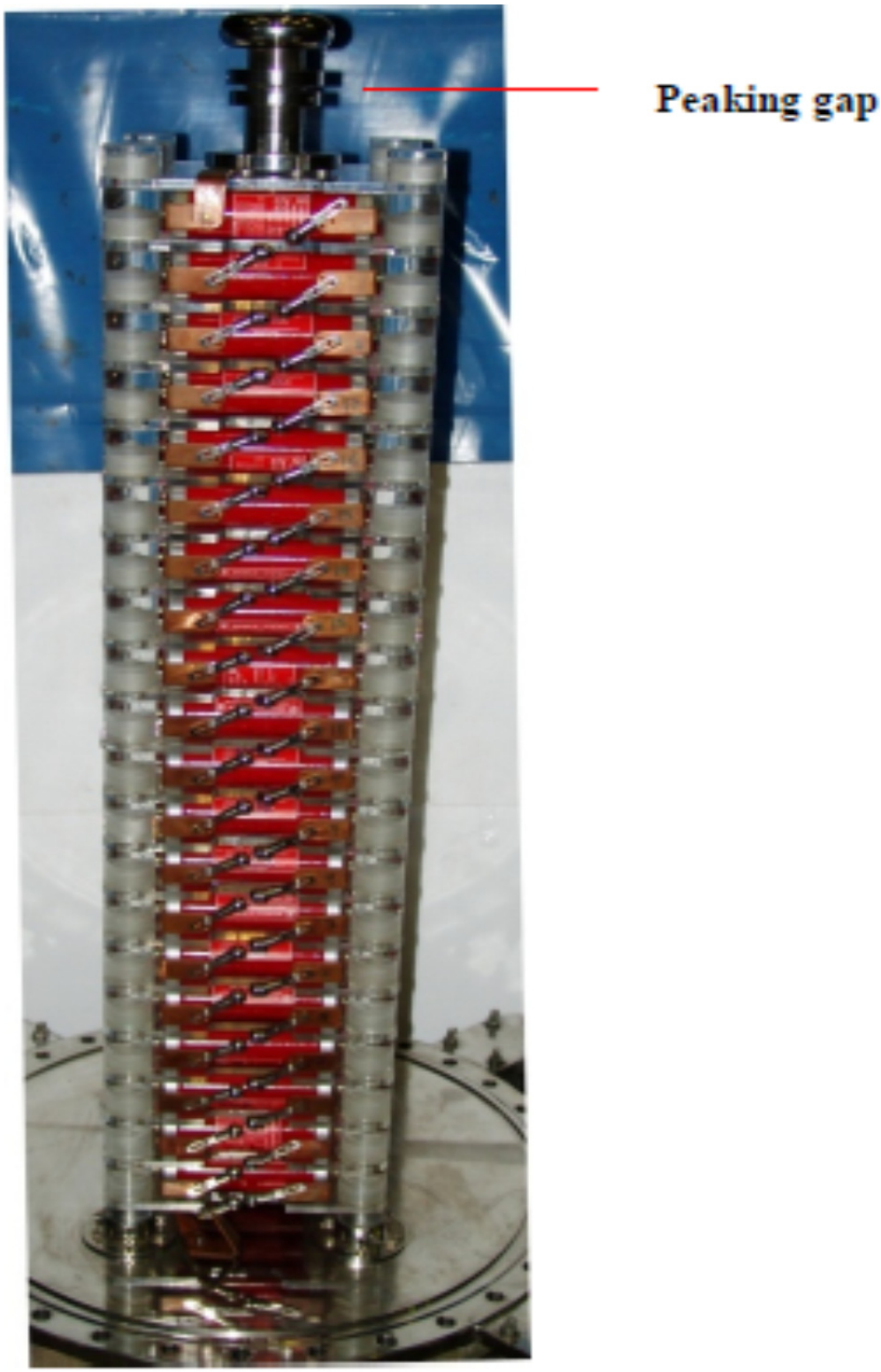

Figure 5.5 Marx generator with a peaking gap.

Table 5.1 Parameters of PFN based Marx generator

Description	Value
Number of stages	20
Capacitor voltage	30kV
Rise time	5ns
Pulse width	150ns
Capacitance per stage	7200pF
Erected capacitance	360pF
Erected inductance	11.25μH
Total stored energy	64J

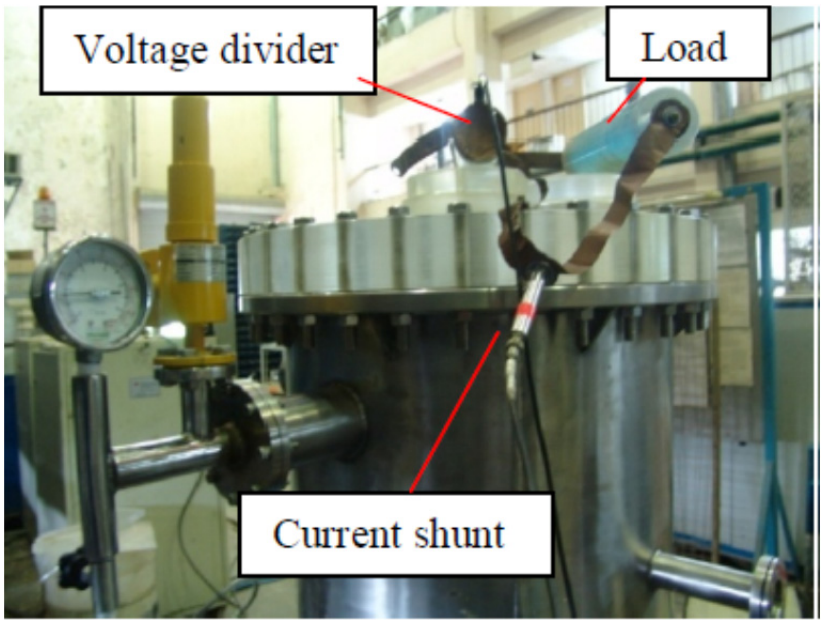

Figure 5.6 Marx generator and peaking capacitor enclosed with an SS chamber with load, voltage divider and current shunt.

5.4 Design of peaking capacitor

The Marx generated output pulse is fed to the load through a peaking spark gap housed within a peaking capacitor .The peaking capacitor is basically a co-axial stainless steel (SS) cylinder having a central bore through which a spark gap is placed which serves as a peaking spark gap. The capacitance is formed between the peaking capacitor tank and the outer SS chamber of the Marx generator as shown in Figure 5.7. It helps in getting sharp rise time at the output. The peaking gap distance and pressure is adjusted such that breakdown voltage is closer to the peak and inductance is small enough to sharpen the pulse and reduce the effect of series spark gap closure time delay [71].Peaking capacitance based on the enclosure geometry with air as dielectric medium is given by equation 5.5.

$$C = \frac{2\pi\varepsilon_0\varepsilon_r}{\ln\left(\frac{R_2}{R_1}\right)} \tag{5.5}$$

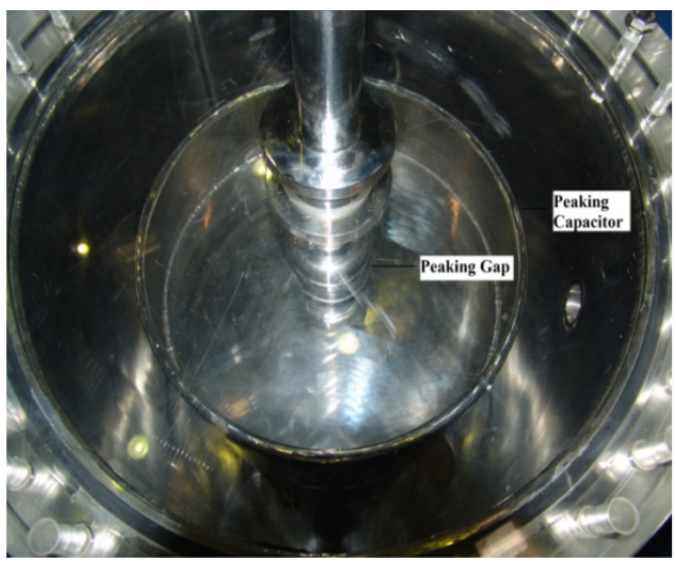

Figure 5.7Peaking capacitor and Peaking gap arrangement.

Where, R_1 is the outer radius of the inner cylinder and R_2 is the inner radius of the outer

cylinder. Peaking capacitance based on the Marx generator parameters [130] is given by equation (5.6).

$$C = \frac{\frac{L_{Marx}}{R_{Load}^2}}{1 + \frac{L_{Marx}}{R_{Load}^2 C_{Marx}}} \tag{5.6}$$

Where, R_{load} is the load resistance, C_{Marx} is the erected Marx capacitance and L_{Marx} is erected Marx inductance. Capacitance of 180 pF based on Marx generator parameter was difficult to achieve and hence a lower value of capacitance of 48 pF for 250 mm length was selected.

5.5 Testing and simulation of Marx generator

5.5.1 Without peaking capacitor

The Marx generator is tested in air till 11.5 kV. To charge the Marx generator beyond 11.5 kV the total system has to be pressurized. The system is robust and a number of shots had taken on the system at charging voltage of 11.5 kV and nearly same waveforms are obtained at the output. The voltage and current waveforms are recorded using a 2.5 GS/s LeCroy oscilloscope. The experimental and simulated waveforms are shown in Figures 5.8 and 5.9 respectively.

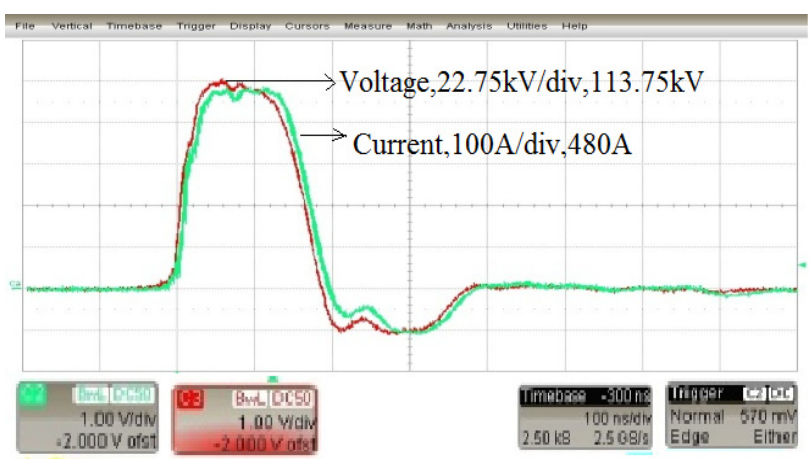

Figure 5.8 Output of 20 stages of the Marx generator in air (Pulse width-150 ns, Rise time -25 ns, Charging voltage -11.5 kV, and time/div-100 ns).

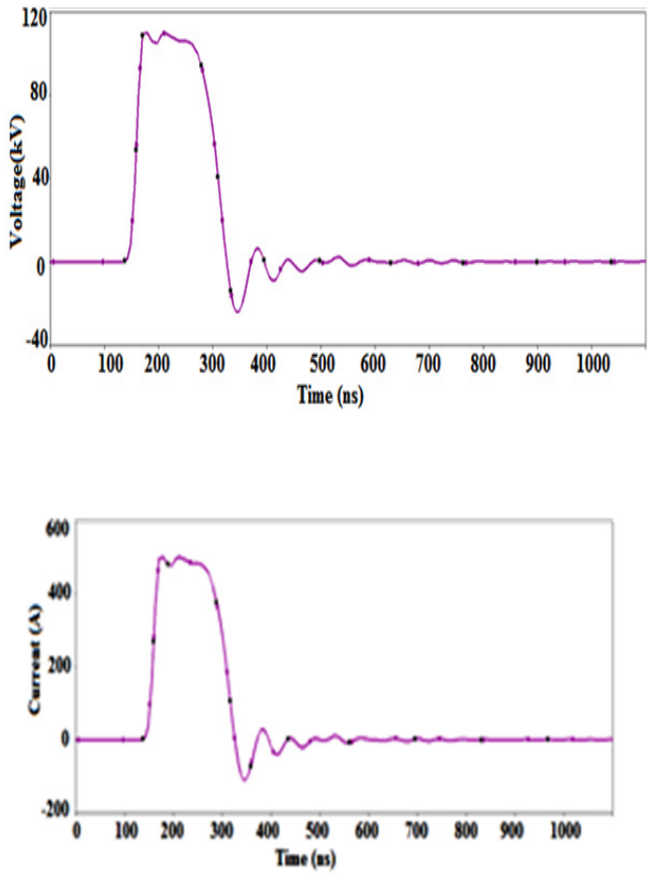

Figure 5.9 Output voltage and current pulse.

5.5.2 With peaking capacitor

The output of the last stage of the Marx generator is connected to a peaking spark gap placed inside a peaking capacitor. The entire system is then placed inside a stainless steel cylinder and sealed at the top by means of a Perspex sheet.

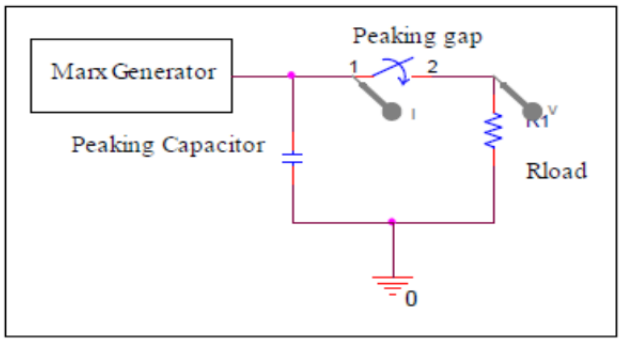

(a)

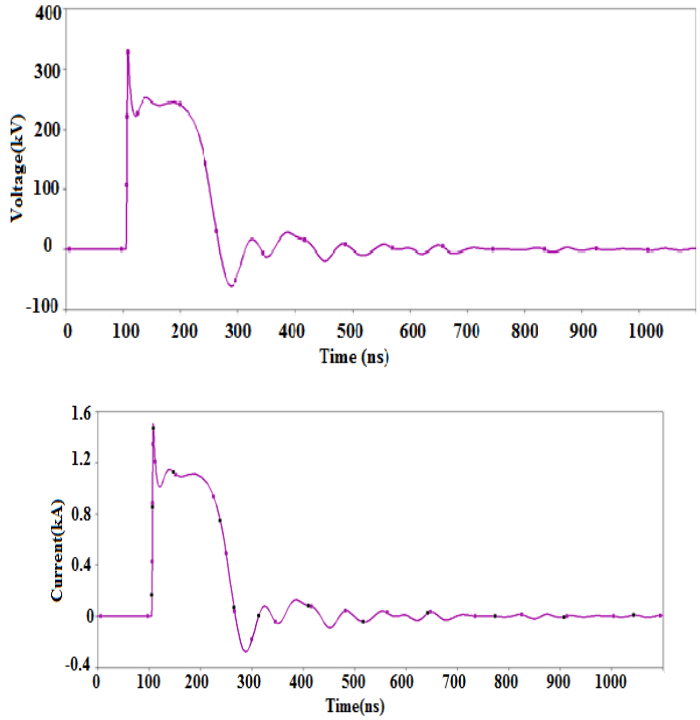

(b)

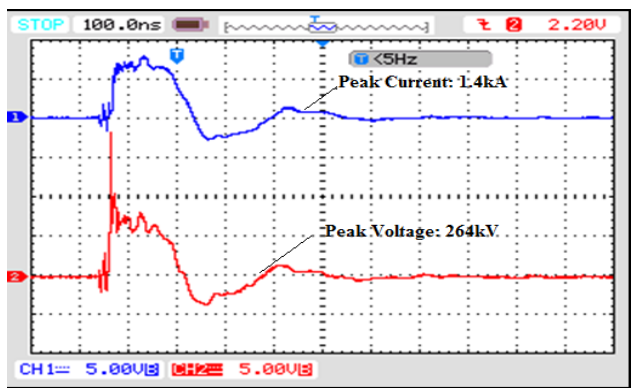

(c.)

Figure 5.10 (a) Block diagram of the Marx generator with peaking capacitor (b) Simulated output voltage and current (c) Experimental results.

The entire system is pressurized by dry nitrogen for charging the Marx at higher voltages. Marx generator is charged up to 26 kVA sharp peak is obtained in the first pulse with a rise time of nearly 4 ns to 5 ns as shown in Figure 5.10 with a pulse width of nearly 150 ns obtained at a charging voltage of 26 kV.

5.6 Calculation of stray capacitance using CST studio

The CST studio suite is utilized for the calculation of stray capacitance. Figure 5.11 below shows the complete structure of the Marx generator. Each of the spark gap electrodes on one arm of the system is fed with a voltage excitation whereas the electrodes on the opposite arm is grounded .A tank of height 1500mm with inner and outer radius of 300 and 306mm respectively enclosing the Marx generator as shown in Figure 5.12 is at ground potential. The capacitance calculated between the Marx generator and the tank as well as between the electrodes and among different stages is a 40 x 40 matrix. The values obtained from the matrix are fed to the simulation circuit and no changes in the output erected voltages are obtained .Thus the tank design is such that no breakdown occurs between system and the tank and the value of the capacitances does not lead to unwanted triggering of spark gaps and reduction in the output voltage. Table 5.2 shows a stray capacitance between first stage, tank and the adjacent stage.

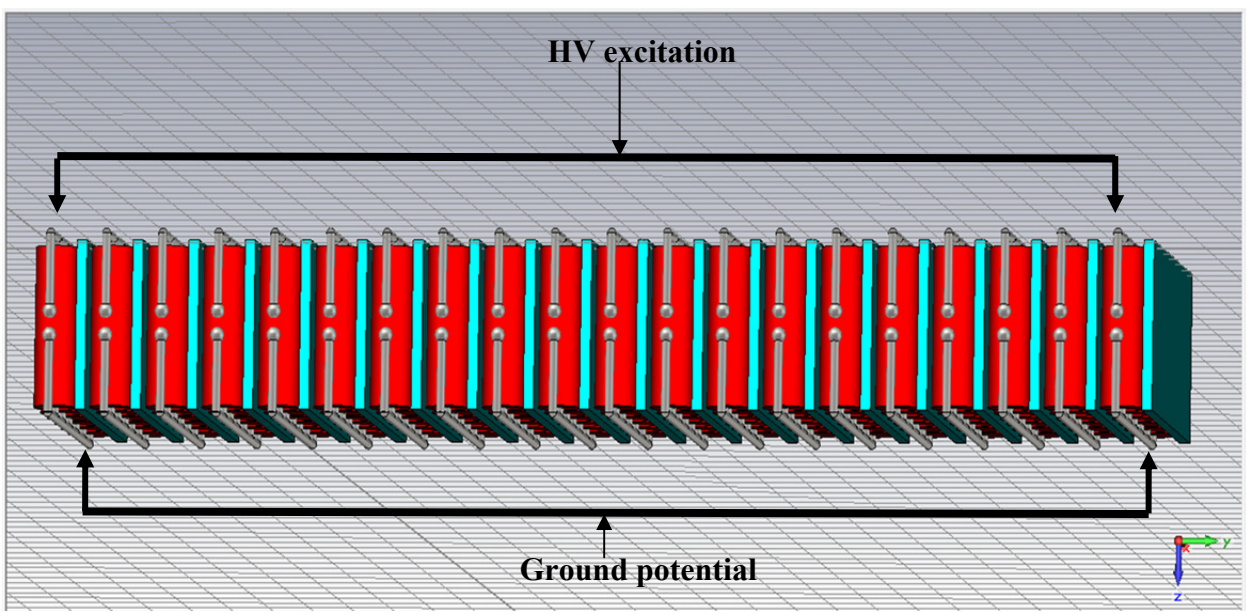

Figure 5.11 Complete structure of the Marx generator with one arm of spark gap subjected to high voltage and the opposite branch is grounded.

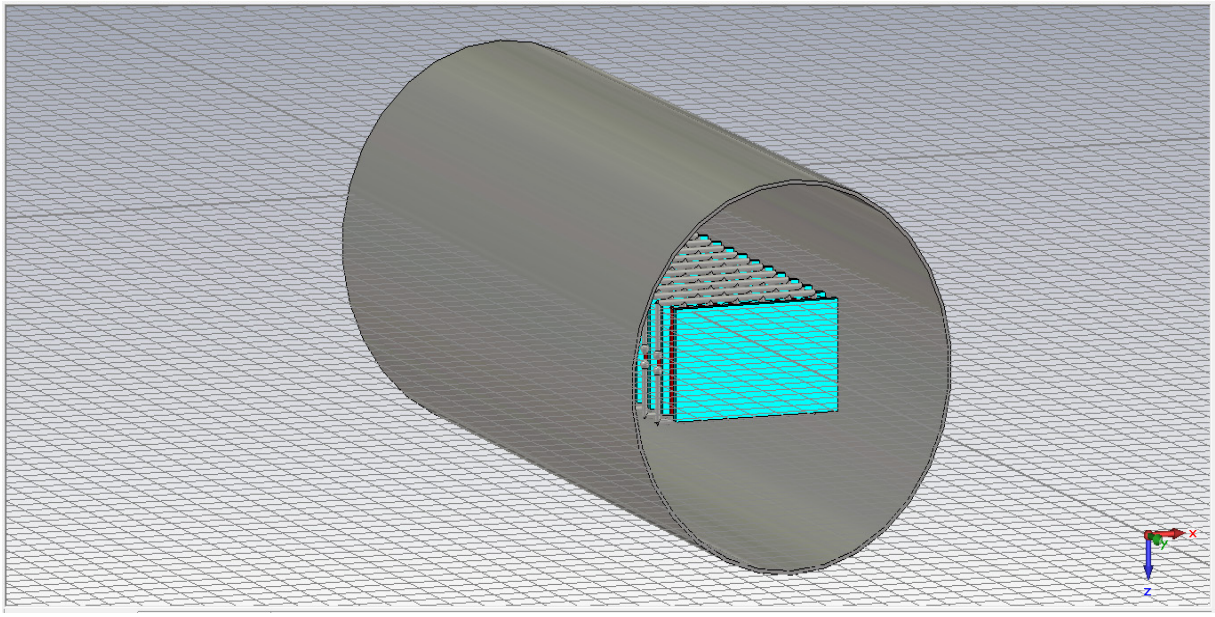

Figure 5.12 The SS tank maintained at ground potential enclosing the Marx generator

Table 5.2 Stray capacitance between first stage, tank and the adjacent stage formed due to voltage excitation at first spark gap

First spark	Adjacent stage	Capacitance (F)
Pot.1	Pot.2	3.7e-18
Pot 1.	Pot.10	2.8e-12
Pot.1	Pot. Tank	5.29e-12

Pot.1 -Potential at first spark gap

Pot.2.-Potential at second spark gap

Pot.10-Potential of grounded electrode opposite to first spark gap

Pot.Tank -Potential of tank

5.7 Experimental results on insulator surface breakdown studies

The nanosecond pulsed output of the Marx generator is utilized as a pulsar for surface flashover studies .The output of the Marx generator is fed to a high pressure spark gap switch designed for surface flashover studies as shown in Figure 5.13.The high pressure spark gap chamber(test cell)

is a Perspex chamber of 125mm outer radius ,105mm inner radius and a length of 237mm.The spark gap chamber is designed so as to withstand pressures up to 5kg/cm^2.Two rogowski profile electrodes each of 90mm diameter and 26mm thickness serves as the spark gap electrodes with a spacer of 10mm thickness placed between the electrodes. The electrodes are located at the center of the chamber. Electrodes are polished to a fine mirror finish using silicon carbide of 800 grade. These electrodes are thoroughly cleaned with laboratory grade acetone before finish. A view port of 100mm inner diameter and 150mm outer diameter is made on the surface of the chamber which serves as a service port, for proper alignment of spacer between the spark gap electrodes, for replacement of worn out spacers after the flashover experiments and also useful for carrying out optical experiments on surface breakdown.

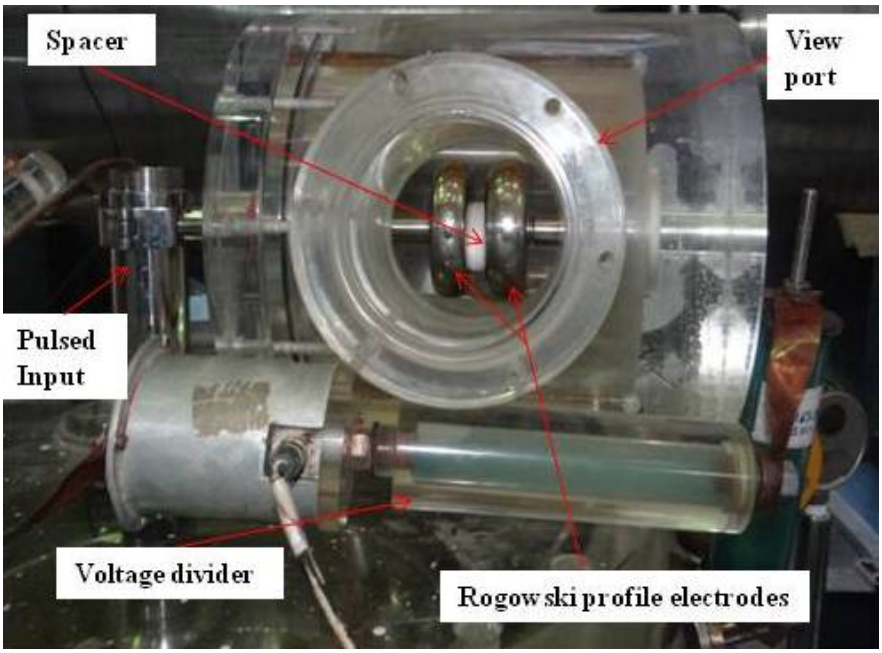

Figure 5.13 High pressure spark gap switch as a test cell for surface flashover studies

The erosion from electrode surface depends on the product of current and applied pulse duration. It depends on the coulomb transfer rate .The mass loss due to electrode erosion for stainless steel is ~380 micrograms/coulomb compared to ~120 microgram/coulomb for copper-tungsten

electrodes. The maximum current is up to 2kA and pulse duration of 100ns, the coulomb transfer rate and hence the material erosion is negligible and does not affect the breakdown experiments. No visual deformation on electrode surface was observed even after five shots for each data point. Both the insulator samples are cleaned with alcohol followed by deionised water and dried before placing it in the test cell. It is ensured that the sample insulators are free from external impurities. The output of the test cell is connected to a load so as to limit the breakdown current which prevents damage of the insulator surface. The breakdown voltage is measured using a calibrated $CuSO_4$ voltage divider. Experiments are carried out to study the effect of pressure on flashover voltage and spacer efficiency.

5.7.1 Effect of pressure on flashover voltage

The surface flashover experiments are carried out in a pressure range from 1kg/cm^2 to 4kg/cm^2 in nitrogen environment. Figure 5.14 shows the variation in breakdown voltage with pressure when perspex and delrin are used as test samples (spacer) along with the bulk breakdown in nitrogen.

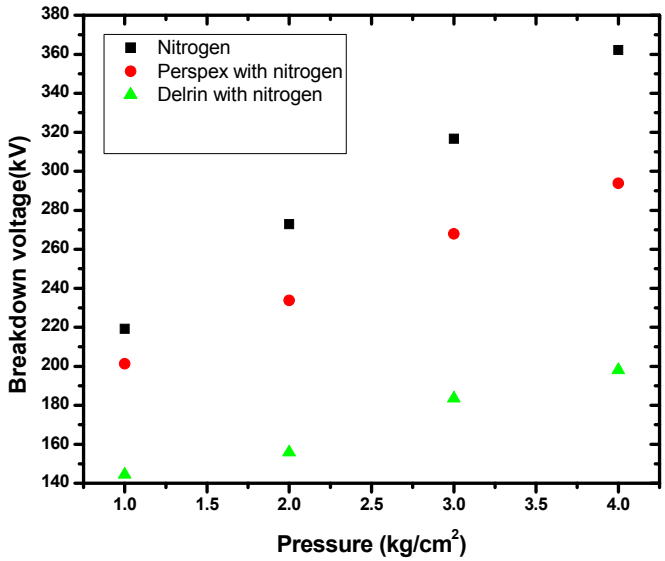

Figure 5.14 Variation in breakdown voltage with pressure

The nitrogen used is the spark gap chamber is IOLAR grade nitrogen with 99.9% purity. Each

shot at a given pressure is an average of 5 shots in order to minimize the statistical variations in the breakdown data .An interval of 1minute is allowed between successive shots which provides sufficient recovery time for gap. The standard deviation in the breakdown data is within 3% for the reported test regime. An increase in the flashover voltage with pressure is observed in both perspex and delrin .However for pressures beyond 3kg/cm^2 a slight saturation in the flashover voltage is observed in both the samples implying higher probability of breakdown along the spacer surface with gas playing a minor role at high pressures. A reduction in flashover voltage is observed in delrin (ε_r=3.7) as compared to perspex (ε_r=2.6) as because a higher permittivity mismatch between the spacer and surrounding gas medium leads to a higher field enhancement resulting in reduction in the breakdown voltage.

5.7.2 Effect of gap pressure on spacer efficiency

Figure 5.15 shows a variation in spacer efficiency with pressure. A reduction in the spacer efficiency [105] which is a ratio of breakdown voltage with and without a spacer is observed with pressure for both the samples. This indicates that breakdown

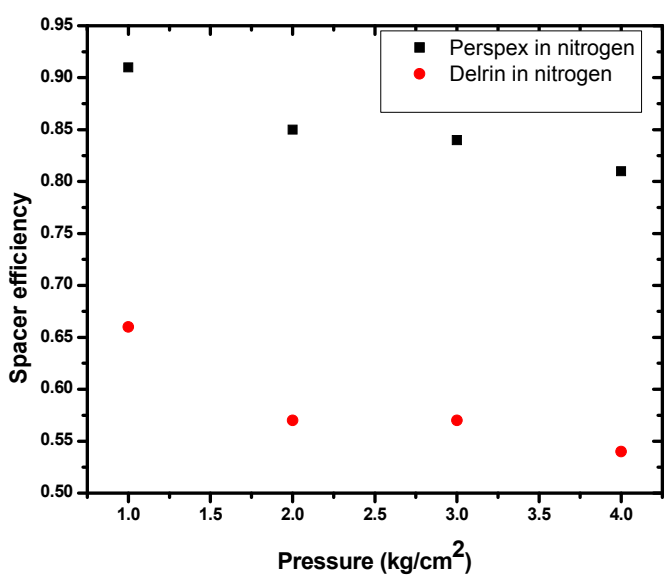

Figure 5.15Variation in spacer efficiency with pressure

occurs mainly along the insulator surface even at high pressures resulting in reduction in spacer efficiency. Highest spacer efficiency of 91% is observed with perspex at a pressure of 1kg/cm^2 . The reduction in spacer efficiency with perspex is 11%as compared to delrin which shows a reduction of 18%. The reduction in spacer efficiency increases with increase in permittivity of the sample.

5.8 Conclusion

A PFN based compact Marx generator with a peaking capacitor is developed and the experimental results are in good agreement with the simulation results and the variations are within 0.05%. The calculations for the capacitance, circuit inductance and characteristic impedance for the Marx generator has been carried out. Peaking capacitor reduces the rise time from 25 ns to 5 ns. A reduction in the breakdown voltage is observed in both perspex and delrin with the highest spacer efficiency of 91% in perspex bridged spark gap. A reduction in spacer efficiency with pressure is observed with a reduction of 11% in spacer efficiency at a pressure of 4kg/cm^2 in perspex as compared to delrin which shows a higher reduction of 18% with pressure.

CHAPTER 6

SURFACE POTENTIAL DECAY OF INSULATING MATERIAL IN AIR AND OPTICAL EMISSION SPECTROSCOPY OF AN INSULATOR SURFACE IN AIR AND NITROGEN.

6.1 Surface potential decay of PMMA and POM insulating material in air

Surface potential decay (SPD) is an important factor when considering the type of insulator to be used in high voltage equipment. Surface potential decay study finds importance in many electrical applications few of them being in testing the suitability of material against static charge [131], determination of electrical properties of insulation materials [132], superficial conductivity of aged insulators [133] and in the analysis of hydrophobicity recovery for insulators used in the outdoor insulation [134].The flashover performance of polymeric insulator deteriorate as a result of charge accumulation on its surface [135]. Potential decay in a charged sample with a metal insulator interface and an air gap between the other electrode and insulator surface involves a number of physical processes like volume polarization, surface conduction, atmospheric neutralization, charge injection at the interface and partial discharge in voids and surface irregularities [136].

The present chapter is divided into two parts .The first part studies the surface potential decay study of PMMA and POM which are commonly used insulators in pulse power systems in air The surface trapping parameters of PMMA is calculated which gives an insight into the variation in decay characteristics with applied voltage polarity and the effect of surface roughness on charge decay is also analyzed.

The second part gives the spectroscopic analysis of flashover along the surface of POM due to particle contamination. Three different conditions of needle protrusion along the surface of

polyoxymethylene are used to study the variation in spectral characteristics due to particle contamination.

6.1.1 Experimental setup

The experimental setup for surface charge measurement is shown in Figure 6.1. The setup utilizes a needle-plane electrode system with a cylindrical insulator of 10 mm thickness and 35 mm diameter each of Polymethyl Methacrylate (PMMA) and Polyoxymethylene (POM) which are used as test samples to study the surface charge decay. The input charging voltage is + 8 kV dc with the sample charging time set to 5 minutes and then of -8kV dc in subsequent experiment with the same sample charging time. It is ensured that there is a complete decay in charge on the surface of the insulator before voltage of negative polarity is applied to the test sample so that there is no effect on the measured data of residual charge on the sample surface. The needle - plane electrode system is used to charge the insulator blocks. The sample is placed on the ground electrode with no gap between the ground electrode and the insulator sample as shown in Figure 6.1 so as to ensure better charging and measurement reproducibility. Before the charging of the sample is allowed to take place using a needle plane electrode arrangement, the sample is placed under the voltage sensor of the electrostatic probe to account for any residual charges present on the sample surface. It is observed that there is no charge present on the surface as observed with zero potential decay on the oscilloscope. The polymers subjected to a dc corona discharging during 5 minutes induces charges on the insulator surface .A number of experiments have been carried out on the same insulator surface and negligible changes have been observed on the potential decay curves .The modification of the surface composition would have resulted in considerable variations in potential decay curve characteristics which is not observed in the present case. Hence such measurements do not induce any surface composition modifications.

The sample is placed on the ground electrode with no gap between the ground electrode and the insulator sample as shown in Figure 6.1 so as to ensure better charging and measurement reproducibility. A gap of 3 mm is placed between the needle electrode and the insulator surface has been maintained to avoid the arc discharge regime and prevent any damage to the sample surface. After charging for the set time duration the HV dc supply is turned off and Trek 341B Electrostatic voltmeter (ESVM) is turned on and the ground electrode with the sample mounted on it is moved towards the ESVM using a thread arrangement and is placed under the voltage sensor of the ESVM.

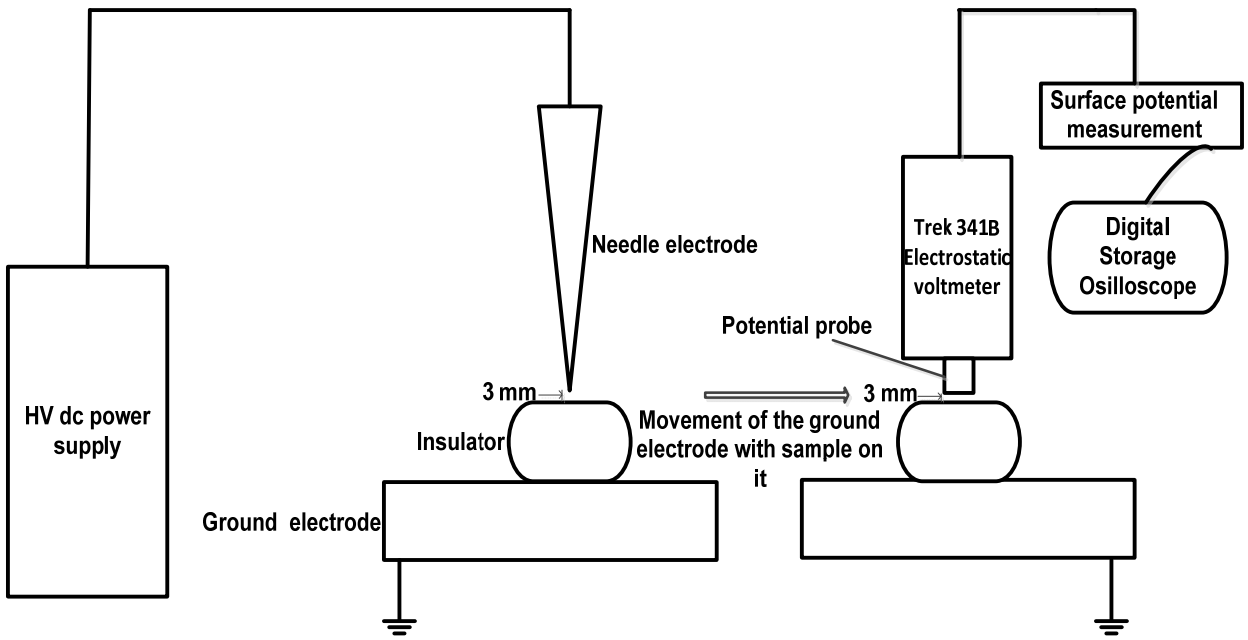

Figure 6.1 Experimental setup for surface charge measurement

The transit time between the end of charging period and first measured potential is 1second.The Trek 341B Electrostatic voltmeter (ESVM) is used for surface charge decay measurements which has a range of 0 $\pm$ 20 kV dc with an accuracy better than $\pm$ 0.1% of full scale [137]. The 3450 probe is used with the ESVM for surface charge measurements which has probe dimensions of 11.8mm ×11.1mm × 76.2mm with an aperture size of 3.05mm ×1.52mm.The

response time of the probe is less than 200µs for a 1kV step in voltage with a noise value of less than 20mV [138]. A 600 MHz Lecroy oscilloscope with a sampling rate of 5Gs/s in rolling mode is used for recording the surface potential decay waveforms. The experiments are carried out in ambient air (temperature of 18ºC -22ºC and relative humidity of 30%-50%). The EVSM is turned on and sufficient time is ensured for the Trek readout to become stable before the sample is placed below the potential probe for surface potential decay measurements. Two different studies of surface potential decay are carried out to understand the effect of applied voltage polarity and nature of the insulator material on charge decay on the insulator surface. A roughness is introduced on the surface of POM and comparisons of the same are made with smooth insulator.

6.1.2 Effect of insulator material on surface potential decay

Two different dielectrics namely PMMA and POM are used and subjected to a dc voltage of 8 kV of positive polarity for 5 minutes and negative voltage of 8 kV for 5 minutes in subsequent experiments. After the applied voltage is removed the sample is placed under the voltage sensor of the electrostatic probe. The applied positive voltage induces negative charge on the surface of the insulator [139]. A capacitive coupling takes place between the voltage sensor and the negatively charge insulator surface which induces positive potential on the voltage sensor of the ESVM which in turn is recorded by the oscilloscope. Similarly negative potential is measured by voltage sensor when the insulator is subjected to negative voltages. An air gap of 3mm between the needle electrode and the insulator. There is no direct contact between the needle electrode and the insulator. Space charges are present in the air gap between the insulator and the electrode. The air gap between the electrode and the insulator creates an air gap capacitance and hence the applied voltage of 8kV cannot be observed on insulator surface. Similar results of

reduced value of initial surface potential of 800V is observed on polytetrafluroethylne (PTFE) when it is subjected to corona charging using a needle electrode .The applied voltage to the needle electrode is 5kV and the applied voltage time duration is for 30 minutes [140]. The surface potential decay curves are shown below in Figure 6.2.

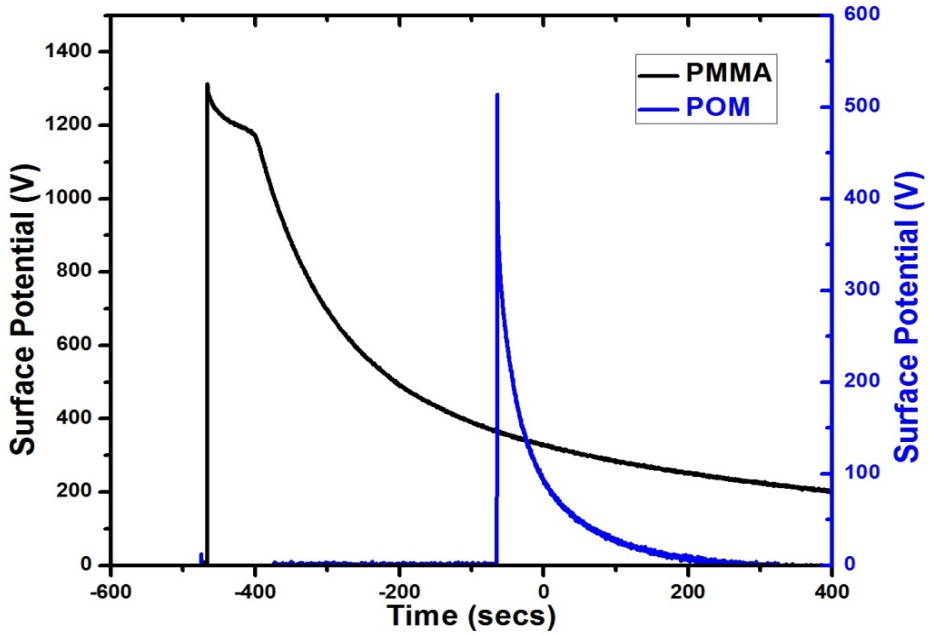

Figure 6.2 Surface potential decay of PMMA and POM subjected to positive potential

The peak surface potential of PMMA is higher than that of POM. The time to decay of surface potential to 50% of its peak value (t_{50}) is 181 seconds for PMMA as against 11.5 seconds for POM, which implies that the ability to retain charge is higher for PMMA than for POM. However the effect is more predominant for negative dc voltage than for positive dc voltage as shown below in Figure 6.3.The charges induced on the surface of different polymers takes different decay time hence the scales have been shifted so that both the curves can be observed with clarity and the time to decay to 50% of its peak value (t_{50}) can also be calculated. A qualitative explanation of the above variations is given in explained in section 6.1.5.

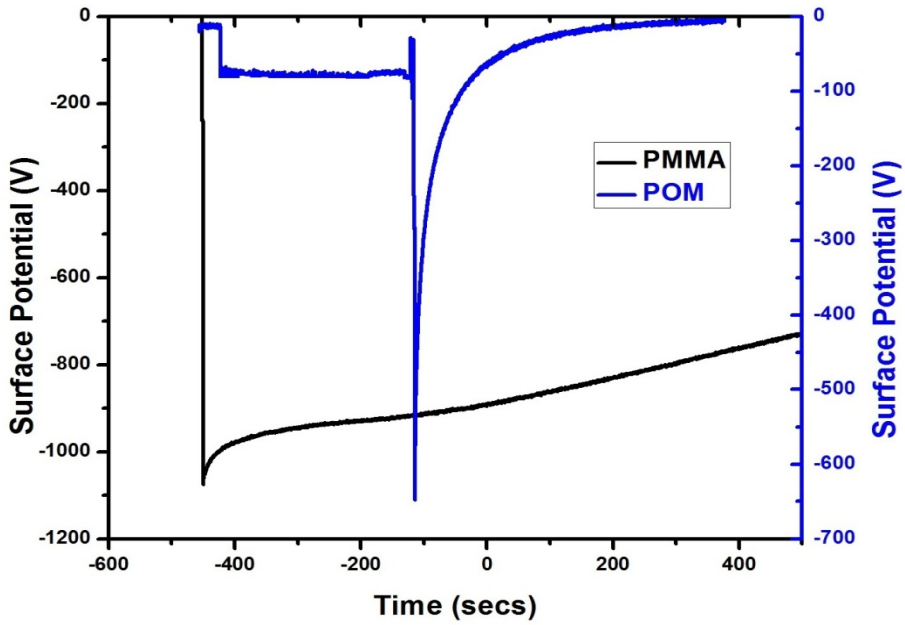

Figure 6.3 Surface potential decay of PMMA and POM subjected to negative potential

6.1.3 Effect of surface roughness on surface potential decay

Roughness introduced on insulator surface is aimed at improving the flashover characteristics of the sample [141].Roughness is introduced on the surface of the POM using an emery paper. The average roughness value (R_a) of emery paper is 268µm with a grit number of 60. After roughness is introduced on insulator surface, the two sides of the sample are shot-circuited to remove any free surface charges. The sample is then placed under the voltage sensor of the electrostatic probe to account for any residual charges present on the sample surface. It is observed that there is no charge present on the surface as observed with zero potential on the oscilloscope. It is observed that for a negatively and positively charged insulator surface the peak surface potential is higher for a rough insulator than for a smooth insulator as shown in Figures 6.4 and 6.5. However the peak surface potential and time to decay (t_{50}) is higher for negative voltages than for positive dc voltages as shown in Figure 6.5 Table 6.1 shows the comparison peak surface potential for a rough and smooth insulator when subjected to positive and negative

dc voltage.

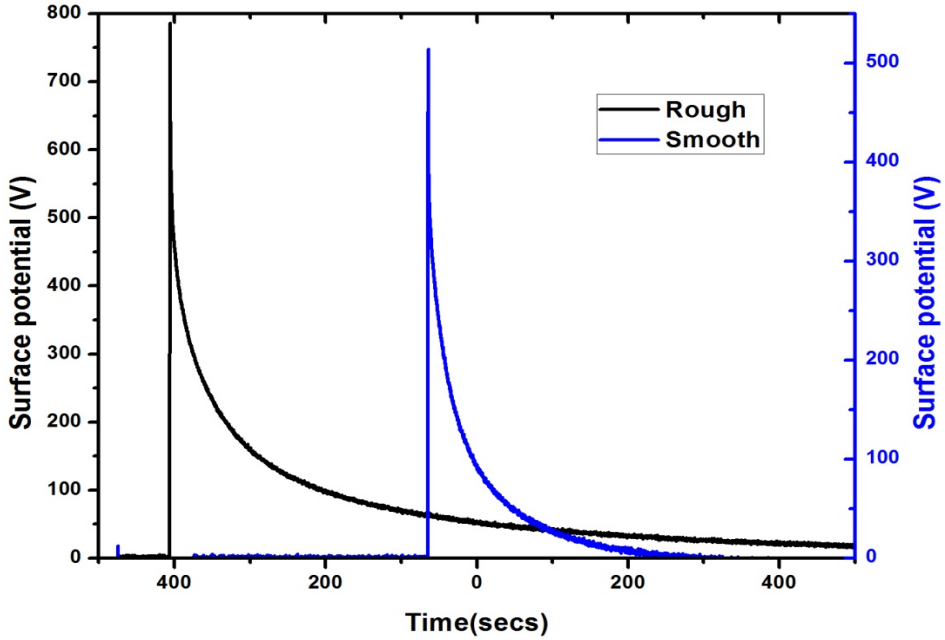

Figure 6.4 Surface potential decay along rough and smooth delrin material subjected to positive potential.

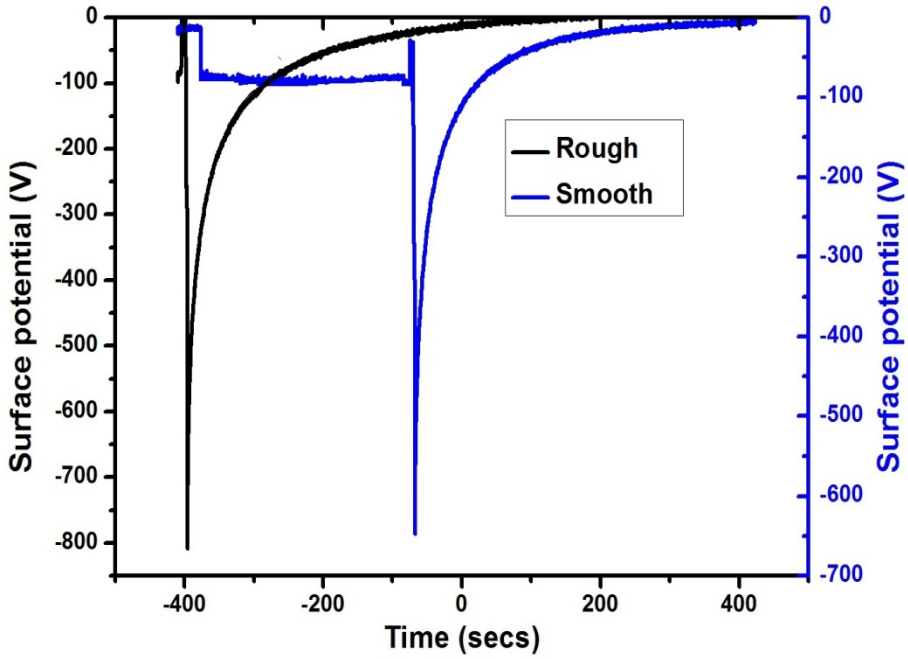

Figure 6.5 Surface potential decay along rough and smooth delrin material subjected to negative potential.

Table 6.1 Peak surface potential for a smooth and rough POM surface

Applied voltage polarity	Smooth	Rough
Positive	510V	790V
Negative	650V	810V

6.1.4 Qualitative description of variation in surface potential decay in PMMA and POM

An increase in surface potential decay in PMMA as against in POM can be explained on the basis of its chemical composition.

1. Polymethyl Methacrylate (PMMA) is a transparent thermoplastic polymer of methyl methacrylate with a chemical composition $(C_5O_2H_8)_n$. Polyoxymethylene (POM) has a chemical composition $(CH_2O)_n$. The chemical structure of PMMA and POM are shown in Figure 6.6.

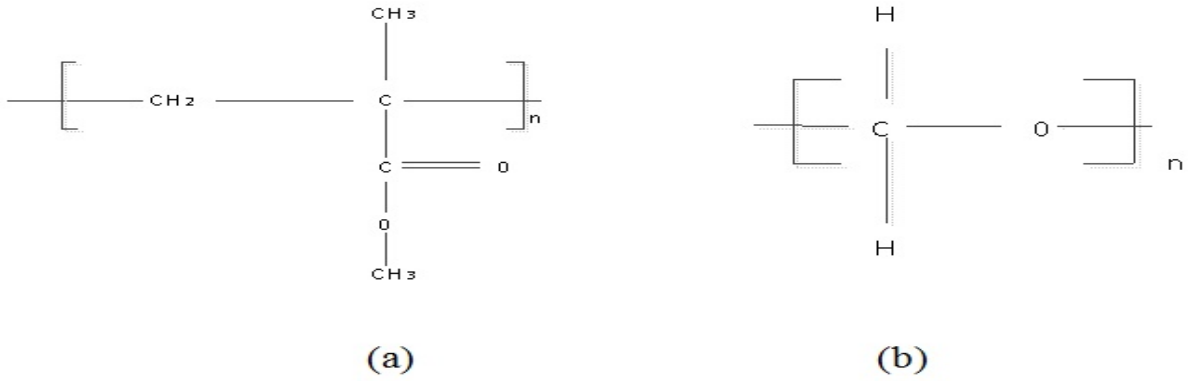

Figure 6.6 Chemical structure of (a) PMMA (b) POM

The increase in surface potential and time to decay for PMMA as against POM can be attributed to the band structure of the insulator. These dielectrics consist of long-chain molecules with strong covalent bonding in the chains and weak Vander Waals bonding between the chains. In a

polymeric structure the bands (conduction and valence band) are localized states rather than extended states so that electron and hole transport occurs by activated hopping [71].

Electrons will move in the periodic potential along the chain interface. However the holes only exist in the valence band. The transport of charge carriers occurs intra molecularly. Chain ends, folds and branching interrupt the periodicity leading to charge localization. Further transport of the charge carriers can proceed only by hopping or tunneling between localized states. The localized states are spatially extended which means the charge trapping centers are extended which depends on the size of polymer molecule chain as shown in Figure 6.7. The numbers of charge trapping centers are increased in case of PMMA as compared to POM which leads to an increase in peak potential and time to decay.

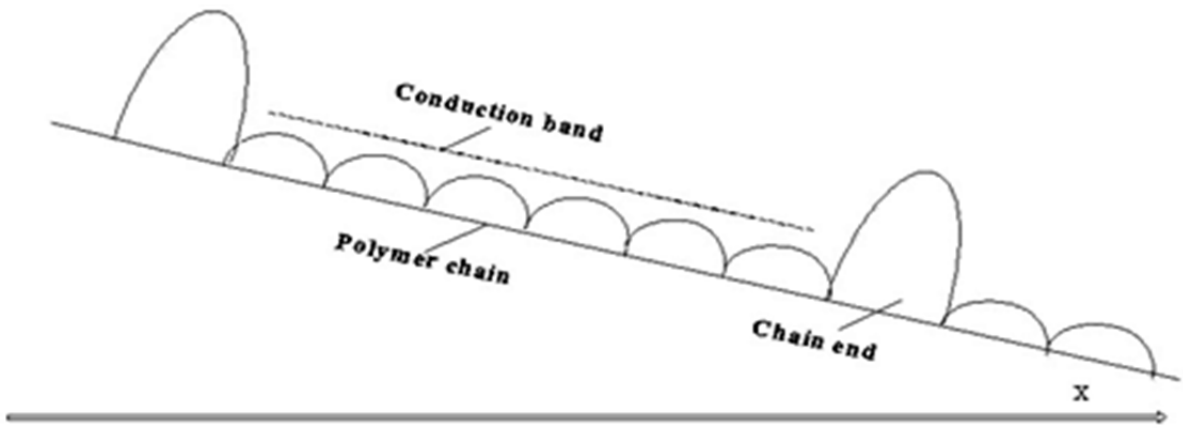

Figure 6.7 Band structure of a section of extended polymer chain. The excess electrons liberated from trap centers can move quasi –freely in conduction band along the chain. The electrons tunnel through a potential well to reach next chain [71].

2. The increase in time to decay of surface potential for negative dc as compared to positive dc is explained on basis of distribution of trap centers with different energy levels present on the surface of the sample. The relationship among the energy level and the density of trapping centers and the isothermal relaxation current density is as follows [140, 142]

$$E_t = kTln(\gamma t) \tag{6.1}$$

$$J = \frac{qdkT}{2t} f_0(E_t) N_t(E_t) \tag{6.2}$$

$$J(t) = \frac{\varepsilon_r \varepsilon_0}{d} \frac{dV_s(t)}{dt} \tag{6.3}$$

where E_t, $N_t(E_t)$, $f_0(E_t)$means the energy level, trap density and initial occupancy of trapping centers respectively, k the Boltzmann constant, q the electron charge, γ the vibrating frequency of electron and T, t, d are the temperature ,time and thickness of the sample respectively.

The current density is calculated using the surface potential decay curve using equation 6.3. Then the relation curve between the density and energy level of trapping centers of PMMA is acquired using equation 6.1 and 6.2 and is shown in Figure 6.8.

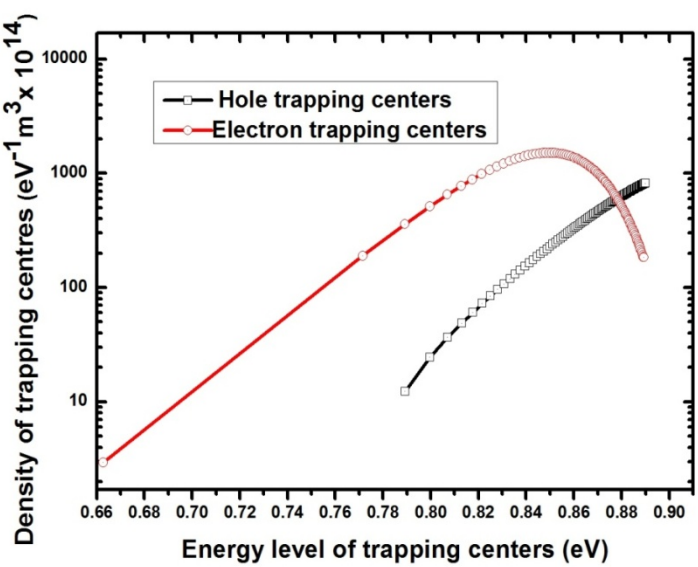

Figure 6.8 The density of trapping centers as a function of its energy level for PMMA sample.

The values of γ and $f_0(E_t)$ are assumed as 10^{12} s^{-1} and 0.5 respectively[140,142].The maximum electron and hole traps in the surface layer of PMMA is of the value ~$1.5x10^{17}eV^{-1}m^3$ and 0.8 $x10^{17}eV^{-1}m^3$ respectively and the energy level of its electron and hole traps are 0.60 -

0.90 eV and 0.78 - 0.9 eV respectively. The charge carriers trapped in low energy trap centers are de trapped more easily then carriers trapped in deep trap centers and hence the time to decay for negative dc is higher than that for a positive dc voltage. Similar results have been observed when studying the trap centers in polytetrafluroethylne block with a slightly higher electron trap density of~ 2.9 x10^{17}eV^{-1}m^{3} as against ~ 2.7 x10^{17}eV^{-1}m^{3} for the density of hole trap centers [140].

3. The introduction of roughness on the surface of the insulator leads to an increase in energy level of electron and hole trap centers from 0.55-0.89 eV as compared to energy range for smooth POM surface from 0.55-0.87 eV. The presence roughness on POM surface leads to an increase in density of electron trap centers from 2.33 ×10^{16}eV^{-1}m^{3} to 2.77 ×10^{16}eV^{-1}m^{3} as shown in Figure 6.9. Similarly the density of hole trap centers increases from 2.85 ×10^{16}eV^{-1}m^{3} to 3.18 ×10^{16}eV^{-1}m^{3} as shown in Figure 6.10.

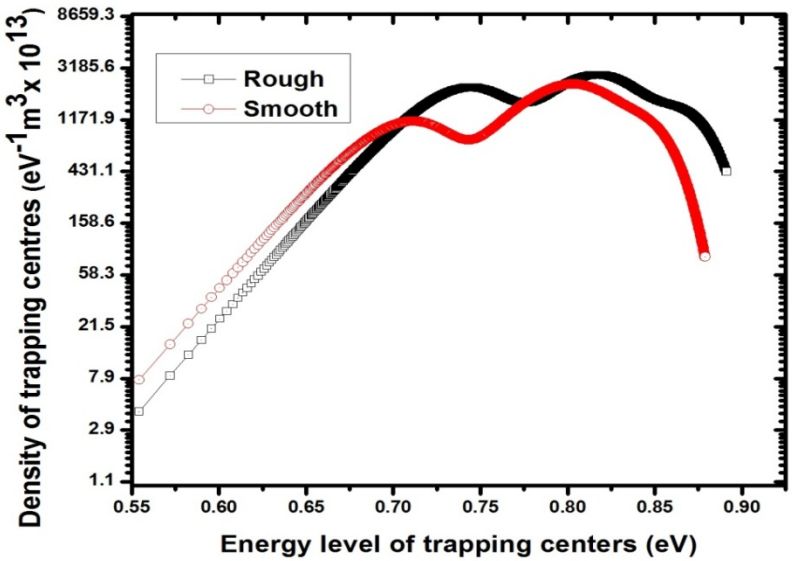

Figure 6.9 The density of electron trapping centers as a function of its energy level for POM sample.

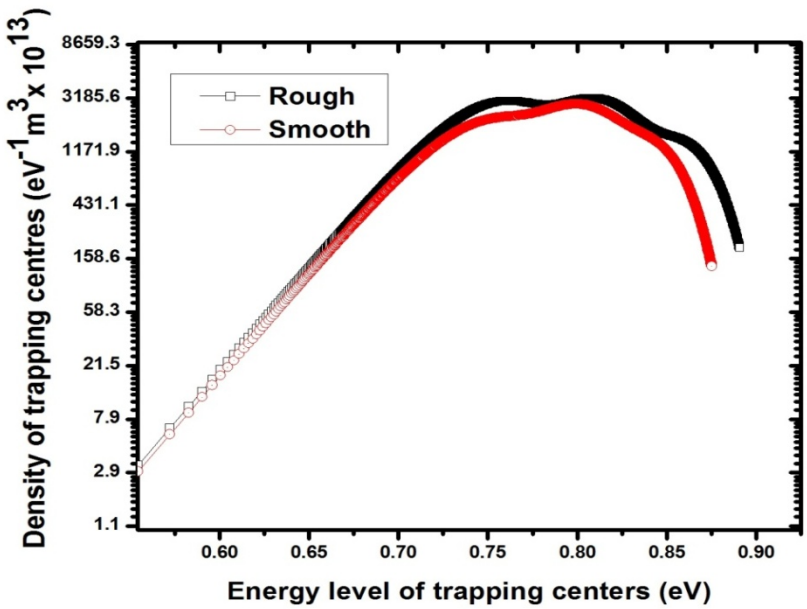

Figure 6.10 The density of hole trapping centers as a function of its energy level for POM sample

Surface roughness leads to the introduction of charge trapping centre on the surface of the insulator and an increase in tracking length on the insulator surface. The increase in density as well as the energy level of both the trap electron and hole centers implies more charge carriers are trapped in deeper trap centers and hence an increase in peak potential and time to decay as observed in Figures 6.4 and 6.5.

6.2 Optical emission spectroscopy study on flashover along insulator surface due to particle contamination

The method of optical emission spectroscopy (OES) is passive and is based on recording light emitted from plasma. The collision with electrons leads to excitation of plasma particles. The relaxation of the excited particles to lower energy state is the reason of emission of photon of light [143]. The ablation of materials by electrical spark plasma forms the basis of analysis of OES. The ablated material is excited in the plasma and the corresponding light in the vacuum ultraviolet to visible range is emitted, the wavelength of which is the characteristic of the element present in the sample and its intensity is a measure its concentration. A number of studies have

been carried out in recent times to study the development of arc and flashover along an ice covered insulator using optical emission spectroscopy (OES) to study the different plasma parameters and the contribution of different particles in the plasma processes [144,145]. The presence of particle on spacer surface provides a local field enhancement and the phenomenon of breakdown was modeled by considering avalanche growth in the surrounding of the particle [146].

This part of the chapter basically emphasizes on the study of the effect of particle contamination (needle protrusion) on spectral characteristics of discharge along insulator surface. It provides an insight into the variation of plasma parameters (plasma temperature and electron density) with distance of particle from cathode. Section 6.2.1 describes the experimental setup of the spectroscopy measurement along with high voltage generation and preparation of the insulator samples. Section 6.2.2 describes the spectroscopic analysis of surface flashover activity in air and nitrogen medium. Section 6.2.3 describes the comparison of H_α due to an insulator in the cathode -anode gap in the two mediums followed by calculation of plasma temperature and density and its effect on distance of the particle contamination from cathode in section 6.2.4.

6.2.1 Experimental methods

The experimental setup for the OES studies on the insulator surface is shown in Figure 6.11. A single phase ac supply is fed to a step up transformer arrangement with a secondary voltage of 100 kV. The output of the step-up transformer is fed to a voltage-doubler circuit for the generation of a high voltage dc output which is fed to the spark gap electrodes enclosed within a Perspex chamber for high pressure studies. The spark gap chamber has a view port arrangement of diameter 150 mm where the lens arrangement is placed perpendicular to path of spark gap discharge to capture the light generated as a result of gap breakdown. Two Rogowski profile

electrodes of 90 mm diameter and 36 mm thickness forms the spark gap electrodes with a cylindrical spacer of 36 mm diameter and 20 mm thickness placed in between the two electrodes. The spacer used is polyoxymethylene (POM) commercially known as delrin which is a commonly used insulator in pulse power systems. The configuration of spark gap electrodes along with the spacer arrangement is very similar to the configurations reported in the literatures for surface flashover study [125,147]. Table 6.2 gives the characteristics of the insulating material used between the electrodes.

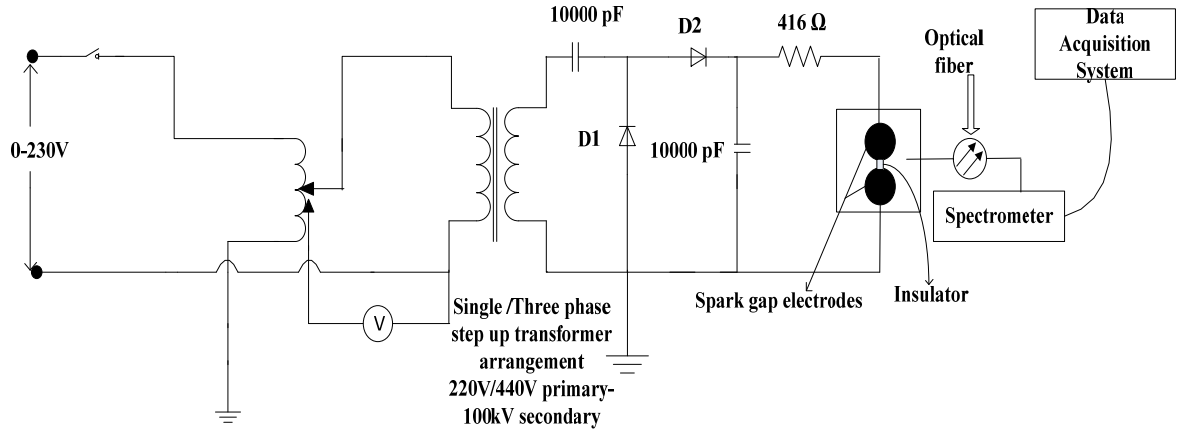

Figure 6.11 Equivalent circuit of the high voltage dc generation and optical spectroscopy measurement

OES is used to determine the spectrum of the plasma with the collected light mainly coming from the bulk of the plasma. However there could be some emissions from regions near the electrodes. The emissions produced as a result of surface discharge in air and nitrogen is collected using a 150 mm focal length lens and is coupled to a time integrated spectrometer (Ocean Optics, USB 2000) using a multimode optical fibre arrangement with a core diameter of 400 μm. The integration time of the spectrometer is 1ms to 65 seconds, baseline corrected wavelength value of 750 nm and the optical fibre used for signal capture subtends an acceptance angle of 25.4^0 with a solid angle of 1.491sr.

Table 6.2: Characteristics of sample (Polyoxymethylene)

Dielectric strength	19.68kV/mm
Dielectric constant (relative to air)	3.7
Loss tangent	0.0085@0.5MHz
Surface roughness	p360
Composition(Chemical formula)	$(CH_2O)_n$

A positive dc voltage of 50 kV was applied to the cylindrical samples of POM with the samples prepared in the following configuration as shown in Figure 6.12.

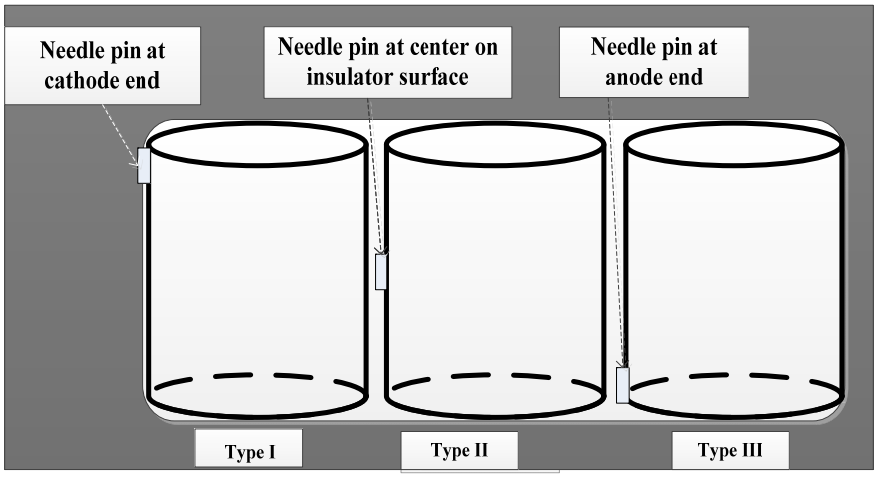

Figure 6.12 Sketch of different types of sample used in the OES study.

1) needle of 3mm length with a diameter of 1mm connected at the cathode tip of the insulator (Type I)

2) needle of 3mm length with a diameter of 1mm connected at the centre on the surface of the insulator (Type II)

3) needle of 3mm length with a diameter of 1mm connected at the anode tip of the insulator (Type III)

The intensity lines were studied with the three sample configurations in air and nitrogen compressed at a pressure of 1kg/cm^2 to analyze the effect of location of particle contamination at different positions on the flashover path.

6.2.2 Results and analysis

A. Analysis of surface flashover activity in air ambience by OES

The phenomenon of surface flashover is analyzed based on the relative intensity of the constituents present in the emission spectra during the discharge phase. However emphasis is laid on the study of the variations in the emission spectra as a result of the introduction of particle contamination at different positions along insulator surface. The need of needle protrusion along the surface of the insulator creates field non-uniformity and initiates discharge along a particular path. Each spectral data is an average of five shots. The emission spectra profile of a spark gap discharge with air as the background medium in the absence of an insulator is shown in Figure 6.13. A high intensity count of singly ionized nitrogen is observed in emission spectra of air.The spectra clearly shows a part of the molecular band emission spectrum of N_2 (C-B) second positive system (SPS) which covers a range 300-450 nm and N_2 (B-A) first positive system (FPS) in the range 600-850 nm. The N_2^+ (B-X) first negative system (FNS) has a spectral band at 391nm is present in the emission spectra but is not very prominent. Other lines observed in the spectra originate from excited N and N^+ species [148]. Air has nitrogen in maximum composition in it which leads to the highest intensity of N^+ in the emission spectra at 500.5 nm and 656 nm as compared to other excited constituents like N and N^+ species. The line at 777 nm is of resonant O I as both nitrogen and oxygen form the major constituents of air. The different spectral lines are identified with the use of molecular nitrogen database [149] and the NIST database [150].

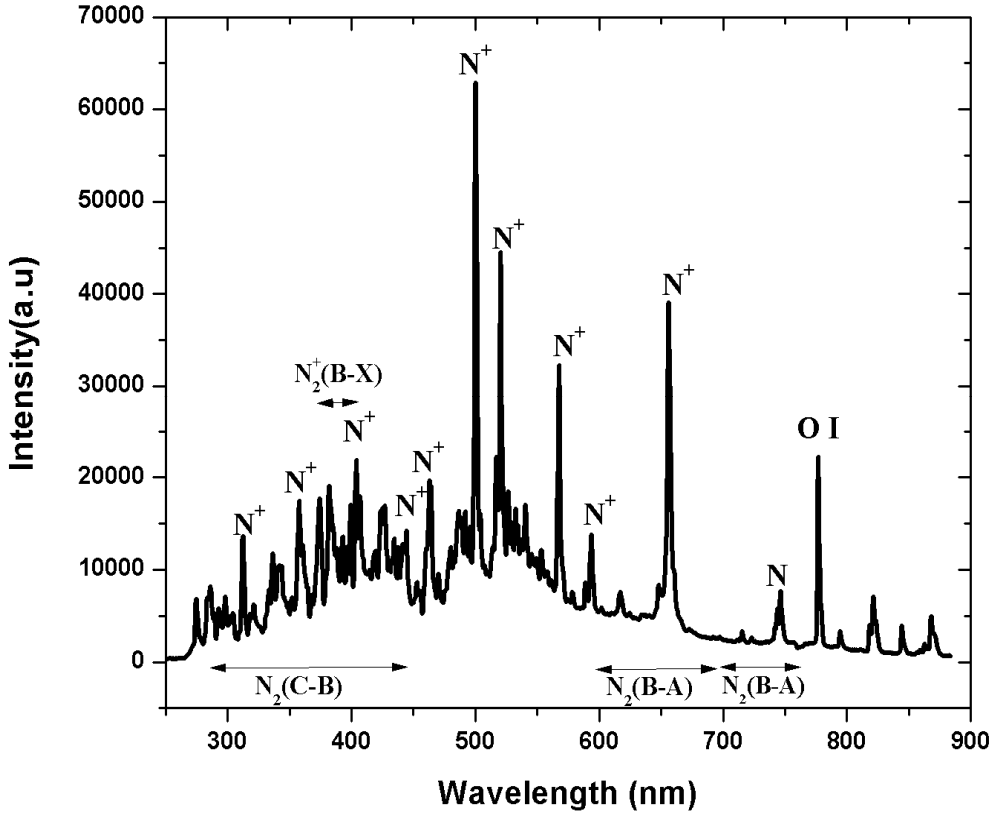

Figure 6.13 Optical emission spectra of spark gap discharge in air

The experiment is repeated with an insulator placed between the two electrodes. It is a polymeric insulator known as polyoxymethyene (delrin) with a chemical formula $(CH_2O)_n$. A needle protrusion as shown in Figure 6.12 is placed at cathode and the emission spectra are observed in Figure 6.14. The spectra shows an increase in the intensity of hydrogen (H_α) at 656.3nm [151] unlike in air which signifies the fact that discharge takes place along insulator surface in a gas insulated system bridged by a solid dielectric. However a peak observed near 656 nm is that of N^+ [150] on which H_α is superimposed leading to an increase in intensity at 656.3nm in the presence of an insulator. Figures 6.15 and 6.16 shows the emission spectra of spark gap discharge when needle is placed at centre and at the anode end along the surface of the insulator respectively .

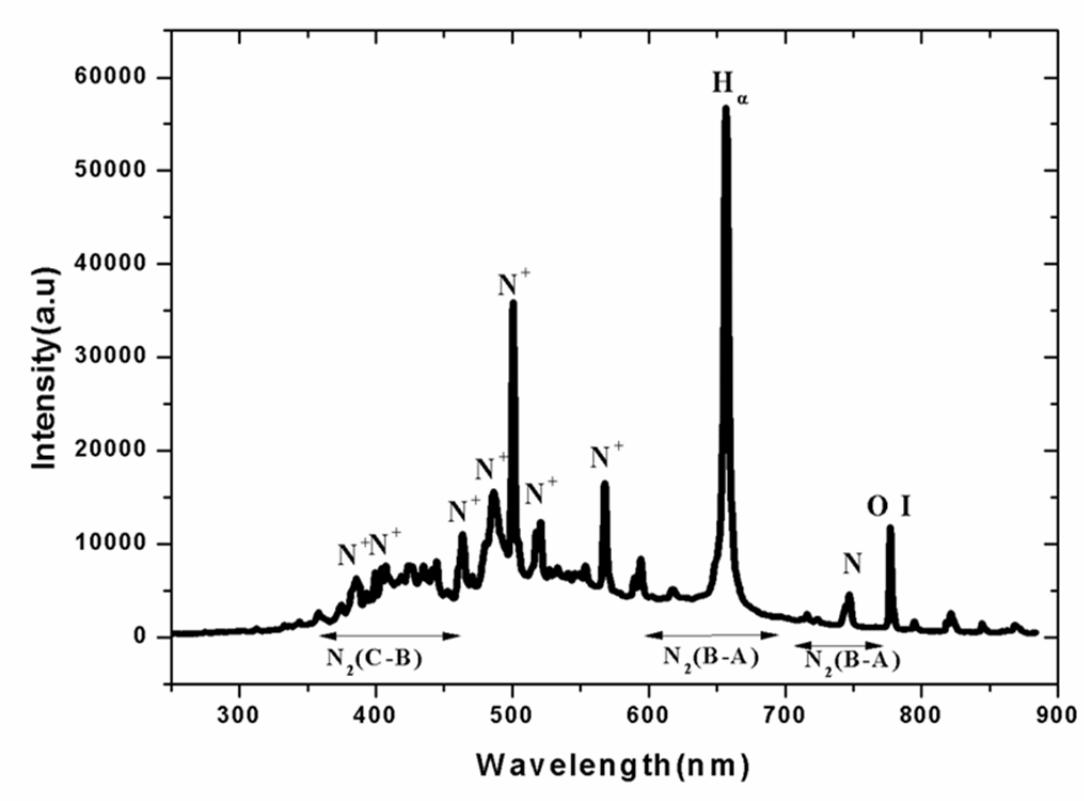

Figure 6.14 Optical emission spectra of spark gap discharge in air along insulator surface when needle protrusion is at the cathode

The maximum intensity of H_α is observed when needle electrode is placed at centre which implies that placing a needle at centre reduces the effective gas gap and discharge paths are formed between the needle and both the electrodes in either direction leading to greater removal of the material from insulator surface in turn leading to highest intensity of H_α in the atomic spectral lines.

However with needle protrusion placed at the anode end comparable intensities of nitrogen N^+ and H_α lines are observed in the atomic spectra which explain the fact that the spark bifurcates and multichannel discharge takes place both in the gas and along the surface of the insulator leading to nearly same intensities of both the elements.

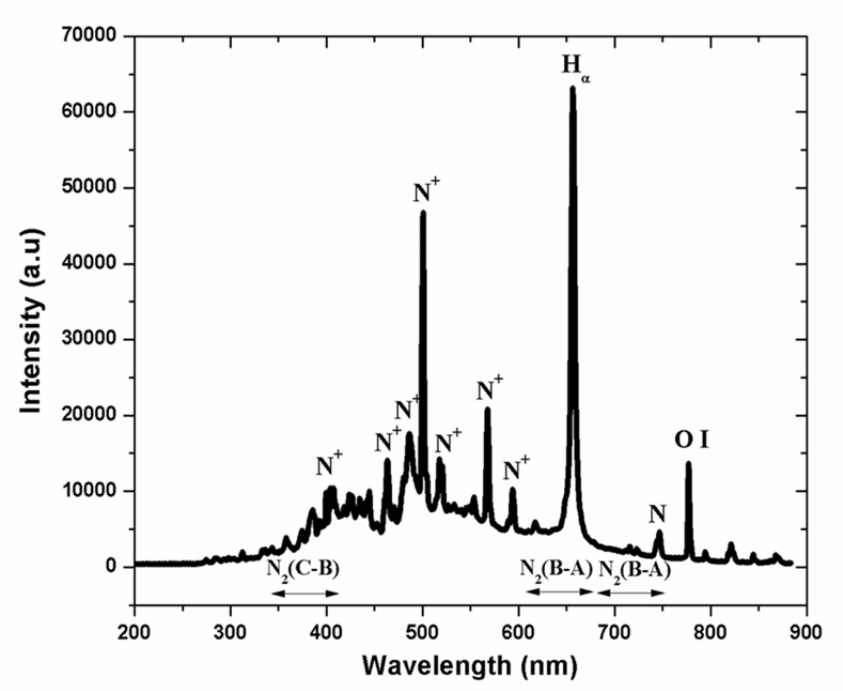

Figure 6.15 Optical emission spectra of spark gap discharge in air along insulator surface when needle protrusion is at the centre

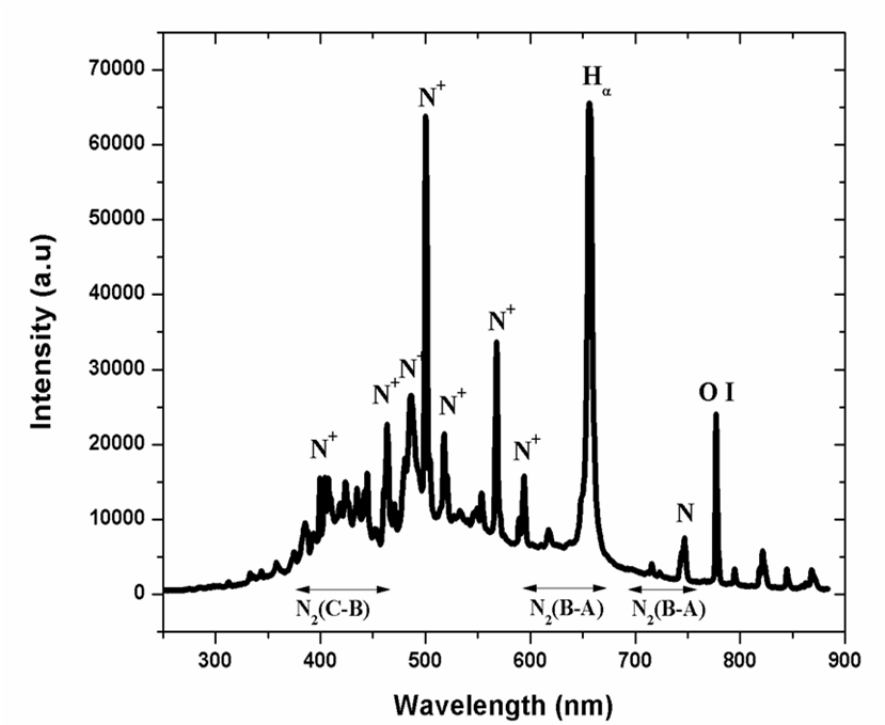

Figure 6.16 Optical emission spectra of spark gap discharge in air along insulator surface when needle protrusion is at the anode

B. Analysis of surface flashover activity in nitrogen ambience by OES

The experiments are repeated to optically study the discharge in nitrogen at a pressure of 1kg/cm^2 as the background gas instead of air. Figure 6.17 shows the spectral lines of spark gap discharge in compressed nitrogen gas. A slight reduction in the values of intensities of singly ionized nitrogen is obtained which signifies suppression in the intensity of spark discharge in compressed gases. The spectra show a peak in the range of 391nm which is a molecular band spectrum of N_2^+ (B-X) first negative system (FNS) which is clearly visible in the spectrum. The spark gap breakdown consists of mainly the ignition and spark phase. The line band around 568 nm is that of N^+ which implies that there is no significant molecular emission during the spark phase and the emission of FPS in the spark phase is mainly because of the overlap between the N_2 (B-A) and atomic nitrogen lines[148].

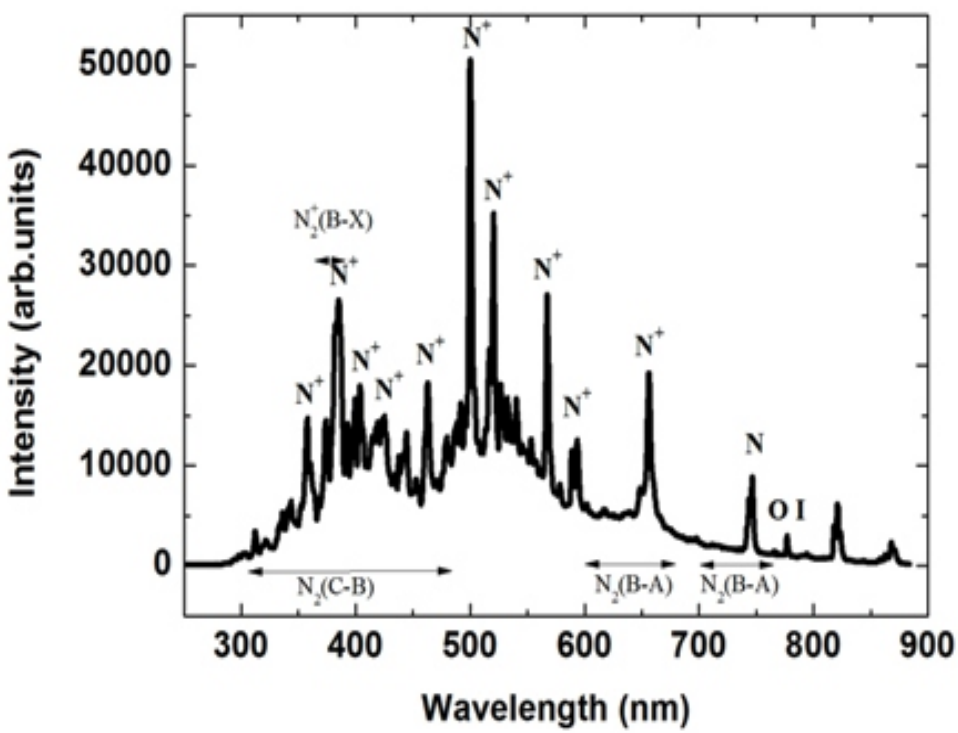

Figure 6.17 Optical emission spectra of spark gap discharge in nitrogen

Similarly the peak around 525 nm is that of presence of atomic nitrogen in the spark phase of

discharge. However in the presence of an insulator the lines at 568 nm and 525 nm is suppressed as shown in Figures 6.18, 6.19 and 6.20 which shows that the H_α line plays the major role at 656.3 nm which suggest that discharge takes place along the insulator surface. However when the needle is present at the anode end of the insulator the discharge phenomenon is very similar to the one taking place in the air medium with needle at anode. The emission in the ignition phase of discharge mainly comes from the FPS, SPS and FNS of nitrogen [148].

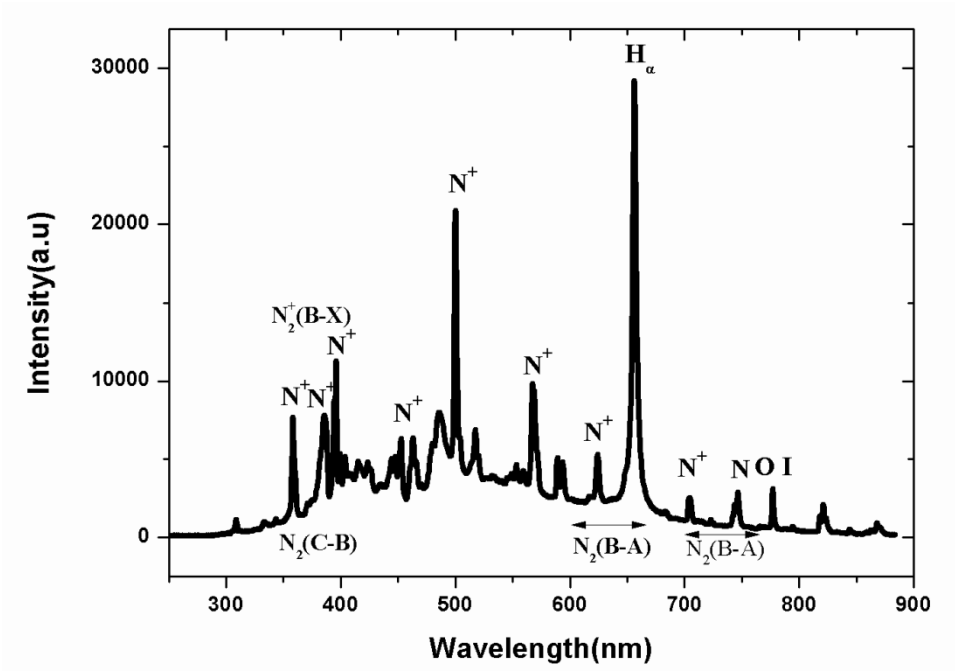

Figure 6.18 Optical emission spectra of spark gap discharge in nitrogen along insulator surface when needle protrusion is at the cathode

In the presence of insulator these band intensities are drastically reduced due a decrease in voltage withstand strength and emission taking place from any point on the surface of the insulator. The nitrogen used in the flashover study is an IOLAR grade with two percent oxygen as impurity. This results in the presence of a resonant O I at 777 nm. However the intensity value is very less when compared to flashover along the insulator surface in ambient air medium in which oxygen is 20% by volume which contributes to the high intensity value of O I line.

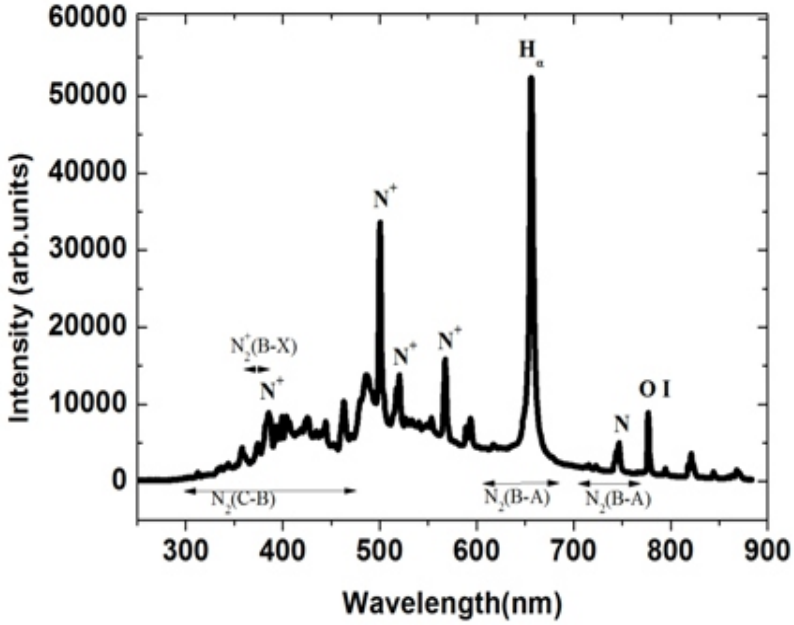

Figure 6.19 Optical emission spectra of spark gap discharge in nitrogen along insulator surface when needle protrusion is at the centre

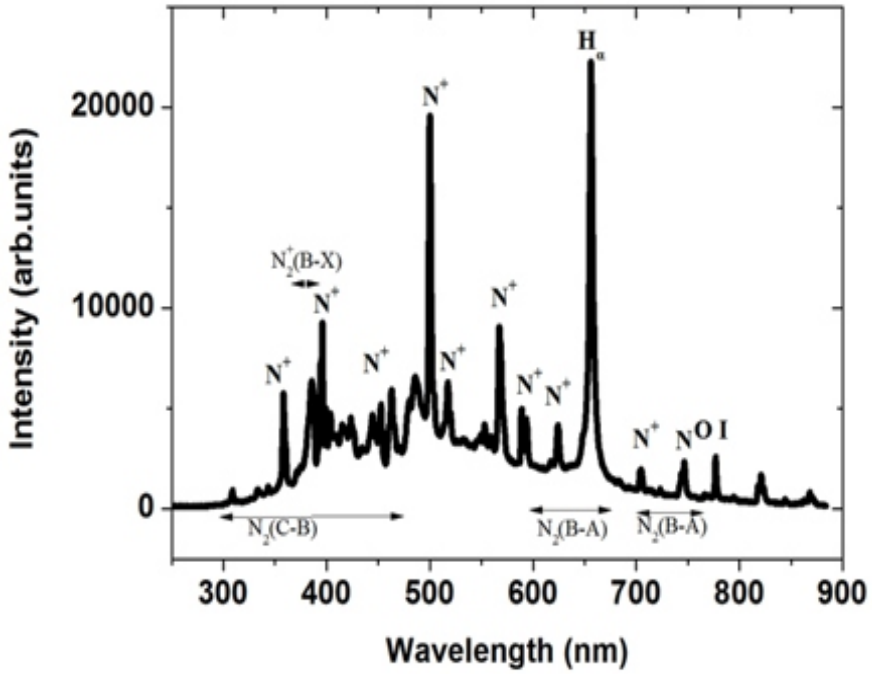

Figure 6.20 Optical emission spectra of spark gap discharge in nitrogen along insulator surface when needle protrusion is at the anode

6.2.3 Comparison of H_{alpha} in air and nitrogen medium

The effect of needle protrusions at different points along the insulator surface between the spark gap electrodes is analyzed on the basis of H_α by using the line broadening of H_α in nitrogen and air with insulator. The measured H_α is fitted with a Lorentizian line shape. The FWHMs are then calculated from the line shape. The discharge initiates at the triple point (cathode +insulator +gas) and arc begins to develop close to the surface leading to slight ionization and arc development. The FWHM estimated from the H_α line broadening are (3.90$\pm$ 0.06) nm and (3.327$\pm$ 0.12) nm in air and nitrogen respectively. Figure 6.19 shows line broadening of H_α in air and nitrogen with needle (protrusion) at anode.

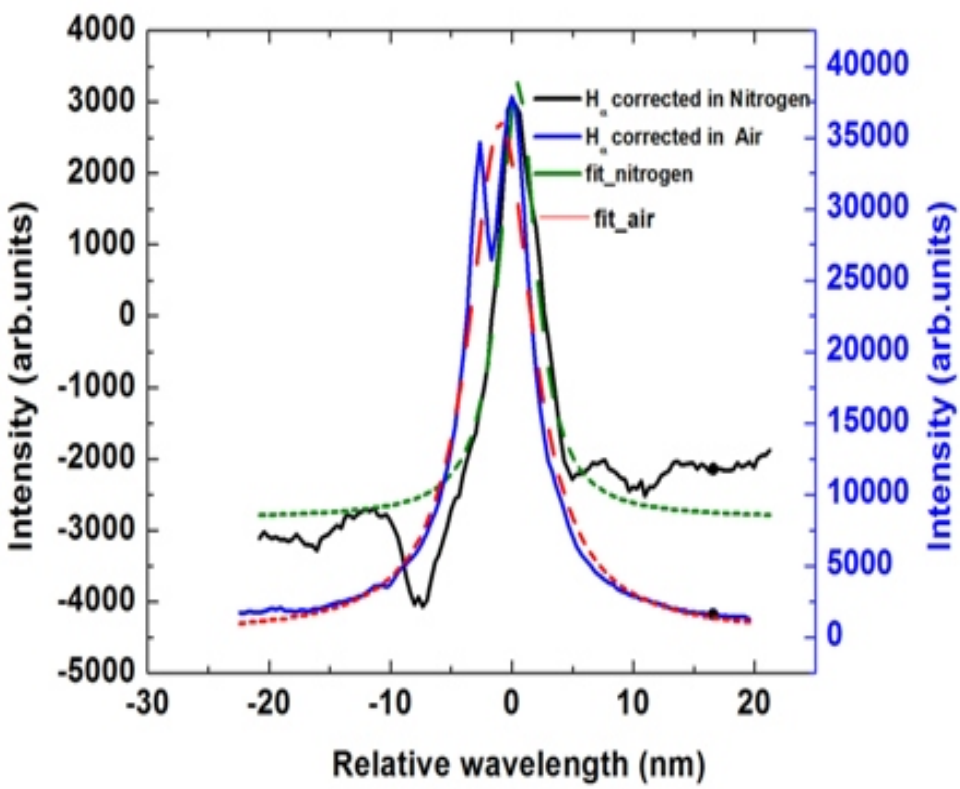

Figure 6.21 Line broadening of Hα in nitrogen and air with insulator (needle at anode). The spectrum of N is subtracted from the spectrum of H_α and N to obtain only the H_α line.

When the needle is placed at the centre along the insulator surface there is further increase in

ionization and expansion of arc leading to increase in FWHM. The maximum value of FWHM is observed when the needle is at anode where the arc has completely expanded leading to maximum line intensity. This suggests that Doppler broadening of the lines to be dominant. The continuous increase in FWHM in air as the protrusion moves away from the cathode is mainly due to the presence of moisture in air. The hydrogen present in moist air ionizes more readily than the ionization of hydrogen along the insulator surface. However such freely available hydrogen is not present in a pure nitrogen environment which leads to an increased value of intensity and hence an increased FWHM in air than in nitrogen. Table 6.3 shows a comparison of FWHM in air and nitrogen for different positions of the needle protrusions.

Table 6.3 Comparison of FWHM in air and nitrogen for different positions of the needle protrusions

Needle position	Air	Nitrogen
At cathode	(3.90±0.06) nm	(3.32±0.12)nm
At centre	(4.32± 0.05) nm	(4.32±0.05)nm
At anode	(6.44±0.22) nm	(3.37±0.02)nm

6.2.4 Estimation of plasma temperature and electron density

The variation in plasma temperature and electron density is studied as function of distance of the particle protrusion from the cathode along the surface of the insulator. The line pair approach was used to estimate plasma temperature and density in which relative intensities of emission lines were used. The plasma temperature and density estimations are based on the assumption of local thermodynamic equilibrium [152]. For the plasma in local thermodynamic equilibrium

(LTE), the energy level population of the different species is given by the Boltzmann's law [153].

$$\frac{n_{a,z}}{n_z} = \frac{g_{a,z}}{P_z} \exp(\frac{-E_a Z}{K_B T}) \tag{6.4}$$

Z refers to the ionization stage of the species (Z=0 and 1 correspond to neutral and single ionized atoms respectively)

k_B is the Boltzmann's constant, T is the plasma temperature , $n_{a,z}$, E_a,and $g_{a,z}$are the population, energy and degeneracy of the upper energy level a, n_z is the number density and P_z is partition function of the species in ionization stage Z. The integrated intensity I_Z of a spectral line occurring between upper and lower energy level i of the species in the ionization stage Z is given by

$$I_z = \frac{hc}{4\Pi\lambda_{ai,Z}} A_{ai,Z} \frac{n_{a,z}}{P_z} g_{a,z} L \exp(\frac{-E_{k,z}}{K_B T}) \tag{6.5}$$

where h is the Planck's constant, c is the speed of light, L is characteristics length of plasma, $\lambda_{ai,Z}$ is the transition line wavelength and $A_{ai,Z}$ is the transition probability .

The intensity ratio of the two lines of the same species of the ionization stage Z is given by

$$\frac{I_1}{I_2} = \frac{\frac{hc}{4\Pi\lambda_{ki}} A_{ki,Z} g_{k,z} L\exp(\frac{-E_{1,z}}{K_B T})}{\frac{hc}{4\Pi\lambda_{nm}} A_{nm,Z}\, g_{n,z} L\exp(\frac{-E_{2,z}}{K_B T})} \tag{6.6}$$

where I_1 is the line intensity from k-i is transition and I_2 is the line intensity from n-m transition. Using equation 6.6 we have

$$T = \frac{(E_2 - E_1)}{K_B \ln(\frac{\lambda_{ki} A_{nm,z}\, I_1 g_{n,z}}{\lambda_{nm} A_{ki,z} I_2 g_{k,z}})} \tag{6.7}$$

The wavelengths $\lambda_{nm}$and λ_{ki} of N^+ lines used in the temperature calculation are 567.4nm and 500.5nm respectively. The Figure 6.22 shows a variation of plasma temperature with distance of needle from cathode along the insulator surface. However there is not much variation in

temperature with distance of particle contamination from cathode. A slight increase in plasma temperature in nitrogen as compared to air can be attributed to reduction in the mean free path in nitrogen with pressure which leads to more number of collisions between the particles leading to an increase in temperature. The ratio of the intensities which is evaluated using two similar wavelengths of nitrogen or air increases implying more ionization as observed with an increase in electron density as shown in Figure 6.23.

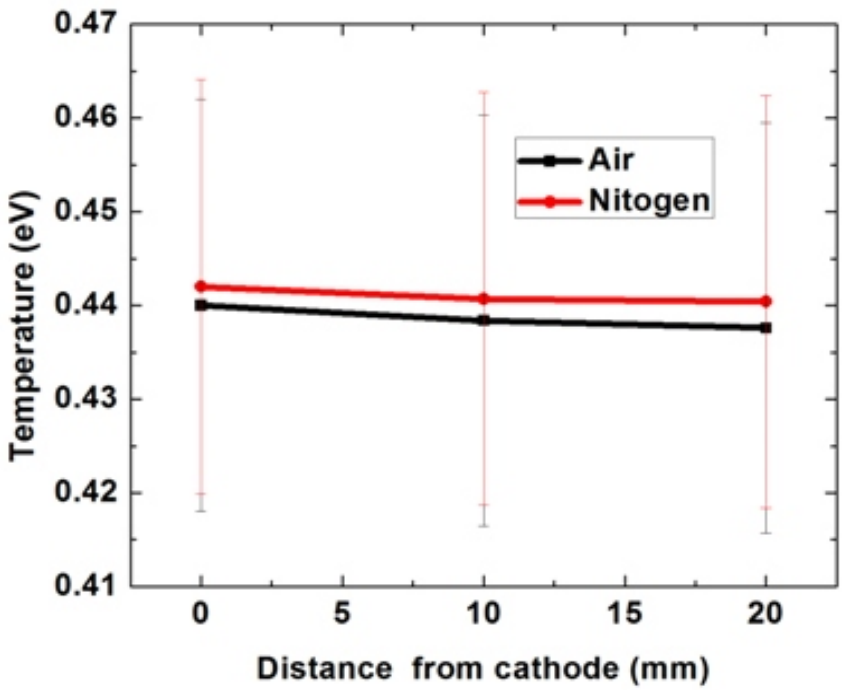

Figure 6.22 Variation of plasma temperature with distance of needle from cathode

This increased intensity ratio leads to reduction in plasma temperature as the particle moves away from the cathode. The effect is independent of the nature of the gas medium surrounding the particle. The results are similar to the study on laser produced carbon plasma in which the temperature shows a decreasing behavior with distance [154]. The electron density calculated using the atom and ion spectral lines which is emitted from the plasma produced by the discharge

between the cathode anode (AK) gap is determined by the Saha-Boltzmann's equation and is given by

$$n_e = \frac{I_a}{I_i} 6.6 * 10^{21} \frac{A_i g_i}{A_a g_a} \exp\left(\frac{E_{ion}+E_i-E_a}{T}\right) \quad (6.8)$$

where n_e is the electron density, $I_a$and I_i are the intensity values of same species in different ionization stages i.e of N and N^+,E_i $A_{i,}g_i$ and E_a, $A_{a,}g_a$, are the energy, transition probabilities of states and degeneracy of the upper energy level and E_{ion} is the minimum energy required to create an ion pair respectively obtained from the NIST database[150].The wavelengths of N^+ and N used in the density calculation are 500.5nm and 746.8nm respectively. Figure 6.23 shows the variation in electron density with the distance of particle (needle) from cathode.

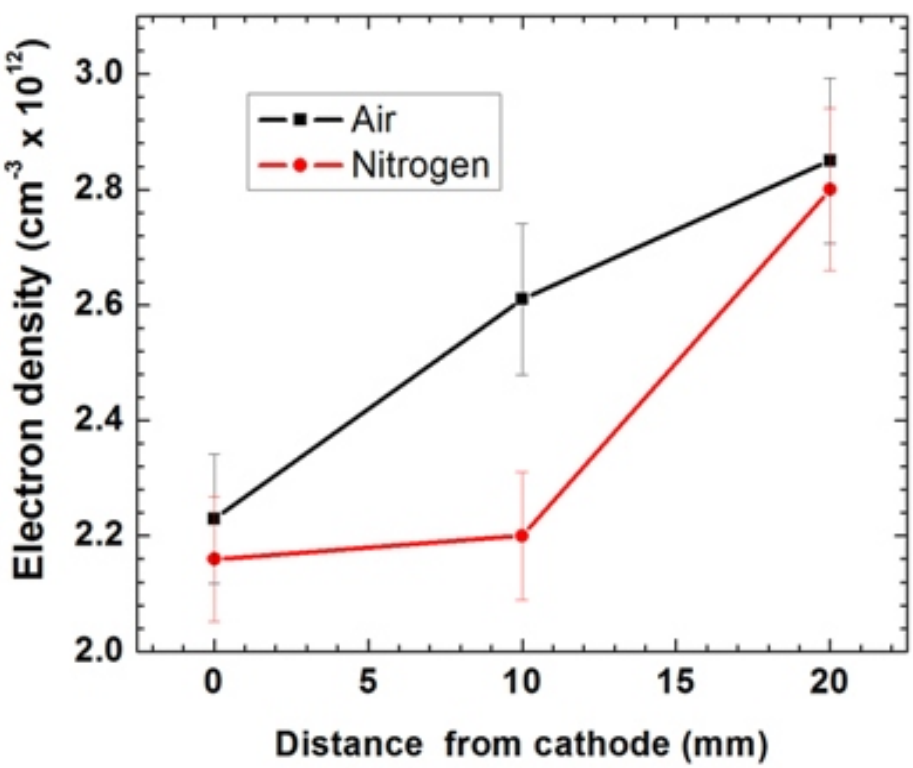

Figure 6.23 Variation of electron density with distance of needle from cathode

An increase in the distance of particle away from cathode serves as conducting medium along the insulator surface which leads to more desorption of material along the surface. Also the cumulative effect of secondary electron multiplication along the insulator surface leads to net increase in electron density as the particle moves away from the cathode. However the density growth in nitrogen is less compared to that in air proves the fact of higher breakdown voltage in nitrogen insulated gap .The additional electrons generated in the gap helps in rapid ionization of the gap causing the gap breakdown at a reduced voltage.

6.3 Conclusion

The surface trapping parameters and energy levels for PMMA is determined both for positive and negative dc voltages. The increase in peak potential and time to decay for PMMA as against POM is due to the length of the polymeric chain which increases the electron travel time and also electron tunneling through a potential well. The sudden termination of lattice structures causes atoms present on the surface of solid to remain active due to the presence of unsaturated chemical bonds which is generally covered with layers of impurity. These create imperfections on the surface of the sample which act as trap centers with very high density on the surface as compared to bulk of the sample .Thus the nature of surface of an insulating material influences its flashover characteristics.

Further the technique of optical emission spectroscopy is used to study the dc discharge along polyoxymethylene subjected to particle contamination in air and nitrogen medium. A variation in the intensities of the constituent atoms which implies material erosion and electron desorption from insulator surface being dependent on the position of the particle contamination along the insulator surface. A reduction in the intensity of spark is observed in nitrogen medium which could be due to the reduction in energy gained between successive collisions as the

pressure is increased and hence the collective intensity is less when the excited atoms return to the ground state. A reduction is observed in the value of plasma temperature from 0.441eV to 0.437eV with increase in the distance of particle contamination from cathode. The increase in electron density from 2.1×10^{12} cm^{-3} to 2.8×10^{12} cm^{-3} can be attributed to increased material desorption and secondary electron multiplication with increase in distance of particle from cathode.

CHAPTER 7

SUMMARY AND FUTURE PERSPECTIVE

The fundamental study is on the discharge characteristics along the gas-solid interface along with the effect of spacer shape and surface on discharge behavior in gaseous medium. The following conclusions were made on the above studies:

1. A finite difference time domain (FDTD) based particle-in-cell (PIC) code was developed to understand the mechanism of discharges along gas-solid interface under nanosecond pulse voltage. The profiles of phase space of electron movement in the cathode anode gap shows a reduction in the momentum of electrons in a spacer bridged gap is observed unlike the plain gas gap condition. The peak value of electron number densities is 3.38 $x10^{12}$ m^{-3} in the presence of dielectric as compared 6.14 $x10^{11}$ m^{-3} in a plain gas gap condition in a velocity range from 0-20 $x10^{7}$ m/s which highlights secondary electron emission along the insulator surface leading to an increase in electron density and serves as a dominant factor for insulator flashover.

2. Different spacer profiles comprising of conical angled insulators, bush bar insulators, double ended frustum insulators and protrusions on insulator surface are used to study the effect of spacer profile and shape on spacer efficiency. An increase in spacer efficiency from 86% in case of cylindrical insulators to 97% with negative angled and bush bar spacer is observed for a 20mm gap length with nitrogen as background gas.

3. A compact Marx generator based on pulse forming network (PFN) is developed with a maximum output voltage of 300kV on a matched load and output energy of 64J. A peaking capacitor connected at the output of the Marx generator significantly improves the rise time from 25ns to 5ns. A reduction in the breakdown voltage is observed in both Perspex

(PMMA) and Delrin (POM) with the highest spacer efficiency of 91% in Perspex bridged spark gap. A reduction in spacer efficiency with pressure is observed with a reduction of 11% in spacer efficiency at a pressure of 4kg/cm^2 in Perspex as compared to Delrin which shows a higher reduction of 18% with pressure.

4. An increase in peak surface potential and time to decay in PMMA as compared to POM is attributed to the length of the polymeric chain responsible for chain retentivity in the material. The maximum electron and hole traps in the surface layer of PMMA is ~1.5 x 10^{17} $eV^{-1}m^3$ and 0.8 x 10^{17} $eV^{-1}m^3$ respectively, with energy level in the range of 0.60 - 0.90 eV and 0.78 - 0.9 eV respectively. The charge carriers trapped in low energy trap centers are de trapped more easily then carriers trapped in deep trap centers and hence the time to decay for negative dc is higher than that for a positive dc voltage in PMMA.

5. The needle protrusion at three different locations on insulator surface which serves as a particle contamination are used to study the variation in spectral characteristics in an insulator bridged gas gap in air and nitrogen at a pressure of 1kg/cm^2. The plasma temperature during bulk breakdown in air is 0.433eV and increases to 0.44eV and from 0.434eV with pressure in nitrogen to 0.441eV in the presence of insulator. The plasma temperature decreases and the electron density increases with increase in distance of particle contamination from cathode.

Further research is open for studying and analyzing different insulators, dielectrics, metals and use of different diagnostics for understanding and minimizing the problem of surface flashover. Finally some suggested future work is outlined

- The application of different pulse durations to study its effect on the flashover phenomena.

- The use of different gases like argon and helium and different insulator materials to further study the variations in the discharge phenomena.
- The use of streak camera to study the spatial and temporal variation of streamer growth along different insulator materials.

Present work has contributed to a better understanding of insulation aspects of high voltage pulse power systems. The study carried out in this thesis is useful in the development of reliable and efficient insulation structure in pulse power systems.

REFERENCES

[1] S.T.Pai and Qi Zhang ,*Introduction to high power pulse technology* Published by World Scientific, 1995

[2.] R.A. Anderson and J.P.Brainard, “Mechanism of pulsed surface flashover involving electron simulated desorption,” J.Appl.Phy.Vol 51, pp.1414-1421, 1980.

[3] R.A. Anderson and W.K.Tucker, “Vacuum surface flashover from bipolar stresses,” J.Appl. Phys.Vol 58, pp.3346-3349, 1985.

[4]J.D.Cross,“High speed photography of surface flashover in vacuum,” IEEE Trans. Electr.Insul.Vol13, pp.145-148, 1978.

[5] A.A.Avdienko and M.D.Malev, “Flashover in vacuum,” Vacuum. Vol 12, pp.643-651, 1977.

[6] A.A.Avdienko, “Surface breakdown of solid dielectrics in vacuum I. Characteristics for breakdown along vacuum surface,” Sov.Phys.Tech Phys.Vol22, pp.982-985, 1977

[7] A.A.Avdienko and M.D.Malev, “Surface breakdown of solid dielectrics in vacuum II. Mechanism for surface breakdown,” Sov.Phys.Tech .Phys, Vol.22, pp.986-991, 1977

[8] J.P.Vigauroux, O.Lee Deacon, C.LeGressus, I.Juretand ,and C.Borzau, “Surface processes during occurring breakdown of high voltage devices,” IEEE Trans. Electr. Insul. Vol. 18, pp. 287-291, 1983

[9] C.L.Enloe "The equilibrium charge distribution and electric field at a vacuum/dielectric interface" J.Appl.Phys.Vol.65, pp.3329-3334,1989

[10] H Singer, H Steinbigler, and P Weiss" A charge simulation method for the calculation of high voltage fields," IEEE Trans. Power Apparatus Syst.Vol. PAS-92 ,pp.871-876, 1973

[11] H. Craig Miller, “Surface Flashover of Insulators,” IEEE Trans. Electr. Insul. Vol. 24, pp. 765-786, 1989.

[12] J. Lewis, T. S. Sudarshan, J. E. Thompson, D. Lee, and R. A. Dougal, “Pre-Breakdown and Breakdown Phenomena along PMMA Surfaces in Vacuum and Nitrogen Gas Stressed by 60 Hz Voltages,” IEEE Trans. Electr. Insul. Vol. 19, pp. 512-518, 1984.

[13]C.M. Jones, K.A. Erb, D.L . Haynes, J.T . Mitchell ,N.F. Ziegler, J.E . Raatz ,and R.D. Rathmell "Tests of compressed geometry acceleration tubes in the oak ridge 25URC tandem accelerator," Nuclear Instruments and Methods in Physics Research. Vol.A268 ,pp.361-367, 1988

[14]W. Assmann, G. Korschinek,and H. Munzer"Test of NEC tubes in compressed geometry," Nuclear Instruments and Methods in Physics Research.Vol.220,pp.86-89,1984

[15]Amitava Roy, Rakhee Menon, Sabyasachi Mitra, D. Durga Praveen Kumar, Senthil Kumar, Archana Sharma, K. C. Mittal, K. V. Nagesh, and D. P. Chakravarthy "Intense relativistic electron beam generation and prepulse effect in high power cylindrical diode," J. Appl. Phys. Vol. 103, pp. 014905(6pp) ,2008.

[16]Amitava Roy, Sabyasachi Mitra, Rakhee Menon, D. Durga Praveen Kumar, Senthil Kumar, Archana Sharma, K. C. Mittal, K. V. Nagesh, and D. P. Chakravarthy "Prepulse Suppression on a High-Power Electron Beam Accelerator Using a Dielectric Cathode Holder," IEEE Trans. Plasma Sci.Vol. 37, pp. 67–75, 2011.

[17]Tadasu Takuma and Boonchai Techaumnat , *Electric fields in composite dielectrics and their applications* Published by Springer 2010

[18]J. R. Laghari and A. H. Qureshi "Surface flashover of spacers in compressed gas insulated systems," IEEE Transactions on Electrical Insulation. Vol.EI-16 No.5, pp.373-387, 1981.

[19]Chathan M.Cooke and Alan .H.Cooke "The nature and practice of gases as electrical insulators," IEEE Trans. Electr. Insul.Vol.EI-13 ,pp.239-248, 1978.

[20]G.R.Nagabhushana"Breakdown mechanism and insulation design with vacuum,gas, liquid and solid,"Proc.of technology and electrical insulation and high voltage pulse techniques,BARC,Mumbai,March1-5,pp.43-65,1982

[21]M.S.Naidu, *High Voltage Engineering* Tata McGraw Hill Education Published by 2004

[22]E. E. Kunhardt, and W. W. Byszewski "Development of overvoltage breakdown at high gas pressure," Physical Review A. Vol 21,pp.2069-2077,1980

[23]Yukimitsu Kawada, Sumikazu Shamoto and Tatsuzo Hosokawa "Nanosecond-pulse breakdown of gas-insulated gaps," J. Appl. Phys.Vol. 63, pp. 1877-1881,1988

[24]John Mankowski, James Dickens and Magne Kristiansen, "High Voltage Subnanosecond Breakdown," IEEE Trans. Plasma Sci.Vol. 26, pp. 874-881,1998

[25]T. H. Martin, “An empirical formula for gas switch breakdown delay,” Res.Sci.Pulsed Power, Sandia Nat. Labs., pp. 73–79, 1991.

[26]R.C.Fletcher "Impulse Breakdown in the 10^{-9} -Sec. Range of Air at Atmospheric Pressure," Physical Review. Vol 76,pp.1501-1511,1949

[27]G.A.Mesyats, Yu. I. Bychkov, and V. V. Kremnev ,"Pulsed nanosecond electric discharges in gases," Soviet Physics Uspekhi. Vol.15, No. 3, pp.282-297,1972

[28]J.Koppitz,“Nitrogen discharge of large cross section at high overvoltage in a homogeneous field,”J. Phys. D: Appl. Phys. Vol. 6, pp. 1494-1502, 1973.

[29]S. J. Levinson and E. E. Kunhardt ,"Investigation of the Statistical and Formative Time Lags Associated with the Breakdown of a Gas in a Gap at High Overvoltage," IEEE Trans. Plasma Sci.Vol. PS-10, pp. 266-270,1982

[30]L. M. Vasilyak, S. P. Vetchinin and D. N. Polyakov, “Effect of the rise rate of nanosecond high-voltage pulses on the breakdown of air gaps,” Tech. Phys. Lett. Vol. 25, pp. 749-751,

1999.

[31]Yukimitsu Kawada and Tatsuzo Hosokawa," Observation of nanosecond-pulse breakdown of gas - insulated gaps by image converter camera," J. Appl. Phys. Vol. 67, pp. 1249,1990

[32]Tao Shao, Guangsheng Sun, Ping Yan and Shichang Zhang" Breakdown phenomena in nitrogen due to repetitive nanosecond-pulses," IEEE Trans. on Dielec. Elec. Insul. Vol. 14,pp. 813-819,2007

[33]Tao Shao, Guangsheng Sun, Ping Yan and Shichang Zhang ,"Repetitive Nanosecond-Pulse Breakdown in Tip–Plane Gaps of Air," IEEE Trans. Plasma Sci.Vol. 34, pp. 1620-1625,2006

[34]S.J. MacGregor, F. A. Tuema, S. M. Turnbull and O. Farish, “The operation of repetitive high-pressure spark gap switches,” J. Phys. D: Appl. Phys.Vol. 26, pp. 954–958, 1993.

[35]M. M. Pejovic and G.S. Ristic, “Memory effects in argon, nitrogen, and hydrogen,” IEEE Trans. Plasma Sci., Vol. 30,pp. 1315-1319, 2002.

[36]Xinxin Wang, Member, Haiyun Luo and Yuan Hu, "Numerical Simulation of the Gas Discharge in a Gas Peaking Switch," IEEE Trans. Plasma Sci., Vol. 35, pp. 702-708, 2007

[37]K.Takaki and H. Akyama "Resistance of pulsed arc discharge in air and SF_6,"IEEE Pulsed Power Conference, Vol-2,pp.1758-1761,2001

[38]V.Carborni, D.Giri and J.Lehr, "The breakdown fields and rise times of select gases under the conditions of fast charging (- 20 ns and less) and High Pressures (20 - 100 atmospheres)," IEEE Pulsed Power Conference,Vol-1,pp.482-486,2001

[39]J.L. Liu, Y. Yin, T.W. Zhan, J.H Feng, and H.H Zhong," Application of a self-breakdown hydrogen spark gap switch on high power pulse modulator,"16th IEEE Pulsed Power Conference, pp.-455-458, 2007

[40]B.S. Manjunath, K. Dwarakanath, K.S. Arunachala Sastry, and K.N. Ravi,"Uniform field

breakdown in SF_6 gas at high pressures under lightning and switching surge voltages," Annual Conference Report on Dielectric and Electric Insulation Phenomena,pp.329-333,1988

[41]Y. Kawaguchi,K. Sakata and S. Menju, " Dielectric breakdown of sulphur hexafluoride in nearly uniform fields," IEEE Trans. Power Apparatus Syst. Vol. PAS-90, pp. 1072-1078, 1970.

[42]Koshi ltaka,and Giichi Ikeda, "Dielectric strength of compressed gas insulated cables," IEEE Trans. Power Apparatus Syst. Vol. PAS-89, pp. 1986-1994, 1970.

[43]S. H. Nam, H. Rahaman, H. Heo, S. S. Park, J. W. Shin, J. H. So, and W. Jang ,"Empirical analysis of high pressure SF_6 gas breakdown strength in a spark gap switch," IEEE Trans.on Dielec. and Elec. Insul.Vol. 16, pp.1106-1110, 2009

[44]E. Kuffel and W.S. Zaengl, *High Voltage Engineering Fundamentals* Published by Pergamon Press, 1984.

[45]M. S. Di Capua, E. K. Freytag, W. R. Dixon, and R. A. Hawley, “A Simple Self-Breaking 2 MV Gas Switch,” IEEE 6th Pulsed Power Conf., pp. 518-521, 1987.

[46]D.A. Goerz, M.J. Wilson, and R.D. Speer, “A Low Profile High Voltage Compact Gas Switch”, IEEE 11th Pulsed Power Conference, pp. 328-333, 1997.

[47]G. Olivier, Y. Gervais, and D. Mukhedkar, “A New Approach to Compute Uniform Field Breakdown of Gases,” IEEE Trans. Power Apparatus Syst. Vol. 97, pp. 969-976, 1978.

[48]Peter Felsenthalt and Joseph M. Proud," Nanosecond-Pulse Breakdown in Gases," Physical Review. Vol 139,pp-1796-1804 ,1965

[49]Laird P. Bradley, "Preionization Control of Streamer Propagation" J.Appl.Phys.43(3) ,pp.886-890,1972

[50]Chathan M.Cooke, "Ionization, electrode surfaces and discharges in SF_6 at extra-high-voltages," IEEE Trans. Power Apparatus Syst. Vol.PAS-94,pp. 1518-1523,1975

[51]Alan H. Cookson and Owen Farish," Particle-initiated breakdown between coaxial electrodes in compressed SF_6" IEEE Trans. Power Apparatus Syst. Vol. PAS-92, pp.871-876, 1973.

[52]Alan H. Cookson, "Electrical breakdown for uniform fields in compressed gases" Proc. IEE, Vol. 117, pp.269-280, 1970.

[53]J.H.Mason, " Breakdown of solid dielectrics in divergent fields" Proc. IEE. part-1, Vol. 98, pp,44-59,1951.

[54]J.H.Mason,"The deterioration and breakdown of dielectrics resulting from internal discharges," Proc. IEE. Part-C. Vol. 102, pp,254-263,1955.

[55]K.H.Stark and C.G.Garton, "Electrical Strength of irradiated polyethylene", Nature. Vol. 176,pp.1225-1226,1955.

[56]H. Frohlich "On the Theory of Dielectric Breakdown in Solids" Proc. R. Soc. Lond. Vol.188 A ,pp 521-532, 1947.

[57] N.Klein,"Electrical breakdown of insulators by one carrier impact ionization" J. Appl. Phys. Vol.53, pp.5828-5839, 1982.

[58]Paul P.Budenstein, "On the mechanism of dielectric breakdown of solids, "IEEE Trans.on Electr. Insul. Vol. EI-15, pp.225-240,June 1980

[59]I. Kitani, and K. Arii, “Impulse Tree and Discharge Light in PMMA Subjected to Nanosecond Pulse,” IEEE Trans. Electr. Insul.Vol. 19, pp. 281-287,1984

[60]H. Yamada., T. Fujiwara, K. Tamada, S. Kimura and T.Sato, "Optical measurement of breakdown process in polymethylmethacrylate under nanosecond Pulse Voltage application” ,Proc. of the 4th International Conference on Conduction and Breakdown in Solid Dielectrics,pp.348-352,1992

[61]Liang Zhao, Jiancang Su, Xibo Zhang, Yafeng Pan, Limin Wang, Jinpeng Fang, Xu Sun,

Rui Li, Bo Zeng and Jie Cheng,"An experimental and theoretical investigation into the “worm-hole” effect ," J. Appl. Phys. Vol. 114, pp. 0363306,2013

[62]Liang Zhao Jiancang Su, Xibo Zhang and Yafeng Pan, "Experimental investigation on the role of electrodes in solid dielectric breakdown under nanosecond pulses" IEEE Trans. on Dielec. and Electr. Insul. Vol. 19 ,pp.1101-1107,2012

[63]Hiroshi Yamada, Tamiya Fujiwara,and Koji Tamada, "High-speed photography of PMMA breakdown under ns pulse voltages," IEEE Trans. on Dielec. and Electr. Insul. Vol. 1 ,pp.754-756,1994

[64] B. Halpern and R. Gomer, “Field Ionization in Liquids,” J. Chem. Phys. Vol. 51, pp. 1048-1056,1969

[65]D.W. Auckland, A.B. Borishade and R.Cooper, "Photographic investigation of breakdown of composite insulation" Proc. IEE. Vol. 124, No. 12pp.1236-1266,1977

[66]James A.Knaur and Paul P. Budenstein, "Impulse breakdown in PMMA under megavolt, nanosecond excitation," IEEE Trans. Electr. Insul. Vol. EI-15 No. 4,pp.313-321,1980

[67]D.B.Watson, "Dielectric breakdown in Perspex" IEEE Trans. Electr. Insul. Vol. EI-8,pp.73-75,1973

[68]M. Treanor, J. R. Laghari and A. K. Hyder," Repetitive phenomena in dielectrics" IEEE Trans. Electr. Insul., Vol.EI-22,pp.517-522,1987

[69]D W Auckland, A B Borishade, and N Gravill, "A self-triggered high speed camera for the photography of pre breakdown luminescence in solid dielectrics," J. Phys. E: Sci . Instru.Vol. 8, pp. 847-849, 1975.

[70]L. A. Dissado, J. C. Fothergill, S. V. Wolfe and R. M. Hill, “Weibull statistics in dielectric breakdown; Theoretical basis, applications and implications,” IEEE Trans. Electr. Insul. Vol. EI-

19, pp. 227–233,1984.

[71] Hansjoachim Bluhm, *Pulsed Power systems: Principles and Applications* Published by Springer-Verlag ,2006

[72]M. P. Wilson, M. J. Given, I. V. Timoshkin, S. J. MacGregor, M. A. Sinclair, K. J. Thomas,and J. M. Lehr, “Impulse-breakdown characteristics of polymers immersed in insulating oil,” IEEE Trans. Plasma Sci.Vol. 38, pp. 2611–2619, 2010.

[73]Liang Zhao, Guo-zhi Liu, Jian-cang Su, Ya-feng Pan and Xi-bo Zhang, "Investigation of Thickness Effect on Electric Breakdown Strength of Polymers Under Nanosecond Pulses," IEEE Trans. Plasma Sci.Vol. 39,pp. 1613-1618,2011

[74]George.L.Jackson, “Pulsed flashover of solid dielectrics in vacuum and gases” Ph.D thesis, Texas Tech University,1983

[75]N.L.Allen and P.N.Mikropoulos, “ Streamer propagation along insulating surface” IEEE Trans. on Electr. Insul. Vol.6 ,pp. 357-362,1999

[76]C. Heitz, M. Piemontesi and G. Salge, "Surface discharge along solid dielectrics in atmospheric air" IEEE International Symposium on Electrical Insulation,pp.341-344,2000

[77]S.Tentbohlen and G.Schroder, “The influence of space charge on lightening impulse breakdown of spacers in SF_6,” IEEE Trans. on Electr. Insul. Vol.7,pp. 241-246, 2000

[78]Feng Wang,Yuchang Qiu,Wolfgang Pfeiffer and Edmund Kuffel, “Insulator surface charge accumulation under impulse voltage, ” IEEE Trans. Electr. Insul. Vol.11 ,pp. 847-854, 2004

[79]J.T Kennedy,"Study of the Avalanche to Streamer Transition in Insulating Gases,". Ph.D. thesis, Eindhoven Univ. of Techn., Eindhoven, The Netherlands,1995

[80]C.Wen, "Time-Resolved Swarm Studies in Gases with Emphasis on Electron Detachment and Ion Conversion". Ph.D. thesis, Eindhoven Univ. of Techn., Eindhoven, 1989

[81]H.F.A Verhaart, "Avalanches in Insulating Gases".Ph.D. thesis, Eindhoven Univ. of Techn., Eindhoven, 1982.

[82]H. Hama,H. Yamamoto, S.Sakuma, K. Takatsuka and T. Yamauchi," Surface flashover characteristic of disc-type spacer system initiated by wedge shaped gas gap and its improvement," IEEE Trans. Power Apparatus Syst.Vol.8,,pp.1070-1079,1993.

[83]N. Giao Trinh, Garry Mitchel and Claire Vincent, "Influence of an insulating spacer on the V-t characteristics of a coaxial gas-insulated cable Part I: Study on a reduced-scale coaxial conductor," IEEE Trans. Power Apparatus Syst.Vol.3,pp.16-25,1988

[84]Toshiyuki Shimazaki and I.Tsuneyasu,"Flashover processes on the surface of solid insulators under positive impulse voltage in atmospheric air," IEEE Trans. Electr. Insul. Vol.27,pp. 488-495, 1992

[85]Toshiyuki Shimazaki,"Flashover characteristics and surface processes under negative impulse voltage in atmospheric air," IEEE Trans. Electr. Insul. Vol.25,pp. 1161-1169, 1990

[86]Chandima Gomes, Vernon Cooray and Mahbubur Rahman, "Breakdown characteristics and optically visible discharge paths of surface flashover, "IEEE Conference on Sustainable Development and Utilization in Engineering and Technology,pp.111-116,2012

[87]Halim Ayan, Gregory Fridman, Alexander F. Gutsol, Victor N. Vasilets, Alexander Fridman, and Gary Friedman," Nanosecond-pulsed uniform dielectric-barrier discharge," IEEE Trans. Plasma Sci.,Vol. 36, pp. 504-508,2008

[88]H. Ayan, D. Staack, G. Fridman, A. Gutsol, Y. Mukhin, A. Starikovskii, A. Fridman and G. Friedman, “Application of nanosecond-pulsed dielectric barrier discharge for biomedical treatment of topographically non-uniform surfaces,” J. Phys. D: Appl. Phys. Vol. 42, pp. 125202 (5pp), 2009.

[89]Tao Shao, Yang Yu, Cheng Zhang, Dongdong Zhang Zheng Niu, Jue Wang and Ping Yan, "Excitation of atmospheric pressure uniform dielectric barrier discharge using repetitive unipolar nanosecond-pulse generator," IEEE Trans. on Dielec. and Elect. Insul. Vol. 17 ,pp.1830-1837,2010

[90]Huijuan Ran, Jue Wang, Tao Wang, Cheng Zhang, Ping Yan and Lei Wang, "Spacer flashover characteristics in SF_6 under repetitive nanosecond pulses," IEEE Trans. on Dielec. and Elect. Insul. Vol. 20 ,pp.1161-1167,2013

[91]B. B. Pati, K. C. Patra and M.S.Naidu," Variation of surface flashover voltage in SF_6 with pressure," IEEE Trans. on Dielec. and Elect. Insul. Vol.1,pp.1175--1179,1994

[92]Kim P. Morales, John T. Krile, Andreas A. Neuber and Hermann G. Krompholz, "Pulsed dielectric surface flashover in nitrogen at atmospheric conditions," IEEE Trans. on Dielec. and Elect. Insul. Vol.13,pp.803-809,2006

[93]John T. Krile, Member,Andreas A. Neuber and Hermann G. Krompholz,"Effects of UV illumination on surface flashover under pulsed excitation," IEEE Trans. Plasma Sci.Vol. 36, pp.332-340,2008

[94]Kim P. Morales, John T. Krile, Andreas A. Neuber and Hermann G.Krompholz, "Dielectric surface flashover at atmospheric conditions with unipolar pulsed voltage excitation," IEEE Trans. Plasma Sci., Vol. 36, pp.774-782,2008

[95]George Laity, Andreas Neuber, Andrew Fierro, James Dickens, and Lynn Hatfield, "Phenomenology of streamer propagation during pulsed dielectric surface flashover," IEEE Trans. on Dielec. and Elect. Insul.Vol.18 ,pp.946-953,2011

[96]T. S. Sudarshan and R. A. Dougal ,"Mechanisms of surface flashover along solid dielectrics in compressed gases: a review," IEEE Trans. Electr. Insul. Vol. EI-21, pp.727-746, 1986

[97]C. W. Mangelsdort and C. M. Cooke, "Bulk Charging of Epoxy Insulation under dc stress," Proc. IEEE Symposium on Electrical Insulation. pp. 146-149, 1980.

[98]S. T. Pai and J. P. Marton, "Filamentary breakdown of gases in the presence of dielectric surfaces," J. Appl. Phys. Vol. 53, pp. 8583-8588, 1982.

[99]L.Niemeyer and F.Pinnekamp,"Surface discharge in SF_6," Proc. of the Third International Symposium on Gaseous Dielectrics,pp.379-385,1982

[100]L.Ludeking,A.Woods and L.Cavey, "Magic User Manual 3.2," Alliant Techsystems, U.S.A, 2011

[101]K.S.Yee, "Numerical solution of initial boundary value problems involving Maxwell's equations in isotropic media," IEEE Trans. on Antennas and Propagation.Vol. 14, pp. 302-307, 1966

[102]Y.P.Raizer ,*Gas Discharge Physics* Published by Springer Verlag, 1987

[103]Yukikazu Itikawa, "Cross Sections for Electron Collisions with Nitrogen Molecules," J. Phys. Chem. Ref. Data, Vol. 35, 2006

[104]K.Dhali and P.F.Williams, "Two-dimensional studies of streamers in gases" J.Appl. Phys.Vol.62,pp.4696-4707 1987.

[105]C.K.Birdshall,and A.B.Langdon, Eds., *Plasma Physics via Computer Simulation*. Published by McGraw-Hill, New York, 1985.

[106]C.K.Birdshall, "Particle-in-cell charged-particle simulations, plus Monte Carlo collisions with neutral atoms," IEEE Trans. on Plasma Sci.Vol. 19, pp.65-85, 1991.

[107]J.R.Laghari,"Spacer flashover in compressed gases," IEEE Trans.Dielect. Elect. Insul. Vol. EI-20, pp.83-92, 1985

[108]W.Pfeiffer, "Gas breakdown in case of steep –fronted pulses and insulator interfaces,"

IEEE Trans.Dielect. Elect. Insul.Vol.EI-17,pp.505-511, 1982

[109]E. E. Kunhardt and W. W. Byszewski, “Development of overvoltage breakdown at high gas pressure,"Physics Review A,Vol-21,pp.2069-2077, 1980

[110]L M Vasilyak, S V Kostyuchenko, N N Kudryavtsev, and I V Filyugin,"Fast ionisation waves under electrical breakdown conditions,"Phys.Usp.Vol.27,pp.247-269 ,1994

[111]D. Levko, S. Yatom, V. Vekselman and Ya. E. Krasik, “Electron emission mechanism during the nanosecond high-voltage pulsed discharge in pressurized air,” Applied Physics Letters.Vol. 100,pp. 084105 ,2012

[112]R. Menon , Amitava Roy, S. K. Singh, S. Mitra, Vishnu Sharma, Senthil Kumar, Archana Sharma, K. V. Nagesh, K. C. Mittal and D. P. Chakravarthy, “High power microwave generation from coaxial virtual cathode oscillator using graphite and velvet cathodes,” J. Appl. Phys. Vol. 107, no. 9, pp. 093301(6pp), 2010.

[113]R. Menon, Amitava Roy, S. Mitra, A. Sharma, J. Mondal, K. C. Mittal, K. V. Nagesh and D. P. Chakravarthy, “ Generation and dose distribution measurement of flash X-ray in KALI-5000 system,” Rev. Sci. Instrum. Vol. 79, pp.103301(5pp), 2008

[114]K.D.Srivastava and Jianping Zhou, “Surface charging and flashover of spacers in SF_6 under impulse voltage,” IEEE Trans.Dielect. Elect. Insul.Vol-26,no.3,pp.428-441,1981

[115]A. Jaksts and J. D.Cross, IEEE Symposium all Electrical Insulation (IEEE, New York, 1978), pp. 149-152

[116]S.M.Mahajan and T.S.Sudarshan,“Avalanches near a solid insulator in nitrogen gas at atmospheric pressure” J.Appl.Phys.Vol.66pp.1095-1102,1989

[117]Chaofeng Sang, Jizhong Sun, Chunsheng Ren and Dezhen Wang," Characteristics of nanosecond pulse needle-to-plane discharges at high pressure: a particle-in-cell Monte Carlo

collision simulation," J. Appl. Phys. Vol. 105, no.4, pp. 043305,2009

[118]Wenxia Sima ,C.Sun,L.Gu,X.Jiang and M.Chen "Study on the shape of suspension insulators influencing development of discharge," ISEIM, pp-290-292, 2001

[119]Amitava Roy,R. Menon, S. Mitra, D. D. P. Kumar, Senthil Kumar, Archana Sharma, K. C. Mittal, K. V. Nagesh and D. P. Chakravarthy," Intense relativistic electron beam generation and prepulse effect in high power cylindrical diode," J. Appl. Phys. Vol.102, pp.064902(5pp), 2008

[120]D.Durga Praveen Kumar, S. Mitra, K. Senthil, Archana Sharma, K. V. Nagesh, S.K.Singh, J.Mondal, Amitava Roy and D. P. Chakravarthy ," Characterization and analysis of a pulse power system based on Marx generator and Blumlein",Rev. Sci.Inst .Vol.78, pp.115107(4pp), 2007

[121]S.Y. Li, G.D. Theophilus and K.D. Srivastava, "Nanosecond Streak Photography of Discharges on Spacer Surface in Gases" IEEE Trans.Dielect. Elect. Insul.Vol-2,pp.114-120, 1995

[122]S.Y.Li, G.D. Theophilus and K.D. Srivastava, "Early stages of discharge development on insulating spacers in gases - a photographic study, ”5th IEEE ICCBSD ,pp-361-365, 1995

[123] Archana Sharma, S. Acharya, K.V. Nagesh and R C. Sethi, “Surface Flashover in Spacer at vacuum/oil interface,” XXth lnternational Symposium on Discharges and Electrical Insulation in Vacuum - Tours,pp.219-222,2002

[124] Archana Sharma , S. Kumar, S. Mitra, Vishnu Sharma, A. Patel, A. Roy, R. Menon, K. V. Nagesh and D. P. Chakravarthy, “Development and Characterization of Repetitive 1-kJ Marx-Generator-Driven Reflex Triode System for High-Power Microwave Generation,” IEEE Trans. Plasma Sci.,Vol. 9.pp. 1262–1267, 2011

[125]Ping Yan, Tao Shao, Jue Wang, Wei Gao, Weiqun Yuan, Ruzheng Pan, Shichang Zhang and Guangsheng Sun, “Experimental investigation of surface flashover in vacuum using nanosecond pulses,” IEEE Trans. on Dielec.and Electr. Insul. Vol. 14, pp. 634–642, 2011.

[126]T. A. Holt, M. G. Mayes, M. B. Lara and J. R. Mayes, "A Marx generator driven impulse radiating antenna,” IEEE,Pulse Power Conference.pp.489-494, 2009.

[127]R. T. Lee and G. S. Smith, “A design study for the basic TEM horn antenna,” IEEE Antennas and Propagation Magazine.Vol. 46, pp.86-92,2004.

[128]D. Goerz, T. Ferriera, D. Nelson, R. Speer and M. Wilson, “An ultra-compact Marx-type high-voltage generator,” Digest of Technical Papers-PPPS.Vol.1, 628-631 ,2001.

[129]G. H Rim, E. P. Pavlov, H. S. Lee ,J.S.Kim and Y.W.Choi, “Pulse forming lines for square pulse generators,” IEEE Trans. Plasma Sci., Vol. 31, pp. 196–200, 2003.

[130]Laura K. Heffernan, "A fast 3 MV Marx generator for megavolt oil switch testing and integrated Abramyan network design," M.S. thesis, 2005.

[131]John Chubb, " New approaches for electrostatic testing of materials, "J.Electrostat. Vol. 54 pp.233-244 ,2002

[132]S. Sahli, A. Bellel, Z. Ziari, A. Kahlouche and Y. Segui, "Measure and analysis of potential decay in polypropylene films after negative corona charge deposition," J.Electrostat. Vol.57 pp.169-181,2003

[133]P Molinie, M Goldman and J Gatellet "Surface potential decay on corona-charged epoxy samples due to polarization processes" J. Phys. D. Appl. Phys. Vol.28,pp. 1601-1610,1995.

[134]D. U. Nguyen , A. Sylvestre, S. Bechu and S. Rowe, "Estimation of surface degradation under immersion plasma by surface potential decay method, "Annual Report Conference on Electrical Insulation and Dielectric Phenomena pp.631-634, 1994

[135]R.Hackman,"Outdoor HV composite polymeric insulators," Proceedings of international symposium on electrical insulating materials pp.1-16, 1998

[136]P.Molinie and P. Llovera, "Surface Potential Measurements: Implementation and Interpretation" 8th Int. Conf. DMMA, Edinburgh, pp.23-25,2000

[137]http://www.trekinc.com/pdf/341BSales.PDF

[138]http://www.trekinc.com/products/probes.asp#vm3450

[139]Frank Mauseth ,"Charge accumulation in rod-plane air gap with covered rod" Norwegian University of Science and Technology Ph.D thesis, pp.1-126, 2006

[140]G J Zhang, K Yang B Zhao and Z Yan, "On the surface trapping parameters of polytetra fluoro ethylene block" Applied Surface Science.Vol. 253,1995-1998 , 2006

[141] OYamamoto ,T Takuma , M Fukuda ,S Nagata and T Sonoda , "Improving withstand voltage by roughening the surface of an insulating spacer used in vacuum," IEEE Trans.on Dielec. and Elect. Insul. Vol. 104,pp. 550-556 ,2003

[142] R Toomer,and T J Lewis, "Charge trapping in corona –charge polyethylene films," J.Phys.D: Appl. Phys.Vol.13 ,pp.1343-1356, 1980

[143] A. Kolpaková, P. Kudrna, and M. Tichý, "Study of Plasma System by OES," Proceedings of 20th Annual Conference of Doctoral Students, Part II, pp 180-185, 2011.

[144] A. Nekahi and M. Farzaneh, "Rotational Temperature Measurement of an Arc Formed over an Ice Surface,"IEEETrans.Dielect.Elect.Insul.Vol.18,pp. 755-759, 2011

[145] Azam Nekahi, Shahab Farokhi, Masoud Farzaneh and Brian G.Stewart, "Arc Energy and Temperature During Its Propagation Over Ice-Covered Surfaces," IEEE Trans.Plasma Sci.Vol. 42,pp.114-119,2014

[146] C.M.Cooke, "Surface Flashover of Gas/Solid Interfaces," Proc. of the Third International

Symposium on Gaseous Dielectrics,pp.337-348,1982

[147] H.Ran, J.Wang, T.Wang, C.Zhang and P.Yan, "Spacer flashover characteristics in SF_6 under repetitive nanosecond pulses," .IEEE Trans.Dielect.Elect.Insul. Vol.20,pp.1161-1167,2013

[148] R M van der Horst, T Verreycken, E M van Veldhuizen and P J Bruggeman,"Time-resolved optical emission spectroscopy of nanosecond pulsed discharges in atmospheric-pressure N_2 and N_2/H_2O mixtures," J. Phys. D: Appl. Phys.Vol. 45, pp. 345201(11pp), 2012

[149]A Lofhtus and P H Krupenie, “The spectrum of molecular nitrogen,” J.Phys.Chem Ref.Data, Vol 6,pp 113-307, 1977

[150]Y Ralchenko ,A E Kramida, J Reader and N A Team, “NIST Atomic Spectra Database (ver. 5.1),” http://physics.nist.gov/asd, 2013

[151] Peter Bruggeman, Daan Schram, Manuel ´A Gonz´alez, Robby Rego, Michael G Kong and Christophe Leys, "Characterization of a direct dc-excited discharge in water by optical emission spectroscopy,” Plasma Sources.Sci.Technol. Vol.18, pp 025017(13pp) ,2009

[152] Jobin K. Antony, Gurneesh Singh Jatana, Nilesh J. Vasa, V. L. N. Sridhar Raja and A.S.Laxmiprasad, "Modeling of laser induced breakdown spectroscopy for very low pressure breakdown conditions," Applied Physics A .Vol.101,pp.161-165, 2010

[153] V K Unnikrishnan, Kamlesh Alti, V B Kartha, C Santhosh, G P Gupta and B M Suri, “Measurements of plasma temperature and electron density in laser-induced copper plasma by time-resolved spectroscopy of neutral atom and ion emissions,“Pramana Journal of Physics.Vol 74,pp.983-993, 2010

[154]S.S.Harilal,C. V. Bindhu, Riju C. Issac, V. P. N. Nampoori and C. P. G. Vallabhana , "Electron density and temperature measurements in a laser produced carbon plasma" J. Appl. Phys, Vol.82, No.5 043302-01-043302-5, 1997.

APPENDIX

1. Electrical Properties of Plastic Materials
2. Specialty Grades of Delrin®—ASTM Data

Professional Plastics

The Global Leader in High Performance Plastics

Electrical Properties of Plastic Materials

Material	Formula	Dielectric constant @1kHz	Dielectric constant @1MHz	Dielectric strength kV mm^{-1}	Dissipation factor @ 1kHz	Dissipation factor @ 1MHz	Surface resistivity Ohm/sq	Volume resistivity Ohm/cm
Cellulose Acetate	CA	-	~5	11	0.06	-	-	5×10^{12}
Cellulose Acetate Butyrate	CAB	-	2.5-6.2	10	0.04	-	-	10^{11}-10^{15}
Ethylene-Chlorotrifluoroethylene copolymer	E-CTFE	-	2.3-2.5	40	0.002	-	10^{14}-10^{15}	10^{15}-10^{16}
Ethylene-Tetrafluoroethylene Copolymer	ETFE	-	2.6	25	-	0.0005	$>10^{14}$	10^{16}
Fluorinated Ethylene Propylene Copolymer	FEP	-	2.1	20 @ 3.2mm	-	0.0007	10^{16}	10^{18}
Polyacrylonitrile-butadiene-styrene	ABS	-	3.2 - 3.3	20-25	-	0.02	-	$>10^{15}$
Polyamide - Nylon 6	PA 6	-	3.6	25	0.2	-	$5x10^{10}$	$5x10^{12}$
Polyamide - Nylon 6, 6	PA 6,6	-	3.4	25	0.2	-	10^{11}	10^{13}
Polyamide - Nylon 6, 6 - 30% Carbon Fiber Filled	PA 6, 6 - 30% CFR	-	-	-	-	-	10^{3}	10^{2}

Material	Formula	Dielectric constant @1kHz	Dielectric constant @1MHz	Dielectric strength kV mm^{-1}	Dissipation factor @ 1kHz	Dissipation factor @ 1MHz	Surface resistivity Ohm/sq	Volume resistivity Ohm/cm
Polyamide - Nylon 6, 6 - 30% Glass Fiber Reinforced	PA 6,6 30% GFR	-	3.9-5.7	-	-	-	-	10^{12}-10^{15}
Polyamide - Nylon 12	PA 12	-	3.5 @ 100kHz	26-30 @ 1mm	0.06	-	10^{13}	10^{12}-10^{14}
Polyamide/imide	PAI	-	3.9-5.4	23 at 1mm	-	0.03-0.042	8-50 x 10^{17}	0.08-2 x 10^{17}
Polybenzimidazole	PBI	-	3.2	21	-	-	-	8x10^{14}
Polybutylene terephthalate	PBT	3.2	-	20	0.002	-	-	10^{15}
Polycarbonate	PC	-	2.9	15-67	-	0.01	10^{15}	10^{14}-10^{16}
Polycarbonate - 30% Glass Fiber Filled	PC - 30% GFR	-	3.3	30	-	0.009	10^{14}	10^{16}
Polycarbonate - Conductive	PC	-	-	-	-	-	100-500	1-100
Polychlorotrifluoroethylene	PCTFE	-	2.24-2.8	14	0.023-0.027	0.01	10^{15}	10^{16}
Polyetheretherketone	PEEK	3.2-3.3 @ 50Hz-10Khz	-	190 @ 50µm	-	0.003	-	10^{15}-10^{16}
Polyetherimide	PEI	3.1	-	30 @ 1.6mm	-	0.0013 @ 1KHz	4.10^{13}	7.10^{15}
Polyethersulfone	PES	-	3.7	16	-	0.003	-	10^{17}
Polyethylene - Carbon filled	PE	-	-	-	-	-	10^{3}-10^{4}	<10^{5}

Material	Formula	Dielectric constant @1kHz	Dielectric constant @1MHz	Dielectric strength kV mm^{-1}	Dissipation factor @ 1kHz	Dissipation factor @ 1MHz	Surface resistivity Ohm/sq	Volume resistivity Ohm/cm
Polyethylene - High density	HDPE	-	2.3-2.4	22	-	1-10 x 10^{-4}	10^{13}	10^{15}-10^{18}
Polyethylene - Low Density	LDPE	-	2.2-2.35	27	-	1-10 x 10^{-4}	10^{13}	10^{15}-10^{18}
Polyethylene - U.H.M.W.	UHMW PE	-	2.3	28	-	1-10 x 10^{-4}	10^{13}	10^{18}
Polyethylene terephthalate	Polyester, PET, PETP	-	3.0	17	0.002	-	10^{13}	>10^{14}
Polyimide	PI	-	3.4	22	0.0018	-	10^{16}	10^{18}
Polymethylmethacrylate	PMMA, Acrylic	-	2.6	15	-	0.014	10^{14}	2-14 x 10^{15}
Polymethylpentene	TPX®	-	2.12	-	0.0002	-	-	>10^{16}
Polyoxymethylene - Copolymer	Acetal - Copolymer POMC	-	3.7 - 4.4	20 @ 2.3mm	-	0.006 - 0.18	10^{15}	10^{15}
Polyoxymethylene - Homopolymer	Acetal - Homopolymer POMH	-	3.7	20	-	0.005	10^{15}	10^{15}
Polyphenyleneoxide	PPO (modified), PPE (modified)	-	2.7	16-20	0.004	-	2x10^{16}	10^{17}
Polyphenyleneoxide (modified), 30% Glass Fiber Reinforced	PPO 30% GFR	-	3.1	15	0.01	-	-	10^{17}
Polyphenylenesulfide - 40% Glass Fiber Reinforced	PPS - 40% GFR	-	3.8 - 4.2	18	-	0.0013-0.004	10^{16}	10^{16}

Material	Formula	Dielectric constant @1kHz	Dielectric constant @1MHz	Dielectric strength kV mm^{-1}	Dissipation factor @ 1kHz	Dissipation factor @ 1MHz	Surface resistivity Ohm/sq	Volume resistivity Ohm/cm
Polyphenylsulfone	PPSu	-	-	-	-	0.005	$>10^{13}$	$>10^{14}$
Polypropylene	PP	-	2.2-2.6	30-40	-	0.0003 - 0.0005	10^{13}	10^{16}-10^{18}
Polystyrene	PS	-	2.4-3.1	20	0.0002	-	-	$>10^{16}$
Polystyrene - Conductive	High Impact Conductive Polystyrene	-	-	-	-	-	10^{2}-10^{7}	10^{2}-10^{7}
Polystyrene - Cross-linked	PS - X - Linked	-	2.5	27-47	-	0.0002	$>10^{15}$	$>10^{15}$
Polysulphone	PSu	3.14	3.10	17	0.0013	0.0050	-	$5x10^{16}$
Polytetrafluoroethylene	PTFE	-	2.0-2.1	50-170	-	0.0003 - 0.0007	10^{17}	10^{18}-10^{19}
Polytetrafluoroethylene filled with Glass	PTFE 25% GF	-	2.2-2.35	40	0.003	-	10^{15}	10^{16}
Polyvinylchloride - Unplasticized	UPVC	-	2.7-3.1	14	0.025	-	-	10^{16}
Polyvinylidenefluoride	PVDF	-	8.4	13	0.06	-	10^{13}	10^{14}
Tetrafluoroethylene-perfluoro(alkoxy vinyl ether) - Copolymer	PFA. Teflon PFA.	2.05-2.06	2.05-2.06	-	0.0001-0.0002	0.0008	-	-

Table 3 (continued)
Specialty Grades of Delrin®—ASTM Data

Property	ASTM	Units	Extrusion Resins		UV Stabilized		Glass-Filled/ Glass-Reinforced			Chemically Lubricated with Teflon® PTFE Fibers and Filler*	
			Delrin® D150E, SA	Delrin® D550SA	Delrin® D127UV	Delrin® D527UV	Delrin® D570	Delrin® D577	Delrin® D525GR	Delrin® D500AL	Delrin® D500CL
ELECTRICAL											
Surface Resistivity	D257	ohm	—	—	1E+15	6E+14	2E+15	—	2E+15	4E+15	6E+15
Volume Resistivity	D257	ohm·cm	—	—	1E+14	1E+14	8E+14	—	4E+13	7E+14	4E+15
Dielectric Constant, 1 MHz	D150	—	—	—	3.3	3.4	3.8	—	3.8	3.6	3.6
Dissipation Factor, 1 MHz	D150	10^{-4}	—	—	—	—	63	—	76	60	70
Electric Strength, 2.3 mm (0.09 in)	D149	kV/mm	—	—	—	—	17.8	—	17.3	17.7	17.3
FLAMMABILITY											
UL94 Rating at Min. Thickness	UL94	—	HB	—	HB	HB	HB	HB	HB	HB	HB
UL94 Min. Thickness Tested	UL94	mm (in)	1.47 (0.05)	—	0.84 (0.03)	0.84 (0.03)	1.47 (0.05)	1.47 (0.05)	0.75 (0.03)	0.75 (0.03)	0.75 (0.03)
MISCELLANEOUS											
Melt Flow Rate, 1.05 kg at 190°C (2.3 lb at 374°F)	D1238	g/10 min	1	7	1	7	4	4	5	6	7
Melt Flow Rate, 2.16 kg at 190°C (4.8 lb at 374°F)	D1238	g/10 min	—	—	—	—	—	—	—	—	—
Specific Gravity	D792	—	1.42	1.42	1.42	1.42	1.56	1.56	1.6	1.39	1.42
Density		g/cm^3	1.42	1.42	1.42	1.42	1.56	1.56	1.6	1.39	1.42
Rockwell Hardness	D785	—	— —	— —	M86 R120	M86 R120	— —	— —	M98 R122	M87 R119	M89 R120
Water Absorption, 23°C (73°F)	D570	%									
Equilibrium, 50% RH			—	—	—	—	0.2	—	—	—	0.24
Immersion, 24 hr			—	—	—	—	0.25	—	0.3	—	0.27
Saturation (Equilibrium)			—	—	—	—	1.0	—	—	—	1.0
Mold Shrinkage, 3.2 mm (0.12 in) thickness	—	%									
Flow Direction			—	—	1.8–2.1	1.9–2.2	0.8–1.1	—	0.3–0.6	1.7–2.0	1.7–2.0
Transverse Direction			—	—	1.8–2.1	1.9–2.2	1.0–1.3	—	1.0–1.3	1.7–2.0	1.8–2.1
PROCESSING GUIDELINES											
Melt Temperature Range		°C (°F)	—	—	210–220 (410–428)	210–220 (410–428)	210–220 (410–428)	210–220 (410–428)	210–220 (410–428)	210–220 (410–428)	210–220 (410–428)
Mold Temperature Range		°C (°F)	—	—	80–100 (176–212)	80–100 (176–212)	80–100 (176–212)	80–100 (176–212)	80–100 (176–212)	80–100 (176–212)	80–100 (176–212)
Processing Moisture Content, max		%	0.2	0.2	0.2	0.2	0.1	0.1	0.1	0.2	0.2

NY = No Yield
NB = No Break
*Teflon® is a registered trademark of DuPont for its brand of fluoropolymer resin. Only DuPont makes Teflon®.

Table 3 (continued)
Specialty Grades of Delrin®—ASTM Data

Property	ASTM	Units	Chemically Lubricated with Teflon® PTFE Fibers and Filler*					Impact Modified		
			Delrin® D100AF	Delrin® D500AF	Delrin® D520MP	Delrin® D510MP	Delrin® D500TL	Delrin® D100ST	Delrin® D500MT	Delrin® D500T
ELECTRICAL										
Surface Resistivity	D257	ohm	—	—	1E+16	6E+15	7E+16	2E+14	3E+14	1E+15
Volume Resistivity	D257	ohm·cm	—	—	3E+14	3E+14	2E+15	3E+14	3E+14	1E+15
Dielectric Constant, 1 MHz	D150	—	—	—	3.4	3.5	3.6	4.2	4.2	3.9
Dissipation Factor, 1 MHz	D150	10^{-4}	—	—	50	50	60	270	250	160
Electric Strength, 2.3 mm (0.09 in)	D149	kV/mm	—	—	18	17.3	16.5	20	15.5	15.5
FLAMMABILITY										
UL94 Rating at Min. Thickness	UL94	—	94	94	94	—	—	94	—	94
UL94 Min. Thickness Tested	UL94	mm (in)	1.47 (0.05)	1.47 (0.05)	1.5 (0.06)	—	—	1.5 (0.06)	—	0.75 (0.03)
MISCELLANEOUS										
Melt Flow Rate, 1.05 kg at 190°C (2.3 lb at 374°F)	D1238	g/10 min	0.5	2	4	5	6	0.8	4	5.5
Melt Flow Rate, 2.16 kg at 190°C (4.8 lb at 374°F)	D1238	g/10 min	—	—	—	—	—	2	—	12
Specific Gravity	D792	—	1.53	1.53	1.54	1.48	1.43	1.34	1.35	1.39
Density		g/cm^3	1.53	1.53	1.54	1.48	1.43	1.34	1.35	1.39
Rockwell Hardness	D785		M79 R118	M78 R118	M78 R119	M87 R121	— —	— —	M98 R122	M87 R119
Water Absorption, 23°C (73°F)	D570	%								
Equilibrium, 50% RH			0.18	0.18	—	—	0.11	0.35	—	0.27
Immersion, 24 hr		0.23	0.2	—	—	0.19	0.44	0.62	0.41	
Saturation (Equilibrium)			0.72	0.72	—	—	0.86	0.85	1.85	0.86
Mold Shrinkage, 3.2 mm (0.12 in) thickness	—	%								
Flow Direction			—	1.8–2.0	1.8–2.1	1.7–2.0	1.7–2.0	0.9–1.2	1.1–1.4	1.3–1.6
Transverse Direction			—	1.5–1.7	1.4–1.7	1.7–2.0	1.7–2.0	1.0–1.3	1.2–1.5	1.3–1.6
PROCESSING GUIDELINES										
Melt Temperature Range		°C (°F)	210–220 (410–428)	210–220 (410–428)	210–220 (410–428)	210–220 (410–428)	210–220 (410–428)	200–210 (392–410)	200–210 (392–410)	200–210 (392–410)
Mold Temperature Range		°C (°F)	80–100 (176–212)	80–100 (176–212)	80–100 (176–212)	80–100 (176–212)	80–100 (176–212)	40–60 (104–140)	40–60 (104–140)	40–60 (104–140)
Processing Moisture Content, Max.		%	0.2	0.2	0.2	0.2	0.2	0.05	0.05	0.05

NY = No Yield
NB = No Break
*Teflon® is a registered trademark of DuPont for its brand of fluoropolymer resin. Only DuPont makes Teflon®.